NTNU

Norwegian University of
Science and Technology

Experimental analysis of the R744 vapour compression rack equipped with the multi-ejector expansion work recovery module

Michal Piotr Haida

NTNU

Norwegian University
of Science and Technology

Department of Energy
and Process Engineering

EPT-M-2015-120

MASTER THESIS

for

Student Michal Haida

Spring 2015

Experimental analysis of the R744 vapour compression rack equipped with the multi-ejector expansion work recovery module

Eksperimentell analyse av R744 butikkjøleanlegg utstyrt med multi-ejektor ekspansjonsarbeidsgjenvinningsmodul

Background and objective

There is a large transition in supermarket refrigeration with a strong focus on Energy consumption. High efficient system configurations with R744 are introduced in various locations throughout Europe; however, further improvements are necessary and possible, for example with the use of ejector-based expansion work recovery.

A multi-ejector expansion pack, intended as a substitute for a standard high-pressure electronic expansion valve (HPV) will be experimentally investigated in the supermarket compressor rack rated for 80 kW at a 35 °C gas cooler outlet temperature and a -3 °C evaporation temperature. The applicability of the multi-ejector pack as a main flashing device shall be verified experimentally. Operational characteristics of the rack (refrigeration capacity, power consumption, COP) shall be recorded for both alternative options: expansion purely in the HPV vs. HPV-assisted expansion in the multi-ejector pack. Additionally, the flash-tank pressure optimization problem shall be addressed for both operation alternatives.

The following tasks are to be considered:
1. Literature review on R744 ejector technology
2. Analysis of operating conditions for a typical R744 compressor rack in supermarket installations
3. Preparation of an experiment plan leading to generation of a set of individual performance maps for the investigated vapour compression rack
4. Practical training at the multi-ejector test facility
5. Test campaign directed to the comparative analysis of energy performance for the standard parallel compression rack vs. multi-ejector supported rack
6. Data processing and analysis of results
7. Conclusions and proposal for further work

-- ” --

Within 14 days of receiving the written text on the master thesis, the candidate shall submit a research plan for his project to the department.

When the thesis is evaluated, emphasis is put on processing of the results, and that they are presented in tabular and/or graphic form in a clear manner, and that they are analyzed carefully.

The thesis should be formulated as a research report with summary both in English and Norwegian, conclusion, literature references, table of contents etc. During the preparation of the text, the candidate should make an effort to produce a well-structured and easily readable report. In order to ease the evaluation of the thesis, it is important that the cross-references are correct. In the making of the report, strong emphasis should be placed on both a thorough discussion of the results and an orderly presentation.

The candidate is requested to initiate and keep close contact with his/her academic supervisor(s) throughout the working period. The candidate must follow the rules and regulations of NTNU as well as passive directions given by the Department of Energy and Process Engineering.
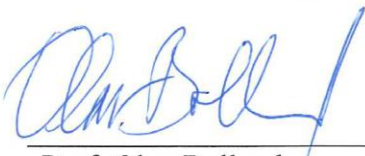
Risk assessment of the candidate's work shall be carried out according to the department's procedures. The risk assessment must be documented and included as part of the final report. Events related to the candidate's work adversely affecting the health, safety or security, must be documented and included as part of the final report. If the documentation on risk assessment represents a large number of pages, the full version is to be submitted electronically to the supervisor and an excerpt is included in the report.

Pursuant to "Regulations concerning the supplementary provisions to the technology study program/Master of Science" at NTNU §20, the Department reserves the permission to utilize all the results and data for teaching and research purposes as well as in future publications.

The final report is to be submitted digitally in DAIM. An executive summary of the thesis including title, student's name, supervisor's name, year, department name, and NTNU's logo and name, shall be submitted to the department as a separate pdf file. Based on an agreement with the supervisor, the final report and other material and documents may be given to the supervisor in digital format.

☒ Work to be done in lab (Water power lab, Fluids engineering lab, Thermal engineering lab)
☐ Field work

Department of Energy and Process Engineering, 3 July 2015

Prof. Olav Bolland
Department Head

Prof Trygve M. Eikevik
Academic Supervisor
e-mail: Trygve.m.eikevik@ntnu.no

Research Advisor: e-mails
Krzysztof Banasiak, SINTEF Energy Research   Krzysztof.Banasiak@sintef.no

Preface

This master thesis was submitted to the Department of Energy and Process Engineering at the Norwegian University of Science and Technology and the Institute of Thermal Engineering at the Silesian University of Technology. The work was carried out from March to August of 2015 within the international exchange program Erasmus+ with EEA scholarship.

My challenge was to carry out of an experimental investigation on advanced test facility, what let me to use my gathered knowledge during my study in a practise. The work on real test rig gave me large portion of experience and abilities to control the CO_2 refrigeration system. I have found motivation in the fact that my work can give information about benefits to use the multi-ejector pack in the commercial refrigeration systems. Thereby, this thesis can promote energy efficient refrigeration technology for the natural, environmentally friendly refrigerant, such as carbon dioxide.

I would like to thank everyone, who help me during this time, which I spent in Trondheim: my SINTEF coordinator Krzysztof Banasiak, my supervisor from the Silesian University of Technology Jacek Smołka, my NTNU supervisor Trygve Magne Eikevik, Armin Hafner from SINTEF, Andrzej J. Nowak from Silesian University of Technology, and my lab partner, roommate and at last colleague Alexander Scheid. All of foregoing persons supported me and they always had time to give me an advice.

I want to thank my fiancée Marta, my parents, and my brother together with his wife, for all of them spiritual help and supporting me during my stay in Trondheim, despite the large distance. Last but not least I would like to dedicate this master thesis my grandmother Brygida. She passed away in the half of my stay in Trondheim- without her support I would never gone so far.

<div align="center">

Trondheim, 26.08.2015

Michał Piotr Haida

</div>

Abstract

Present supermarket refrigeration systems, with carbon dioxide as a refrigerant, indicate high-efficiency performance and they are commonly installed in throughout Europe. The refrigeration systems with R744 have still a large potential to limit power consumption. One of solutions is ejector-based expansion work recovery module.

Aim of this thesis is to present an experimental investigation of standard R744 supermarket refrigeration system, with the high-pressure electronic valve (HPV), and refrigeration system with multi-ejector expansion pack on the same vapour compression rack. Comparison of the R744 multi-ejector refrigeration system, was carried out based on energy performance characteristics: refrigeration capacity, power consumption, COP, and exergy efficiency. Apart from the system performance comparison, influence of the pressure level in the flash tank on the system performance for both alternatives was analysed.

The experimental results indicated COP and exergy efficiency improvement of the multi-ejector refrigeration system up to 7% and 13.7%, respectively. The multi-ejector system was able to operate in smaller range of the tanks pressure lift than the standard system dependent on the refrigeration load and the exit gas cooler section parameters. The highest values of COP and exergy efficiency were obtained by the multi-ejector refrigeration system for the tanks pressure lift value close to the limit value. The values of the overall compressor efficiencies were significantly differentiated, dependent on the operation module (cooling load and heat rejection conditions), which strongly influenced the values of COP and exergy efficiency. Therefore, it was not possible to clearly define the optimum pressure in the flash tank. It was concluded that improvement of compressors efficiencies utilized in the multi-ejector system will indicate high energy performance of the refrigeration system.

Streszczenie

Obecne systemy chłodnicze wykorzystujące dwutlenkek wegla (R744), jako czynnik roboczy, charakteryzują się wysokosprawnościową wydajnością i są instalowane powszechnie w dużych sklepach na terenie całej Europy. Pomimo wysokiej efektywnosci pracy, systemy chłodnicze z czynnikiem R744 mają nadal ogromny potencjał do redukcji konsumpcji mocy elektrycznej. Jednym z rozwiązań jest implementacja modułu eżektorowego w celu częściowego odzysku pracy.

Niniejsza praca przedstawia wyniki badań eksperymentalnych na jednym stanowisku badawczym dla dwóch konfiguracji: standardowego systemu chłodniczego z wysokocisnieniowym elektronicznym zaworem rozprężnym (HPV) oraz dla systemu chłodniczego z zaimplementowanym modułem eżektorowym. Porównanie obu systemów zostało przeprowadzone na podstawie charakterystyk: wydajności chłodniczej, konsumpcji mocy elektrycznej, COP oraz sprawności egzergetycznej. Oprócz porówniania wydajności systemów wykonano analizę wpływu poziomu ciśnienia w średniociśnieniowym separatorze na poprawę efektywności pracy układów chłodniczych.

Wyniki eksperymentalne wykazały poprawę COP oraz sprawności egzergetycznej systemu chłodniczego z modułem eżektorowym, w stosunku do systemu chłodniczego z równoległym sprężaniem o odpowiednio 7% oraz 13,7%. System z modułem eżektorowym byl zdolny do pracy w mniejszym zakresie różnicy ciśnień pomiędzy średniocisnieniowym separatorem, a niskociśnieniowym separatorem w stosunku do standardowego system chłodniczego. Największe wartości COP oraz sprawności egzergetyczne zostały uzyskane przez system chłodniczy z modułem eżektorowym dla wartości różnicy ciśnien w separatorach bliskiej granicznej mozliwej wartości do poprawnej pracy modułu eżektorowego. Wartości całkowitej sprawności kompresorów różniły się od siebie w zależności od trybu pracy (obciążenie chłodnicze oraz warunki oddania ciepła przez czynnik roboczy), co mocno wpłynęło na uzyskane wartości COP i sprawności egzergetyczne. W efekcie różnic sprawności kompresorówjasne zdefiniowanie optymalnej wartości ciśnienia w średniocisnieniowym separatorze nie było mozliwe. Poprawa sprawności kompresorów, wykorzystywanych w systemach chłodniczych z modułem eżektorowym przyczyni się do poprawy wydajnosci energetycznej systemu chłodniczego z CO_2.

Contents

List of Figures

List of Tables

List of Symbols and Abbreviations

Greek Letters

η	Efficiency	
Φ	Mass entrainment ratio	
Π	Pressure Ratio	
ρ	Density	kg m^{-3}
ψ	Specific exergy	kJ kg^{-1}

Roman Letters

c_p	Specific heat capacity	kJ kg^{-1} K^{-1}
d	Diameter	m
$\dot{E}$	Exergy rate	kW
h	Specific enthalpy	kJ kg^{-1}
s	Specific entropy	kJ kg^{-1} K^{-1}
$\dot{m}$	Mass flow rate	kg s^{-1}
N	Power	kW
p	Pressure	bar
T, t	Temperature	K, ^{o}C
u	Standard uncertainty	

w	Velocity	m s^{-1}
W	Work rate	kW
x	Variable	

Subscripts

CO_2	Carbon dioxide
comp	Compressor
ej	Ejector
el	Electric power
evap	Evaporator
ex	Exergy
g	Electromotor losses
gc	Gas cooler
gl	Glycol
hp	High pressure
in	Inlet
incr	Increment
is	Isentropic
me	Electric-mechanical motor
mot	Ejector motive side
max rec	Maximum work recovery
multi-ejector	The multi-ejector system

out	Outlet
parallel	The parallel system
suc	Ejector suction side
vol	Volumetric

Abbreviations

CD1400H	Base-load Compressor Dorin CD1400H
CD1000H	Parallel Compressor Dorin CD1000H
CD380H	Parallel Compressor Dorin CD380H
CFC	Chlorofluorocarbon
COP	Coefficient of performance
HCFC	Hydro-Chlorofluorocarbons
HPV	High-pressure electronic expansion valve
IHX	Internal Heat Exchanger
MT	Medium-temperature level
LT	Low-temperature level
P&ID	Piping and Instrumentation Diagram
R744	Refrigerant signature of carbon dioxide
SLHX	Suction-liquid line heat exchanger
VEJ1	Vapour Ejector number 1
VEJ2	Vapour Ejector number 2
VEJ3	Vapour Ejector number 3

1 Introduction

Increase of using the refrigeration system, based on the natural refrigerant, in the commercial refrigeration is related to the restrictive political regulations about environment protection. The Montreal Protocol and the Kyoto Protocol defined that the annual leakage of synthetic refrigerant, common used in refrigeration, such as Chlorofluorocarbon (CFC) and hydro-chlorofluorocarbons gases (HCFCs), should be significantly reduced, or even replaced by the environmentally friendly refrigerant (United Nations Environment and Ozone, 1987, United, 1997). Thereby, environmentally friendly carbon dioxide (denoted as R744), well known natural refrigerant in the first half of twentieth century, has been commonly used in recent refrigeration systems thanks to Prof Gustav Lorentzen activities to revival of the CO_2 use in refrigeration (Pearson, 2005). In 1990 Prof Lorentzen patented the transcritical carbon dioxide system for automotive air-conditioning, what let to design and manufacture rival refrigeration systems with CO_2 as a main working fluid (Lorentzen, 1990).

Carbon dioxide has the low critical temperature and the high critical pressure. Therefore, for the surrounding temperature above the critical temperature, the refrigeration system has to reject the heat from the R744 cycle in the transcritical mode, which influences on the degradation of the system performance (Kim et al., 2004). As a result of the ambient temperature influence on energy efficiency, the R744 transcritical refrigeration systems are located most frequently in the cold climate regions. Although the development of CO_2 transcritical system configuration and the development of devices included in the system let to introduce the CO_2 commercial refrigeration system in a warm climates. One of the idea to improve R744 refrigeration system energy performance is integration the ejectors module as a main flashing device and partially supported by standard high-pressure electronic expansion valve (HPV). The aim of use the ejector is recover some potential work due to expansion of the high-pressure fluid and compress the low-pressure fluid at the same time inside the ejector in order to improve energy performance of the refrigeration system.

Nowadays SINTEF Energy Research introduces the ejector technology to the R744 refrigeration systems in the supermarket. In collaboration with Enex and Danfoss, world leading companies specialized in the design, control and production of high-efficiency refrigeration systems, and the Silesian University of Technology, SINTEF Energy Research is working on the *Multijet* project, which the main task was to implement the designed multi-

ejector pack to the R744 refrigeration system in two supermarkets: Spiazzo (Italy) and Trondheim (Norway). Hence, the test facility equipped with the designed multi-ejector pack has been installed and commissioned in the research laboratory at NTNU and SINTEF Energy Research. Now the actual goal of the project is to present the system performance improvement of the R744 vapour compression system with the multi-ejector expansion pack.

2 Objectives

The main task of this thesis is an analysis of system performance of the R744 vapour compression rack equipped with the multi-ejector expansion pack based on experimental investigation. The experimental investigation has been carried out with and without the use of the multi-ejector pack for the same operating conditions. Recorded operational characteristics, such as refrigeration capacity, power consumption, COP and exergy efficiency, have been compared to both alternative configurations in order to present system performance improvement of the R744 multi-ejector refrigeration system. In addition, the information about the efficiencies of the rack of compressors has been presented during the experimental investigation for both configuration on the same test facility.

In the literature, there is no precise information about optimum flash-tank pressure in the R744 transcritical refrigeration system. Hence, searching of the optimum pressure level in the liquid receiver tank, based on experimental investigation has been done for both operation alternatives. In addition, for the multi-ejector block, the analysis of the flash-tank pressure can present the upper limit of pressure ratio required for proper work of ejectors (no reversed-flow conditions).

The draft of the research paper has been presented in Appendix A as a result of the experimental investigation of the R744 vapour compression rack equipped with the multi-ejector module.

3 Literature Review

3.1 Overview of Recent R744 Refrigeration Systems

3.1.1 Two-stage Cascade Refrigeration System

The development of recent commercial refrigeration system directs towards to design high-efficient modern system with zero leak (Da Silva et al., 2012). One of solutions to improve system performance for the supermarket refrigeration, contained medium-temperature level (MT) in chiller cabinets and low-temperature level (LT) in freezer cabinets, is applied the two-stage cascade system. The standard two-stage cascade refrigeration system, with two separated vapour compression cycles of both refrigerants, is shown in Figure 3.1. According to Getu and Bansal (2008), foregoing solution is suitable for evaporating temperature in LT level ranging from -30 ^{o}C to -50 ^{o}C. Carbon dioxide can be used as low-temperature refrigerant in separate vapour compression circuit due to excellent thermo-physical properties at low temperature. The typical high-temperature refrigerant is ammonia or other synthetic refrigerant (Bansal, 2012).
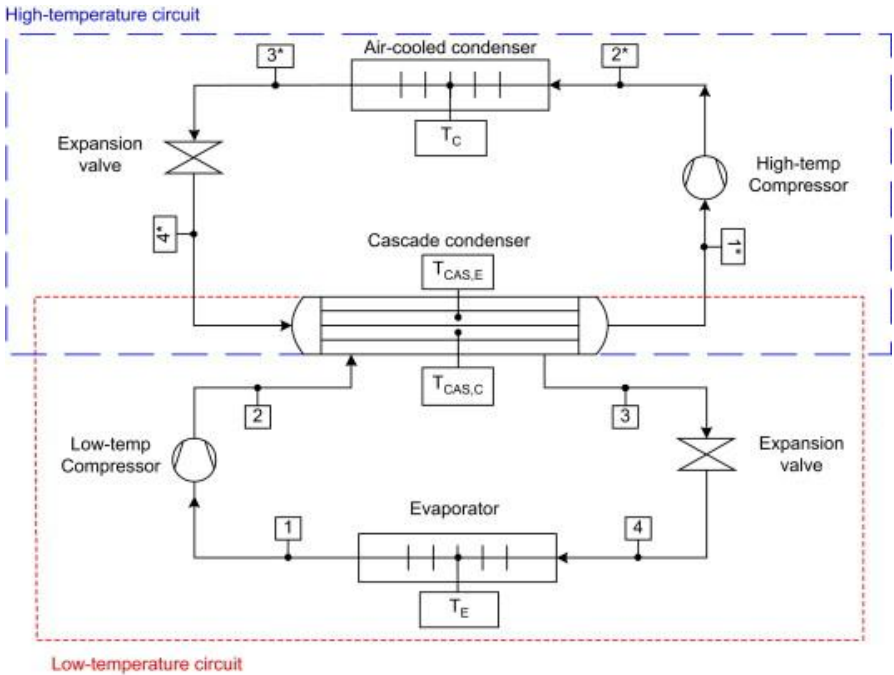
Figure 3.1: Schema of the two-stage cascade refrigeration system. The figure shows two separated loops with different refrigerants, which transfer heat between each other in the cascade condenser. Adapted from Getu and Bansal (2008).

Da Silva et al. (2012) compared system performances of CO_2/ HFC-404A cascade refrigeration system with HCFC-22 and HFC-404A as the conventional systems for supermarkets. Energy analysis indicated reduction of the power consumption per year for the cascade system and the CO_2/R404A refrigeration system improved energy performance up to 22.3% and 13.7% in comparison with the R404A and R22 conventional systems, respectively. According to Da Silva et al. (2012) R744 system in relation to R404A and R22 in cascade system achieved many advantages, such as reduction of the electric energy consumption, increase of the useful life of R744 due to low compression ratio, economical savings by reduction of CO_2 piping diameter size, reduction of all installation and less carbon taxes. Therefore, CO_2 cascade system configurations are competitive solutions in all climates. Although the CO_2 cascade system with synthetic refrigerants in the high-temperature loop such as HCFC-22, or HFC-404A, commonly worked in existing commercial refrigeration systems, only minimizes the annual emission of harmful gases. Da Silva et al. (2012) stated that for global warming potential index (GWP[1]) for the R744/R404A cascade system is around eight and four times smaller than conventional R404A, or R22 systems, respectively. Thereby the development of the purely CO_2 refrigeration system with low energy consumption and harmless for the environment is more expected.

3.1.2 R744 Transcritical Booster System

Designed refrigeration system, including only one circuit at MT and LT levels with CO2 as only refrigerant is simple and cheap in comparison to the cascade system (Ge and Tassou, 2011). The performance of the CO_2 system depends on the surrounding temperature, which determines working condition of CO_2 in transcritical, or subcritical mode. To reduce high pressure ratio in the transcritical mode, the booster system is divided into four pressure levels, what is shown in Figure 3.2. The additional receiver on the intermediate pressure level collects R744 after the heat rejection in the gas cooler and expands the saturated refrigerant liquid into the MT and LT evaporators (Sharma et al., 2014). The saturated vapor of CO_2 from the receiver, named flash gas, is throttled to the medium-temperature pressure level (1-2 in Figure 3.2), before it enters to the high-stage compressors. The internal heat exchanger, set after the intermediate vessel, is set to extend the difference of specific enthalpy in evaporators

---

[1] The potency of a greenhouse gas to the CO_2 emission over a 100-year period

(4-5 in Figure 3.2) and it provides that the flash gas after the throttling process is superheated (2-3 in Figure 3.2).

Girotto et al. (2004) stated that in hot climate region, the annual electric energy consumption of R744 transcritical booster system can be higher than a conventional R404A system, but in cold climate it consumed less electric energy than R404A systems during the year due to operation in subcritical mode for the higher number of hours. The author presented monthly averaged COP of both foregoing systems in the climate of Treviso (Italy) and in July COP of CO_2 and R404A units were equal to 2.0 and 2.8, respectively, when monthly averaged ambient temperature was equal to 24 ^{o}C. In January, for ambient temperature equal to 5 ^{o}C, R744 refrigeration system reached COP up to 4.2, when COP of the conventional system was equal to 3.9 (Girotto et al., 2004). Therefore, R744 transcritical booster system is located mostly in Northern Europe countries (Sawalha et al., 2015).
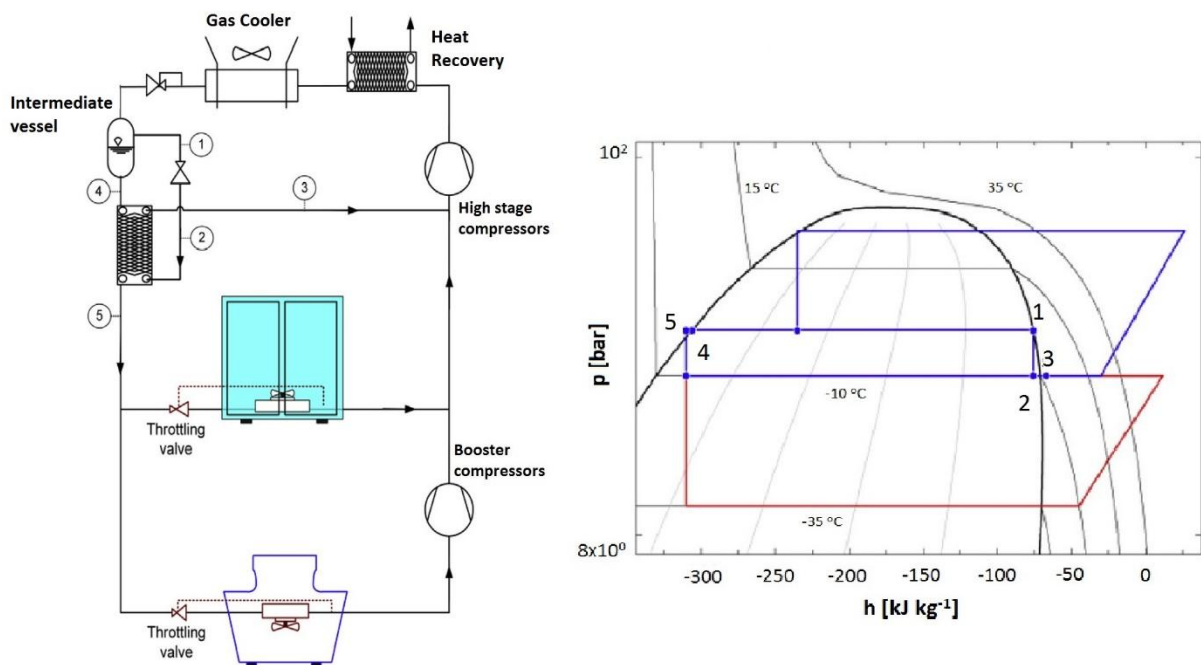
Figure 3.2: R744 Transcritical Booster System with two evaporation levels (MT & LT): simple schematic diagram with pressure-specific enthalpy diagram. Adapted and modified from Sawalha et al. (2015)

3.1.3 R744 Transcritical Parallel Compression System

The booster configuration with flash tank reduces the throttling losses by increase of the specific enthalpy difference in evaporator. Although, throttled flash gas to the MT level do not provide any useful effect. In order to advantageously use of the flash gas, it can be done by means of an auxiliary compressor. The parallel compression concept allows to compression the saturated CO_2 gas phase from the flask tank with a lower pressure ratio (Chesi et al., 2014). This system is applied to increase energy performance of a refrigeration system during summertime in hot climates (Bansal, 2012).

Figure 3.3 shows simplified schema of R744 parallel compression system and CO_2 state points on the pressure-specific enthalpy diagram. The system consists of three racks of compressors, gas cooler, MT and LT evaporators, two suction-liquid line heat exchangers (SLHX), liquid receiver tank, the high pressure expansion valve (2-3), and two metering valves before evaporators (6-7 and 9-10). After heat absorption in the low-temperature evaporator, the CO_2 is superheated in the SLHX2 and compressed through the low-pressure rack of compressors. The LP compressors work with the pressure ratio from low-temperature level to medium-temperature level. Both rest rack of compressors: HP compressors and bypass compressors, also known as parallel compressors, compress the refrigerant to the high discharge pressure but from different suction pressure. The CO_2 enters from medium-temperature pressure level to the HP compressors, previously superheated in the SLHX1, and from receiver tank pressure level to the parallel compressors. Simultaneously, in the SLHXs the refrigerant is subcooled after the gas cooler and the receiver tank, in order to increase the heat pump capacity and refrigeration capacity respectively.
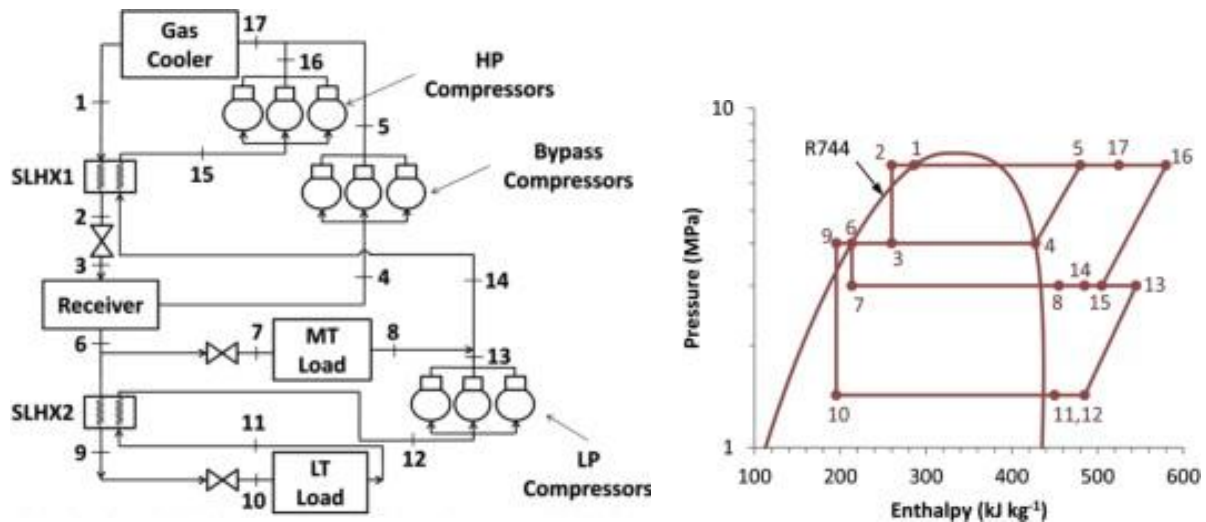
Figure 3.3: R744 Transcritical Parallel System with two evaporation levels (MT & LT): simple schematic diagram with pressure-specific enthalpy diagram. Adapted from Sharma et al. (2014).

Sarkar and Agrawal (2010) compared performance of three different parallel compression configuration. Authors determined that the parallel compression economized system (flash gas directly compressed by the parallel compressors section) achieves 47% COP improvement over the basis CO_2 transcritical refrigeration cycle for the chosen ranges of operating conditions.

Chesi et al. (2014) investigated experimental analysis of the R744 parallel compression system, based on energy performance analysis for different compressors discharge pressures, exit gas cooler temperatures and evaporation pressures. In addition, the influence of the flash tank separation capacity and the compressors volumetric flow ratio were analysed. According to Chesi et al. (2014), the ideal parallel compression cycle can reach COP improvements of over 65% and over 30% in terms of negligible pressure loss, considered perfect liquid-vapour separator and certain controlled value of the superheating. Authors identified the influence of compressors volumetric flow ratio closely linked to the flash tank pressure and the separator efficiency on the system performance.

Sharma et al. (2014) carried out analysis of various CO_2 configurations in supermarket refrigeration systems including the CO_2 cascade system, the transcritical booster system and the transcritical parallel compression system. Besides the R744 refrigeration systems, the multiplex direct expansion system with R404A as a working fluid has been introduced as the baseline. Authors compared each system based on annual average coefficient of performance

evaluation (COP described in section 4.3) for a different climate zones of the United States. Figure 3.4 shows the contour map of the United States with three specified regions for the most efficiently refrigeration systems. It can be noticed that for north part of the USA, the R744 transcritical parallel compression system gains the best energy performance and the similarly efficient as the R404 DX system in the central part of the United States. Sharma et al. (2014) stated that the COP of the R744 parallel compression system is 13% higher than that of the R404A multiplex direct expansion system in zones 5, 6 and 7 shown in Figure 3.4. In the south part of the US in zones 1, 2 and 3, the COP of the parallel compression system is 8.3% lower that of the R404A DX system (Sharma et al., 2014).

The R744 parallel compression refrigeration systems is a competitive commercial refrigeration system in particular in cold climate regions. Although there is still large potential to improve the energy performance of CO_2 systems by reducing of the throttling losses. One of idea is introduced an ejector as a main expansion device in refrigeration system in order to recover some potential work.
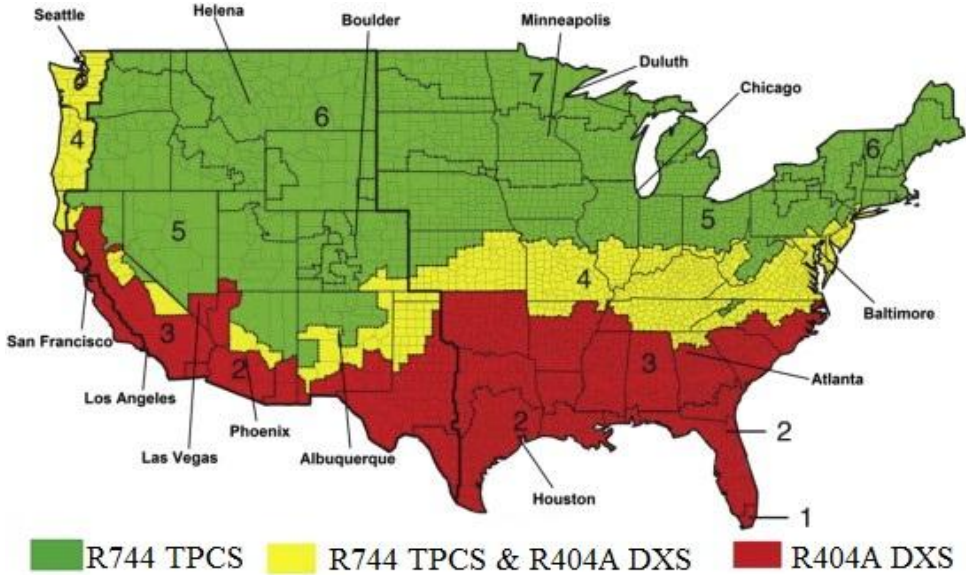
Figure 3.4: The contour map of most efficiently refrigeration system for each climate zones in the United States: the R744 Transcritical Parallel Compression System (R744 TPCS) and the R404A multiplex direct expansion system (R404A DXS). Adapted and modified from Sharma et al. (2014).

3.2 The R744 Two-phase Ejector Technology in Refrigeration System

In the refrigeration cycle, the expansion irreversibility, or the throttling losses in the expansion valves, can be reduced by use of an ejector (Sarkar, 2009). The first ejector, or rather the condensing-type injector, was invented in 1858 by Henry Giffard, but in 1931 Norman Gay patented refrigeration system with applied two phase ejector (Elbel, 2011). The two phase ejector characterizes two-phase flow outside the ejector, where the driving flow and driven flow are in liquid and vapor phase, respectively. According to Sumeru et al. (2012) main objective of using two-phase ejector in refrigeration cycle is energy performance improvement of the system by increasing the cooling capacity and lowering the compressor work. Description of working principles and main characteristics of the two-phase ejector is presented in section 4.5.2.

Kornhauser (1990) carried out energy performance analysis of vapour compression cycle with the two-phase ejector presented for selected refrigerants such as R22, or ammonia. Schematic of standard two-phase ejector refrigeration cycle is shown in Figure 3.5. In this cycle, the motive stream is a liquid CO_2 out of the condenser, the suction stream is a vapour phase of CO_2 after the evaporation process in the evaporator. Out of the ejector, the mixed CO_2 stream is split on two saturated phases in the separator. Author used the set of own equations describing two-phase ejector as a one-dimensional mathematical model. The COP of the ejector refrigeration system in a rate to standard vapour compression system was 1.20 and 1.12 times larger for R-22 and NH_3, respectively. According to Kornhauser (1990) the relative COP of refrigerants in both systems are relatively different, therefore this may impact to use non-CFC refrigerants. In 1996 Menegay and Kornhauser (1996) investigated experimental analysis of the ejector expansion refrigeration cycle with R-12 as refrigerant and they proofed that the COP improvement of the ejector system, in comparison to the standard vapour compression system, varied from 2.3% to 3.1%. The authors expected COP improvements in a range from 7% to 9% and even larger for refrigeration and ice storage application.
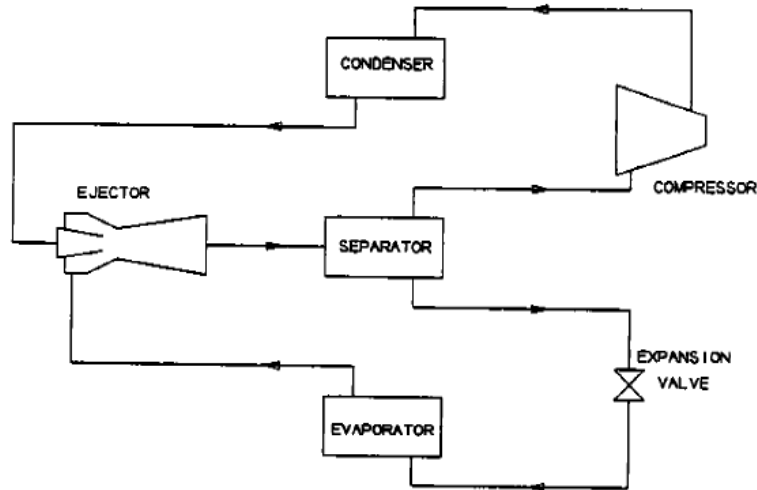
Figure 3.5: Schema of two-phase ejector expansion refrigeration system adapted from Kornhauser (1990).

Kornhauser's iteration model of two-phase ejector led to development of the research from the use of an ejector in refrigeration system for each refrigerant, especially for natural refrigerants like R744. Li and Groll (2005) presented theoretical analysis of transcritical CO_2 refrigeration cycle with the two-phase ejector-expansion device. They recorded the COP improvements of the CO_2 ejector expansion cycle up to 16% in comparison to standard CO_2 vapour compression cycle for typical air conditioning applications.

Deng et al. (2007) presented the system performance of CO_2 transcritical ejector expansion refrigeration cycle, based on the first and second law analysis, in comparison to conventional vapor compression cycle and the internal heat exchange cycle. In foregoing thesis, the ejector expansion refrigeration cycle improved maximum COP by up to 18.6% and by 22.% as the internal heat exchanger cycle and the conventional cycle, respectively. Exergy analysis indicated much less the throttling exergy loss for the ejector expansion refrigeration cycle and reduction of compression and heat rejection exergy losses. Lawrence and Elbel (2013) presented energy and exergy analysis, for the ideal and real cases, of three different R744 two-phase ejector refrigeration cycles, compared to standard expansion cycle. For the ideal case all three ejector refrigeration cycles improved COP and the second law efficiency by up to 23%, but for real case the ejector cycles obtained COP and exergy improvement up to 7% and 8%, respectively.

Elbel and Hrnjak (2008) designed the first prototype ejector with a variable motive nozzle throat area, by introduce a needle, and investigated experimental analysis to compare energy performance of the CO_2 refrigeration system with new designed ejector to a baseline with expansion valve. The needle in motive nozzle allows to the regulation of high-side pressure. According to Elbel and Hrnjak (2008), the R744 ejector refrigeration system improved the COP and the cooling capacity by up to 7% and 8%, respectively. The use of the needle increased the COP during increasing of the high-side pressure, due to reduced area of the motive nozzle throat. Effect of throat diameter of the two-phase ejector on the energy performance of the R744 two-phase ejector expansion refrigeration cycle was investigated by Chaiwongsa and Wongwises (2007). Authors stated that the highest COP was obtained for the smallest throat diameter equal to 0.8 mm as a result of low primary mass flow rate at still high vaporized mass flow rate and refrigeration capacity of the system.

Elbel (2011) compared influence the change of the mixing section length and the diffuser angle on the ejector efficiency and the system energy performance of the R744 transcritical refrigeration cycle. Four diameters of the constant-area mixing section: 7.5 mm, 32.5 mm, 57.5 mm, 82.5 mm, and three angles of the diffuser angle: 5°, 10°, and 15°, were chosen. As a result of investigation, the highest ejector efficiency was reached for the shortest constant-area section up to 15%. Simultaneously, the smallest diffuser angle 5° yielded the best ejector performance. Hence, both foregoing designed parameters can significantly influence the ejector performance (Elbel, 2011). The energy performance analysis indicated COP and cooling capacity improvement of the R744 transcritical ejector expansion cycle up to 7% and 8%, respectively, what confirmed the results presented in Elbel and Hrnjak (2008).

Sumeru et al. (2012) stated that the COP results of the CO_2 vapour compression system with the two-phase ejector given from experimental analysis are still different than theoretical calculations. According to Banasiak et al. (2012), the ejector geometry has to be optimized for a given application in order to maximize COP of the refrigeration system.

3.3 R744 Transcritical Refrigeration System with Ejector Expansion Module in Supermarket

Experimental and theoretical analysis indicates that replacing the expansion valve by the ejector in CO_2 transcritical vapour compression cycle improves energy performance and

reduces exergy losses of the cycle (Sumeru et al., 2012). Therefore, the evaluation of system performance for new, or existing R744 refrigeration system equipped with the ejector expansion pack in the supermarket has to be carried out.

Hafner et al. (2014) presented ejector technology for supermarket applications and carried out analysis of simulation model of the multi-ejector system and the reference CO_2 transcritical booster system for the selected operating conditions like load profiles, controls concept and climate data. The transient simulations were performed based on the annual variable ambient temperature and annual variable load profiles for heating and cooling mode, for three different climate regions: North European, Middle European and Mediterranean. In addition, experimental analysis of both foregoing refrigeration systems was presented. To simplify the refrigeration systems, calculations were done for only medium-temperature evaporation level due to fact that for both systems less than 20% of the overall cooling capacity is provided for the low-temperature cabinets (Hafner et al., 2014).

The R744 multi-ejector concept with non-continuously controllable ejectors is shown in Figure 3.6. It can be seen that the ejectors are applied to maintain and secure a constant pressure difference between both separators. Hence, in this case the multi-ejector installed instead of the expansion valves do not recover the expansion work (Hafner et al., 2014). In addition, the refrigeration system is applied in the heat recovery units.
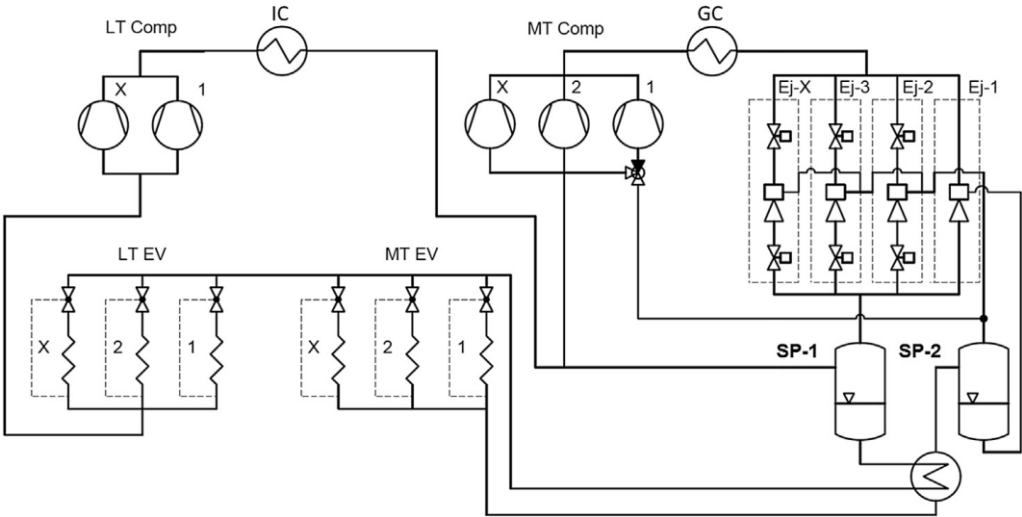
Figure 3.6: Circuit diagram of R744 transcritical refrigeration system in supermarket with controllable ejector module. Adapted from Hafner et al. (2014)

According to (Hafner et al., 2014), for a steady-state analysis, the COP of the R744 multi-ejector refrigeration system improved in comparison to the reference system by up to 10% and 20% at the ambient temperature 15 ^{o}C and 45 ^{o}C, respectively. The transient simulations indicated significant COP improvement of the multi-ejector system for cooling and heating mode. For selected climate zone, the COP for cooling mode increased between 20% and 30% during the winter and 17% in Mediterranean, 16% in Middle European, and 5% in Northern European countries during the summer.

Wiedenmann et al. (2014) presented work of R744 transcritical parallel compression refrigeration system in Migros Bulle supermarket after the integration of the ejectors. Figure 3.7 shows schema of the Migros Bulle refrigeration system with and without the ejectors module. The system consists of two vapour and one liquid ejectors, therefore the additional liquid receiver after the MT evaporator is applied. Wiedenmann et al. (2014) stated that the annual energy power consumption, depending on the climate region, of the refrigeration system with integrated ejectors was in the range of 12% to 20% less than the reference system.
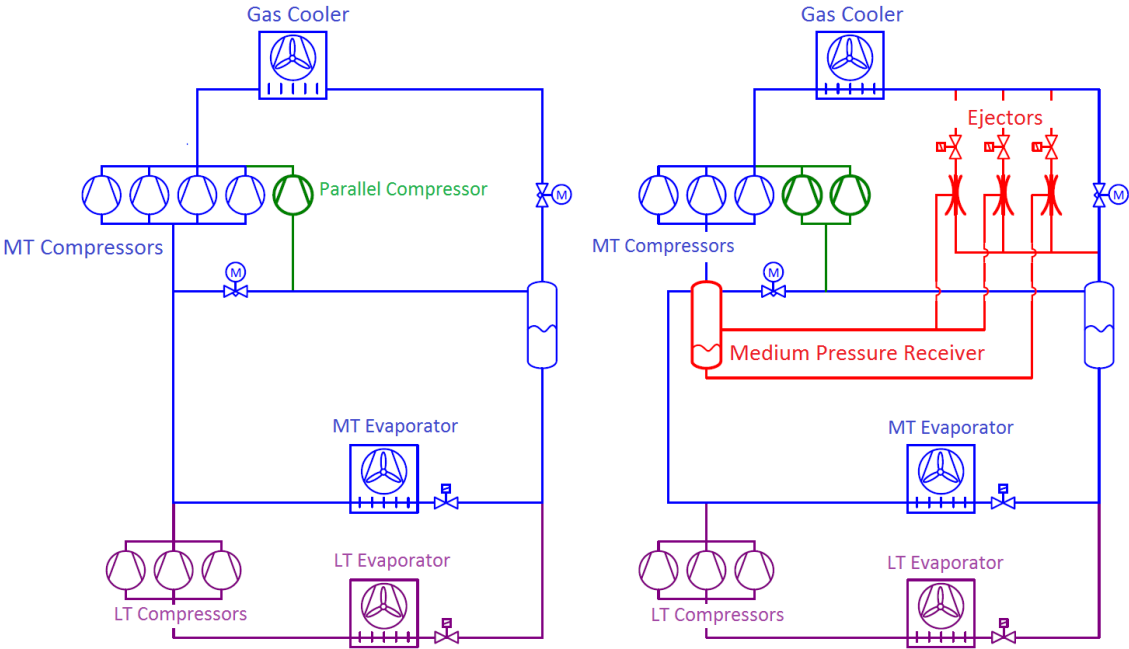
Figure 3.7: Integration of two vapour and one liquid ejectors to the existed CO_2 transcritical parallel compression refrigeration system in Migros Bulle supermarket. Adapted and modified from Wiedenmann et al. (2014).

3.4 Literature Review Summary

In order to improve energy performance of commercial refrigeration system, the two-phase ejector indicates many benefits to use it in CO_2 refrigeration system. In recent times, the most common R744 refrigeration system applied in supermarket is the R744 transcritical parallel compression system. Therefore, integration of the ejectors to support parallel compression can improve the energy performance of the system. Applying multi-ejector module in CO_2 transcritical refrigeration system could reduce the power consumption of overall system in supermarket as has already been proved by Hafner et al. (2014), Wiedenmann et al. (2014). As a result of high-efficiency work, the CO_2 refrigeration system equipped with the ejector pack can be much more competitive solution in throughout climate regions including especially in cold climates, hot climates or even tropical countries and desert areas (Sumeru et al., 2012). However, there are still small number of papers interested in the modern R744 transcritical refrigeration system equipped with ejector expansion module. Hence, the study on the ejector technology in commercial CO_2 refrigeration system is required.

4 Theory

4.1 Properties of CO$_2$

Present refrigeration systems in supermarkets have CO_2 as a refrigerant due to limit of global warming and ozone depletion effects. Properties of carbon dioxide are well known, therefore analysis of the system performance can be investigated. Table 4.1 presents a comparison of CO_2, or R744, properties and characteristics with some other refrigerants. Carbon dioxide is non-flammability, non-toxicity, and non-ozone depletion natural refrigerant. The high value of volumetric refrigeration capacity (VRC) for R744 forces to compress working fluid as a vapor. Critical point of CO_2, has a temperature of 31.1 ^{o}C, and a pressure of 73.8 bar. The heat transfer cannot be rejected by using condensation process as in the standard vapour compression cycle, when the ambient temperature is above the critical temperature of CO_2. Therefore, R744 vapour compression system has to work in transcritical mode for the ambient temperature higher than critical temperature of carbon dioxide.

Table 4.1: Characteristics of common refrigerants. Adapted and modified from Kim et al. (2004).

	Unit	R-12	R-22	R-134a	R-717	R-290	R-744
ODP/GWP[2]	-	1/8500	0.05/1700	0/1300	0/0	0/3	0/1
Flammability/toxicity	-	N/N	N/N	N/N	Y/Y	Y/N	N/N
Molecular mass	kg/kmol	120.9	86.5	102.0	17.0	44.1	44.0
Critical pressure	MPa	4.11	4.97	4.07	11.42	4.25	7.38
Critical temperature	^{o}C	112.0	96.0	101.1	133.0	96.7	31.1
Volumetric refrigeration capacity[3]	kJ/m^3	2734	4356	2868	4382	3907	22545

---

[2] ODP-Ozone depletion potential, GWP- Global warming potential.
[3] Volumetric Refrigeration Capacity at 0 ^{o}C.

4.2 Vapour Compression Cycle

In a supermarket the refrigeration system is designed to achieve established temperature in chiller cabinets and freezer cabinets. Hence, the standard vapour compression cycle, represented the conventional refrigeration cycle, is divided into three pressure level: discharge high-pressure level, medium-temperature pressure level, and low-temperature pressure level. Figure 4.1 shows layout, T-s and P-h diagrams of R744 standard vapour compression cycle with mentioned pressure levels. Both diagrams show work of refrigeration cycle in subcritical mode and the cycle can be divided into four essential thermodynamic processes: compression (process 1-2), condensation, or cooling the supercritical working fluid in transcritical mode (2-3), throttling (3-4, 3-6 and 5-1) and vaporization (4-5 and 6-1).

In evaporators, liquid phase of CO_2, at respectively low temperature, absorbs heat from space of cabinets. As an effect of absorption, the refrigerant boils at constant temperature and pressure. During vaporization, CO_2 is working in two-phase flow region until it turns into saturated vapour outside the evaporator. In real refrigeration system, the vapour is superheated and secured by additional liquid receiver for a safety of compressors. The compressor pulls out CO_2 away from the evaporator and compresses to a higher pressure level, which depends on the refrigerant parameters outside the condenser (in subcritical mode), or gas cooler (in transcritical mode). In subcritical cycle, the specific enthalpy outside the condenser is a function of temperature, as a result of condensation process at constant pressure. At the supercritical high-side conditions, the specific enthalpy is dependent on temperature and pressure (Kim et al., 2004). Before the refrigerant enters to the evaporators, the high value of pressure has to be reduced to required pressure levels in medium-temperature and low-temperature evaporators, which is controlled by expansion valve. In the expansion valve, the pressure is expanded by viscous effect and by acceleration, thereby the CO_2 is leaving it as a two-phase mixture. Throttling process gains large thermodynamically losses due to increase of an entropy at constant specific enthalpy, which is shown on T-s diagram in Figure 4.1.
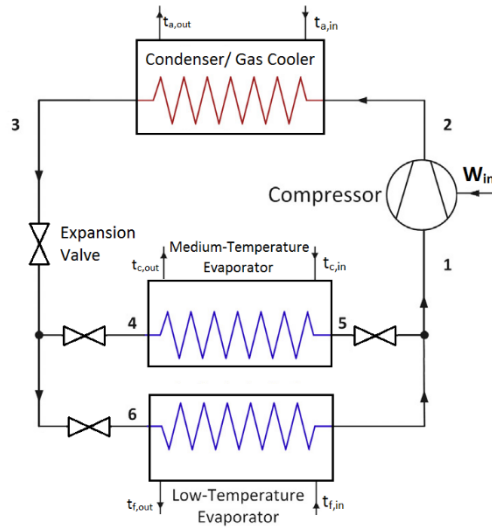
(a) Layout of Standard Vapour Compression Cycle
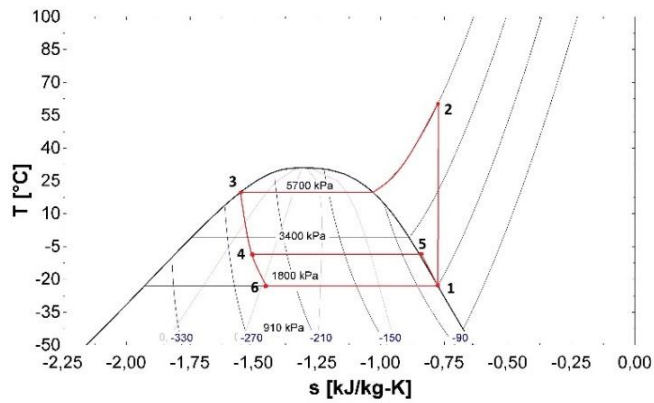
(b) Temperature-specific entropy diagram
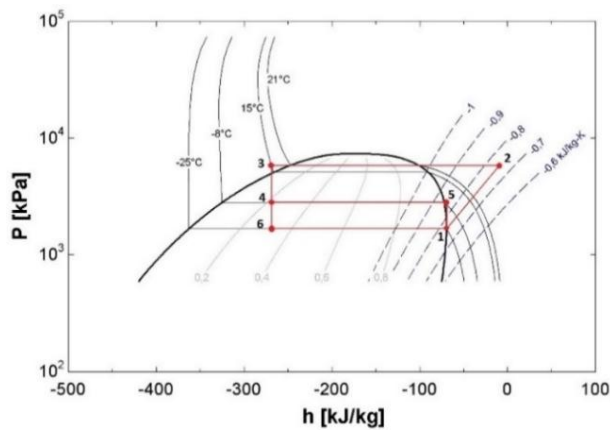
(c) Pressure-specific enthalpy diagram

Figure 4.1: Standard Vapour Compression Cycle with two evaporation temperatures. Adapted and modified from Lawrence and Elbel (2013).

Large irreversible losses in expansion valves, in particular for high pressure ratio in transcritical cycle, force to extending standard vapour compression cycle, by using additional liquid receiver after high-pressure expansion valve, on a pressure level above pressure in MT evaporator. The liquid phase of carbon dioxide from separator is throttled and it flows through evaporator, which increases the specific refrigeration capacity. The saturated vapor, named as flash gas, has more solutions. The flash gas can be throttled to evaporator pressure level, or it can be directly compressed to discharge pressure level, by section of parallel compressors. Integration of the liquid receiver divides pressure reduction in high-pressure expansion valve, which decreases thermodynamic losses of the system.

4.3 First Law Analysis

Discharge pressure in R744 vapour compression cycle is maintained by the compressor work, which has to be supplied by external sources. Performance of the system based on first law of thermodynamics is presented as a coefficient of performance (COP), which is a ratio between absorbed, or rejected heat transfer rate by refrigerant in heat exchanger, into internal power of a compressor. COP for cooling mode of standard vapour compression cycle with one evaporator is described as:

$$COP_{cooling} = \frac{Q_{ev}}{N_i} = \frac{h_{ev,out} - h_{ev,in}}{h_{comp,out} - h_{comp,in}} \tag{4.1}$$

where $\dot{Q}_{ev}$ is a refrigeration capacity in kW, N_i is an internal power of the compressor in kW. The real refrigeration system has many heat exchangers, which damp system performance due to the temperature change associated with pressure drop in heat exchangers. Although for R744 at 0 ^{o}C the temperature change is about 0.01 K for 1 kPa of pressure drop, which is much smaller than other refrigerants (Kim et al., 2004). The coefficient of performance of the present advanced refrigeration systems in supermarket is calculated as a sum of total refrigeration capacity divided by a sum of total electric power of compressors rack:

$$COP_{cooling} = \frac{\sum_{i=1}^{n} Q_{ev,i}}{\sum_{i=1}^{n} N_{el,i}} \tag{4.2}$$

The electric power of compressor presents overall power utilized in refrigeration system, because conversion of electrical power into compression energy involves some energy losses.

Therefore, the compressor has to be characterized by efficiencies describing the quality of compression:

$$N_i = N_{el} \cdot \eta_{me} \tag{4.3}$$

$$\eta_{is} = \frac{N_{is}}{N_i} = \frac{h_{out,isen} - h_{in}}{h_{out} - h_{in}} \tag{4.4}$$

where in Eq. (4.3) η_{em} is the electric-mechanical motor efficiency, in Eq. (4.4) η_{is} is the isentropic efficiency due to irreversible adiabatic process of compression, N_{is} is an isentropic internal power of the compressor. In experimental analysis presented below, the evaluation of compressor exit temperature is impossible due to fact that the temperature sensor could not be installed directly on the discharge side of the compressor. As a result of the missing temperature, the compressor can be characterized only by compressor efficiency, which is calculated as:

$$\eta_{comp} = \frac{N_{is}}{N_{el}} = \frac{\dot{m}_{CO_2} \cdot (h_{out,isen} - h_{in})}{N_{el}} \tag{4.5}$$

The mass flow rate of carbon dioxide $\dot{m}_{CO_2}$ that flows through a compressor, can be either measured by mass flow meter or calculated using volumetric efficiency. According to Lambers (2008), volumetric efficiency is a ratio of the real inlet gas mass flow to the inlet gas mass flow in reference process and it is defined as:

$$\eta_{vol} = \frac{\dot{m}_{CO_2}}{\dot{m}_{CO_2,ref}} \tag{4.6}$$

The reference mass flow of R744 can be defined as positive displacement of compressor multiplied by the density at the CO_2 suction parameters. The positive displacement compressor is a device that confines successively volumes of fluid within a closed space with the pressure of the fluid is increased as the volume of the closed space is decreased (Mobley, 1999). Therefore, the positive displacement can be defined as the most possible volume flow rate of the fluid that can be discharged in the selected compressor. The positive displacement is the parameter of the individual compressor and the information about the value of displacement is delivered by the supplier.

$$\dot{m}_{CO_2,ref} = \dot{V}_{displ} \cdot \rho_{CO_2}(T_{suction}, p_{suction}) \tag{4.7}$$

Data about working of compressor, electric power consumption, refrigeration capacity of evaporators and losses linked to imperfection of processes allow to create the performance characteristic of refrigeration system.

In the subcritical mode value of COP decreases during increasing of the discharge pressure. In transcritical cycle, a maximum value of COP depends on the high-side pressure and the gas cooler exit temperature, which is shown in Figure 4.2 (Kim et al., 2004). The isotherm above the critical temperature has a specific shape, where above the critical pressure, it is gliding. The optimal gas cooler pressure is reached, when the partial derivative of COP with respect to the gas cooler pressure equals zero for the set gas cooler exit temperature (Liao et al., 2000):

$$\left(\frac{\partial COP}{\partial P_{GC}}\right)_{P_{gc}=P_{opt}} = 0 \qquad (4.8)$$

As a result of the gliding temperature, there exists a pressure level, for which the drop of specific enthalpy at the exit of gas cooler is equal to the same as the gain of specific enthalpy at the exit of compressor. The drop of specific enthalpy at the exit of gas cooler is expressed as:

$$\Delta h_{gc,out} = h'_{gc,out}\big(T_{gc,out}, P_{gc} + \Delta P\big) - h^0_{gc,out}\big(T_{gc,out}, P_{gc}\big) \qquad (4.9)$$

where $h'_{gc,out}$ is the exit gas cooler specific enthalpy with increased refrigeration output in kJ kg^{-1}, $h^0_{gc,out}$ is the exit gas cooler specific enthalpy without increased refrigeration output in kJ kg^{-1}.

The gain of specific enthalpy at the exit of compressor is expressed as:

$$\Delta h_{comp,out} = h'_{comp,out}\big(s_{comp,out}, P_{gc} + \Delta P\big) - h^0_{comp,out}\big(s_{comp,out}, P_{gc}\big) \qquad (4.10)$$

where $h'_{comp,out}$ is the exit compressor specific enthalpy with increased refrigeration output in kJ kg^{-1}, $h^0_{comp,out}$ is the exit compressor specific enthalpy without increased refrigeration output in kJ kg^{-1}, $s_{comp,out}$ is the constant specific entropy of the compressor in kJ kg^{-1}K^{-1}.

In that case, COP of the cycle has a maximum value:

$$COP_{cooling,max} = \frac{h_{ev,out} - (h_{ev,in} - \Delta h_{gc,out})}{(h_{comp,out} + \Delta h_{comp,out}) - h_{comp,in}} \Leftrightarrow \Delta h_{gc,out} = \Delta h_{comp,out} \qquad (4.11)$$
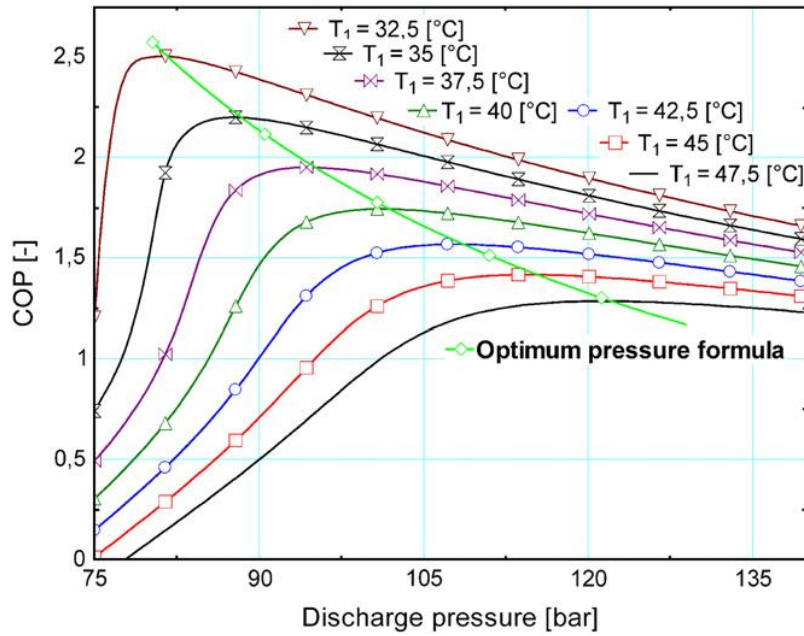
Figure 4.2: COP-discharge pressure diagram at different gas cooler exit temperature. Adapted from Sawalha (2008).

The optimal parameters of CO_2 at outside the gas cooler ensure maximum performance of the refrigeration system.

COP is a common rate used to compare performances of each refrigeration systems. To evaluate the performance result after introducing modification can be expressed by COP improvement defined as the difference between COP after and before (baseline) system modification divided by COP of the baseline system.

$$COP_{improvement} = \frac{COP_{modification} - COP_{baseline}}{COP_{baseline}} \cdot 100\% \qquad (4.12)$$

However, COP does not give any information about maximum of system performance and how large are the losses in each component. Exergy balance can show real cooling efficiency of the refrigeration system. Thereby, comparison of two refrigeration systems in supermarket based on the exergy analysis need to be done as well.

4.4 Second Law Analysis

The first law analysis delivers information of the refrigeration system performance and losses following with irreversibility of processes in each component. In exergy analysis of the refrigeration system, the important information is where and how much the system

performance is degraded (Yumrutaş et al., 2002). Carnot cycle has a maximum performance as a refrigeration system, because it consists of two isentropic processes and two isothermal processes. According to Lawrence and Elbel (2013), COP of the Carnot cooling cycle can be evaluated as the ratio of the absolute evaporation temperature to the difference between condensation temperature and evaporation temperature.

$$COP_{Carnot} = \frac{T_{evap}}{T_{cond} - T_{evap}} \tag{4.13}$$

where T_{evap} is a saturated evaporation temperature in K, T_{cond} is a condensation temperature in K. The second law efficiency of refrigeration system, or the exergy efficiency, can be defined as the COP of refrigeration system divided by the COP of Carnot cooling cycle.

$$\eta_{ex} = \frac{COP}{COP_{Carnot}} \tag{4.14}$$

The definition of exergy efficiency presented in (4.14) evaluates real cooling ability of refrigeration systems, but it does not give an information about decomposed exergy losses in the cycle. Energy balance and exergy balance of each component need to be done. Exergy balance equation is defined as:

$$E_{in} = E_{out} + \sum I_i \tag{4.15}$$

where $\sum I_i$ is a sum of irreversibility of the system components in kW.

Ahamed et al. (2011) presents energy and exergy balance for the standard vapour compression cycle for following assumptions:

- Analysis is conducted for steady-state conditions.
- Pressure drop in pipelines is neglected.
- Heat losses and heat gains in whole system are not considered.
- Potential and kinetic energy is not considered.
- Exergy losses are not considered.

Specific exergy in any state is calculated as:

$$\psi_i = (h_i - h_{amb}) - T_{amb} \cdot (s_i - s_{amb}) \tag{4.16}$$

where ψ_i is a specific exergy in kJ kg^{-1}, h_{amb} is a specific enthalpy in ambient conditions in kJ kg^{-1}, T_{amb} is an ambient temperature in K, s_i is a specific entropy in kJ kg^{-1}K^{-1}. According to Fang et al. (2005), exergy of amount of heat q may be expressed as the exergy increment:

$$\psi_{incr} = q \cdot \left(1 - \frac{T_{amb}}{T}\right) \tag{4.17}$$

where T is the temperature, for which the environment absorbs (heat sink temperature), or rejects (heat source temperature) the amount of heat. During experimental investigation, presented in this thesis, the temperature T of heat source, or heat sink changed from T_1 to T_2. According to Fang et al. (2005), the exergy increment can be defined as:

$$\psi_{incr} = q \cdot \left| 1 - \frac{T_{amb} \cdot \ln\left(\frac{T_1}{T_2}\right)}{(T_1 - T_2)} \right| \tag{4.18}$$

The positive sign of the exergy increment is set due to negative sign of the removed heat from the evaporator, where the temperature of refrigerant is below the ambient temperature ($T < T_{amb}$).

Energy balance equations and exergy destruction equations of each specific component are presented below, respectively.

- For evaporator:

$$\dot{Q}_{ev} = \dot{m}_{CO_2} \cdot \left(h_{ev,out} - h_{ev,in}\right) \tag{4.19}$$

$$I_{ev} = \dot{m}_{CO_2} \cdot \left(\psi_{ev,out} - \psi_{ev,in}\right) + \dot{m}_{CO_2} \cdot \psi_{ev,incr} \tag{4.20}$$

- For condenser/ gas cooler:

$$\dot{Q}_{cond} = \dot{m}_{CO_2} \cdot \left(h_{cond,in} - h_{cond,out}\right) \tag{4.21}$$

$$I_{cond} = \dot{m}_{CO_2} \cdot \left(\psi_{cond,in} - \psi_{cond,out}\right) + \dot{m}_{CO_2} \cdot \psi_{gc,incr} \tag{4.22}$$

- For compressor:

$$N_{el} \cdot \eta_{me} = \dot{m}_{CO_2} \cdot \left(h_{comp,out} - h_{comp,in}\right) \tag{4.23}$$

$$I_{comp} = \dot{m}_{CO_2} \cdot \left(\psi_{comp,in} - \psi_{comp,out}\right) + N_{el} \tag{4.24}$$

- For expansion valve

$$\dot{m}_{CO_2} \cdot h_{cond,out} = \dot{m}_{CO_2} \cdot h_{ev,in} \tag{4.25}$$

$$I_{valve} = \dot{m}_{CO_2} \cdot \left(\psi_{ev,in} - \psi_{cond,out}\right) \tag{4.26}$$

Total destruction of refrigeration system is a sum of exergy destruction of each components:

$$I_{total} = \sum I_i = I_{ev} + I_{cond} + I_{comp} + I_{valve} \tag{4.27}$$

Thereby the second law efficiency can be expressed as:

$$\eta_{ex} = \frac{E_{out}}{E_{in}} = \frac{E_{in} - I_{total}}{E_{in}} = 1 - \frac{I_{total}}{E_{in}} \tag{4.28}$$

Set of energy and exergy balance equations presented above allows for identification of the component with the largest irreversibility. According to Ahamed et al. (2011), the largest irreversibility has condenser followed by compressor, expansion valve and evaporator, respectively. Temperature of evaporating and condensing strongly influences the value of COP, the second law efficiency, and the exergy losses (Yumrutaş et al., 2002). Evaluation of exergy destruction in expansion valve proves that some potential of work can be recovered to improve the exergy efficiency and the COP of the refrigeration system. Influence of modifications in refrigeration system on the exergy efficiency value should be calculated similarly as in case of COP, by using exergy efficiency improvement:

$$\eta_{ex,improvement} = \frac{\eta_{ex,modification} - \eta_{ex,baseline}}{\eta_{ex,baseline}} \cdot 100\% \tag{4.29}$$

4.5 The Two-phase Ejector Characteristics

4.5.1 Working Principles

The ejector is a simple device without rotational pieces. Figure 4.3 shows simple geometry of an ejector in axially section, with velocity and pressure profiles along the ejector. Generally, three principles phenomena can be distinguished in an ejector:

- Supersonic stream occurring in converging-diverging motive nozzle (A).
- The momentum conservation between motive and entrainment stream (B) in the mixing chamber.

- Conversion of the kinetic energy of the mixed fluid into pressure energy (C).

The motive fluid from high-pressure collector gets accelerates due to the Venturi-effect in converging-diverging nozzle. Thereby, in throat, speed of the motive stream is equal to speed of the sound and behind the throat the fluid flows in supersonic condition. The throat has the smallest dimension in the ejector. Therefore, the maximum mass flow rate of the motive fluid flowing through the ejector can be expressed as:

$$\dot{m}_{motive,max} = \frac{\pi \cdot d^2_{throat}}{4} \cdot w \cdot \rho \qquad (4.30)$$

where w is a speed of sound of the motive fluid in m s^{-1}, d is a throat diameter in m, ρ is a density of the motive fluid in a throat in kg m^{-3}. The high-pressure motive stream expands to the mixing-chamber pressure level and increases the kinematic energy of the fluid due to supersonic flow. When the pressure level in mixing chamber is lower than the low-pressure level of suction fluid, the motive stream entrains the low-pressure stream. Both streams are mixing as a result of many complicated phenomena associated with the momentum transfer. Mixed fluid flows through diverging diffuser, where kinematic energy is conversed into pressure energy due to the turbulence flow. Therefore, stream outside the ejector has a higher pressure than low-pressure suction fluid.
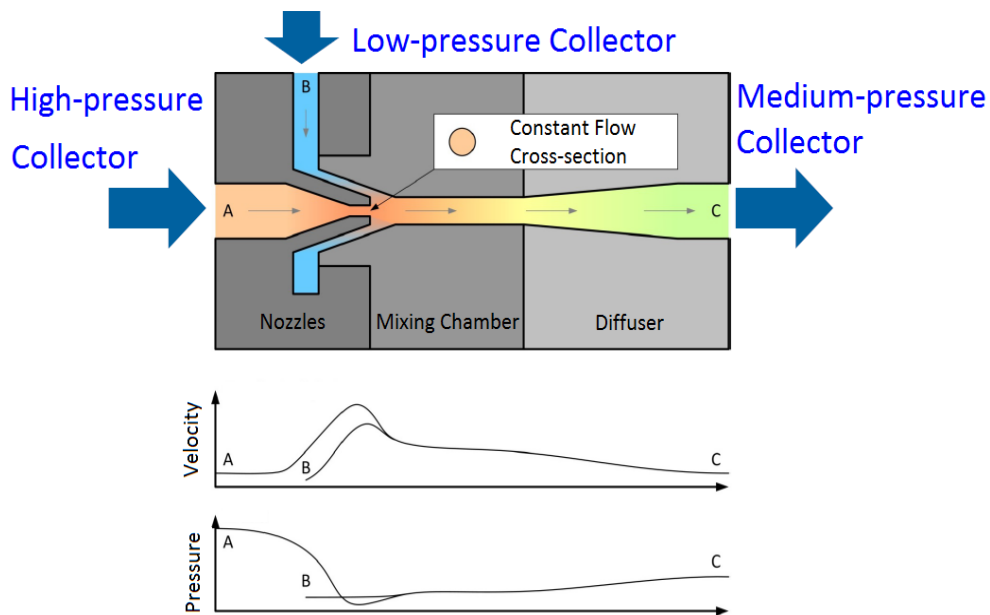
Figure 4.3: Conceptual drawing of the R744 two-phase ejector. Velocity and pressure profiles of motive and suction stream along the ejector. Adapted and modified from Schönenberger (2014).

4.5.2 Ejector Parameters

The ejector can entrain the low-pressure fluid until the pressure in mixing chamber is lower than the pressure of suction fluid. Entrainment depends on the difference between medium-pressure level and the low-pressure level, which can be presented by two ejector parameters. Pressure ratio is a division of the outlet pressure level to the suction nozzle pressure level.

$$\Pi = \frac{P_{outlet}}{P_{suction}} \tag{4.31}$$

Pressure lift is calculated as a difference between both pressure levels.

$$p_{lift} = p_{outlet} - p_{suction} \tag{4.32}$$

Besides foregoing parameters, an information about the mass flow rate of the motive and suction fluids is needed to evaluate of the ejector work and ability to pumping of the low-pressure stream. The mass entrainment ratio shows the ratio between mass flow rate of the entrainment fluid and mass flow rate of the motive fluid, which is expressed as:

$$\phi = \frac{\dot{m}_{suction}}{\dot{m}_{motive}} \tag{4.33}$$

In this thesis the ejector efficiency is defined as the ejector efficiency definition proposed by Elbel and Hrnjak (2008). The one of the benefit to use foregoing definition is that it can be applied for an experimental investigation, because it avoids the measured static pressure in the mixing chamber. The ejector efficiency is the amount of expansion work recovered divided by the maximum potential to recover expansion work rate by the ejector.

$$\eta_{ejector} = \frac{\dot{W}_{rec}}{\dot{W}_{max,rec}} \tag{4.34}$$

where $\dot{W}_{rec}$ is an expansion work rate recovered in kW, $\dot{W}_{max,rec}$ is a maximum potential to recover expansion work rate in kW. Figure 4.4 illustrates expansion of motive fluid and compression of suction fluid as a recovery potential of R744 two-phase ejector work. The maximum work, which can be recovered by an ejector, is a difference of enthalpies from state A, which represents throttling process to state B, which represents isentropic expansion process on the same outlet pressure level.

$$\dot{W}_{max,rec} = \dot{m}_{motive} \cdot (h_A - h_B) \tag{4.35}$$

Work rate recovered is expressed as an isentropic compression of the suction stream with respect to its surroundings (Elbel and Hrnjak, 2008). In Figure 4.4, the amount of work rate recovered is shown as a change of the entrainment fluid from state D to state C, calculated as:

$$\dot{W}_{rec} = \dot{m}_{suction} \cdot (h_C - h_D) \qquad (4.36)$$

Finally, the ejector efficiency can be expressed as:

$$\eta_{ejector} = \frac{\dot{m}_{suction}}{\dot{m}_{motive}} \cdot \frac{(h_C - h_D)}{(h_A - h_B)} = \phi \cdot \frac{(h_C - h_D)}{(h_A - h_B)} \qquad (4.37)$$
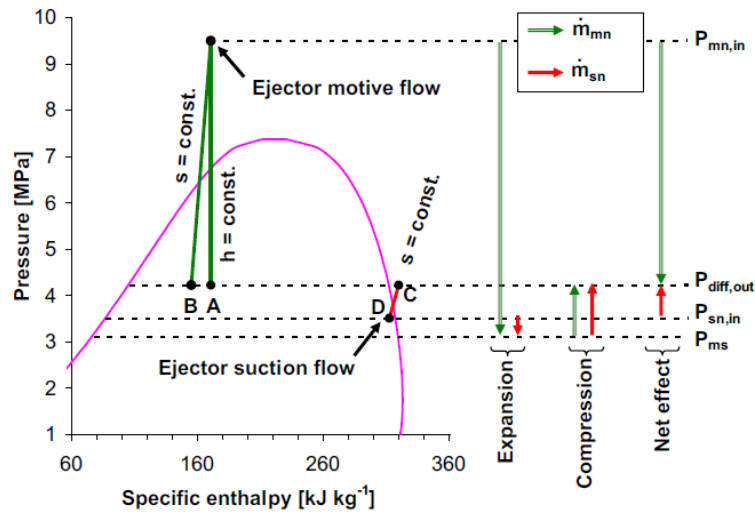
Figure 4.4: Pressure- specific enthalpy diagram of expansion and compression of motive and suction fluid in R744 two-phase ejector. Adapted from Elbel (2011).

5 Experimental Method

5.1 Description of the Test Facility

The R744 multi-ejector refrigeration test rig was manufactured by Enex Company in collaboration with Danfoss Company and SINTEF Energy Research. The test facility is divided into three individual modules: R744 unit with oil management circuit, glycol module and the electrical cabinet. Figure 5.1 shows the view of the experimental test facility, where it can be seen the rack of compressors and table with main pressure gauges.

Figure 5.1:   The R744 Multi-ejector refrigeration test rig.

Figure 5.2 illustrates the pipeline and instrumentation diagram (P&ID) of R744 loop of the test rig, which includes all main components. The system is filling in the pressure receiver tank (liquid separator in Figure 5.2), where the liquid phase of CO_2 flows down on the bottom of the tank, but the vapor phase of CO_2 is created in the top of the tank. The liquid level in liquid separator depends of the pressure level due to constant density of CO_2. Therefore,

pressure level of the receiver can be regulated. The liquid separator has to deliver saturated liquid to the evaporator.

For the experimental investigation presented in this thesis, the peak-load evaporator was not utilized, because the base-load evaporator had enough refrigeration capacity for set loads. The multi-ejector test rig has only medium temperature evaporator in order to simplify the system. The pressure level in the evaporator is controlled by the expansion valve. The suction accumulator tank (liquid receiver in Figure 5.2) delivers saturated, or superheated vapour to the compressor and to the suction side of the vapor ejectors (VEJ) in multi-ejector block. In addition, it can supply liquid phase of CO_2 to the suction side of liquid ejector (LEJ), which enables to utilize the evaporator in flooded mode. From the thermodynamic point of view the decrease of the evaporation temperature in the flooded mode improves the performance of the system. However, during the experimental investigation the liquid ejectors were omitted and the evaporator had set the superheat in order to investigate the system performance improvement of the R744 vapour compression system with the vapour ejectors.

The vapor phase of CO_2 from suction accumulator is delivered to medium temperature compressor, where it is compressed to set discharge pressure. The compressor rack consists of medium temperature compressor and two parallel compressors that compressed the gas from the liquid separator (denoted also as the pressure receiver tank or the flash tank). The system has a flash valve to throttle the vapor from the pressure receiver tank if the parallel compressors do not have to be utilized. The pressure level in the receiver is governed by either parallel compressors or flash valve. The vapor phase of CO_2 from the both receivers flows through the additional internal heat exchangers and absorbs the heat from the high-pressure CO_2, after the gas coolers section, in order to safety of the compressors. After the compression, stream flows through the two gas cooler stages. The high-pressure of CO_2 behind the gas cooler section can be reduced either by high-pressure electronic expansion valve (HPV), or by the multi-ejector pack, with assistance of HPV. During the investigation, the largest vapour ejector number 4 (VEJ4) was omitted due to too high capacity of the ejector module. The multi-ejector block is described in details in section 5.2.5.

In the CO_2 loop some amount of lubricant penetrates to the cycle. Therefore, the test rig has a separate loop of lubricant. The oil receiving loop contains the high-pressure separator, behind the compressor rack, and the receivers installed together with the CO_2 tanks. Integration of

lubricant separators results in the heat transfer improvement in heat exchangers and the minimization of an annual leakage of the lubricant (Wang et al., 2012).
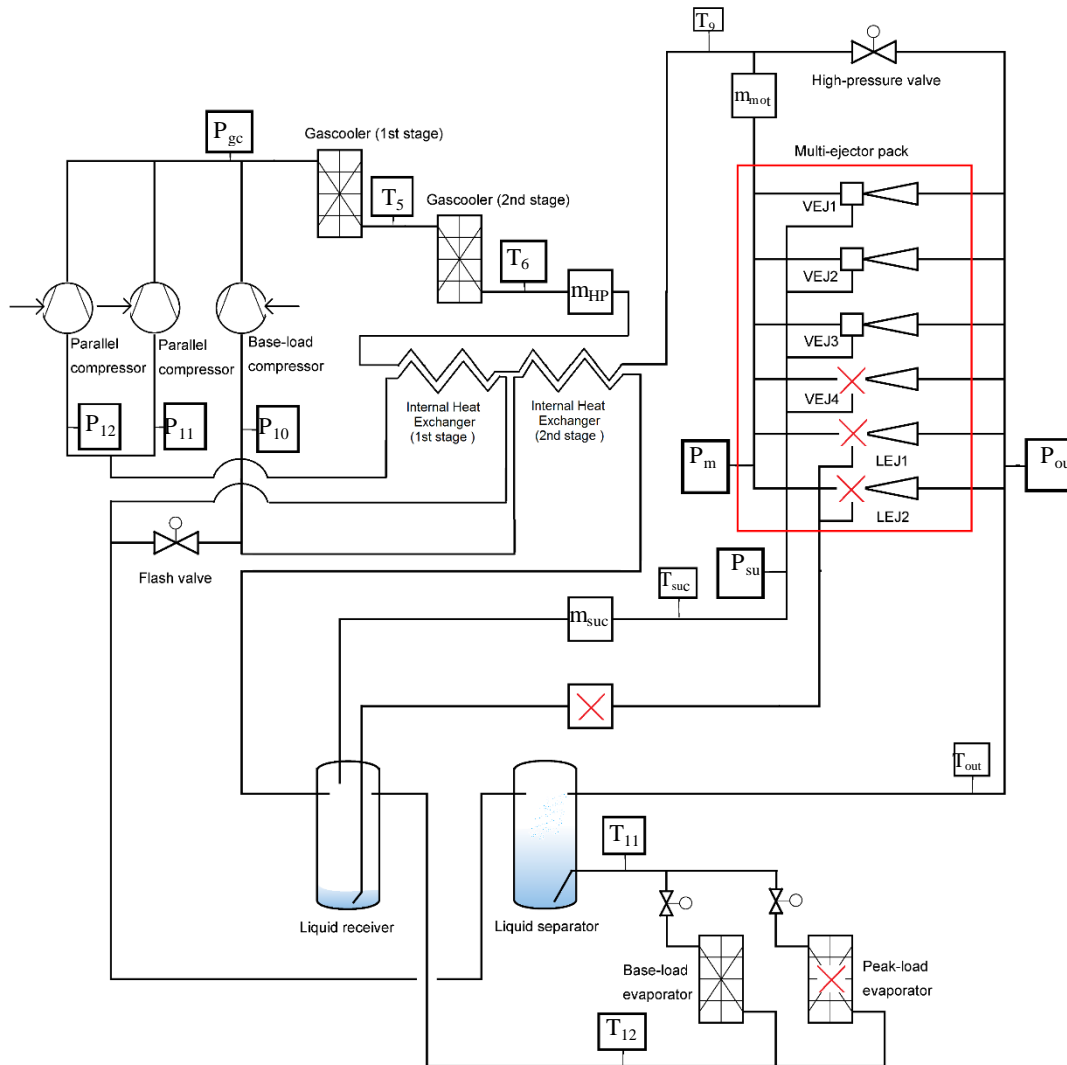
Figure 5.2: P&ID diagram of CO_2 loop in R744 Multi-ejector Refrigeration Test Rig. During the experimental investigation, the peak-load evaporator, the vapour ejector VEJ4 and both liquid ejector were omitted.

In order to provide cooling and heating in the gas cooler section and in the evaporator, the test facility has got an auxiliary glycol loop and additional cooling water loop. Simplified schema of auxiliary loops is shown in Figure 5.3. The glycol unit consists of the glycol tank and two separated evaporator and gas cooler loops, respectively. Aim of both coolant loops was to absorb the heat from first stage of the gas cooler and reject the heat in evaporator. The glycol is delivered to heat exchangers by two pumps manufactured by Grundfos. The cooling water

cycle decreases the temperature of CO_2 in the second stage of the gas cooler until R744 expands to pressure receiver tank. Therefore, the exit gas cooler temperature of R744 is regulated by mass flow rate of cooling water. The glycol stream flowed through the gas cooler can be cooled by additional cooling water network loop, but for presented investigations was not utilized.

Figure 5.3: P&ID diagram of auxiliary loops in R744 Multi-ejector Refrigeration Test Rig. During the experimental investigation, the peak-load evaporator and additional cooling water network were omitted.

5.2 Components description

5.2.1 The Rack of Compressors

Three semi-hermetic, reciprocating compressors, manufactured by Dorin, are incorporated to the test rig and are shown in Figure 5.4. Each compressor alters the capacity depending on the

suction side parameters and the operating conditions. Based on Dorin documentation, the compressor models are named as:

- Base-load compressor - Dorin CD1400H
- Parallel compressor #1 – Dorin CD1000H
- Parallel compressor #2 – Dorin CD360H

Figure 5.4:   The rack of the piston-type R744 compressors. On the left: base-load Dorin CD1400H, parallel #1 Dorin CD1000H, and parallel #2 Dorin CD380H.

In order to regulate capacity of each compressor work by changing the frequency, the electric power is supplied by inverters manufactured by Danfoss. Unfortunately, in the test facility the mass flow rate meters were installed to measure the summarized CO_2 mass flow of the rack of the compressors and the motive stream, and the suction stream in the multi-ejector module. Hence, the evaluation of the CO_2 mass flow rate in each individual compressor was performed by the volumetric efficiency and the compressor efficiency calculation. Compressor supplier Dorin provides polynomial functions, to calculate R744 mass flow rate and electric power consumption for each compressor working at nominal frequency of 50 Hz.

$$y = c_1 + c_2 \cdot t_0 + c_3 \cdot p_c + c_4 \cdot t_0^2 + c_5 \cdot t_0 \cdot p_c + c_6 \cdot p_c^2 + c_7 \cdot t_0^3 + c_8 \cdot p_c \cdot$$
$$t_0^2 + c_9 \cdot t_0 \cdot p_c^2 + c_{10} \cdot p_c^3 \tag{5.1}$$

where y is the CO_2 mass flow rate and power consumption, t_0 is an evaporating temperature in $^{\circ}C$ and p_c is a discharge pressure in bar. Values of the constants c_i are specified for each compressor and given by the Dorin supplier. The volumetric and compressor efficiency for the nominal frequency of 50 Hz was calculated by using equations (4.5) and (4.6). To calculate new values of compressor and volumetric efficiencies, the approximation functions for corrections resulting from alterations in the frequency and the evaporator temperature have been used, based on the manufacturer data (received for internal use only). Figure 5.5 presents the results of auxiliary tests performed in-house for experimental estimation of the volumetric and compressor efficiency correction for the various frequency than the nominal 50 Hz of the base-load compressor Dorin CD 1400H. In addition, the discrepancy between the experimental results and the correction given from Dorin supplier has been shown. The maximum value of the relative error defined as a difference of the experimental and calculated results divided by the experimental result is of 6% for the volumetric efficiency and 4.9% for the compressor efficiency, respectively. The table with a set of the experimental and approximation results is presented in Appendix B.
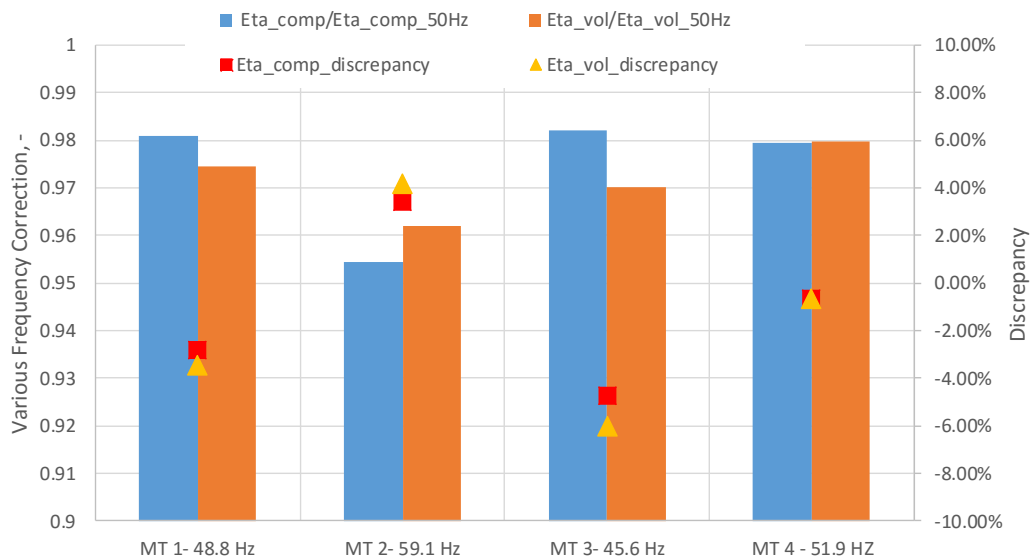
Figure 5.5:   Experimental investigation of the various frequency correction for the volumetric and compressor efficiency for the base-load compressor Dorin CD1400H together with the discrepancy from the Dorin various frequency correction.

5.2.2 Heat Exchanger

The heat exchangers that have been utilized in the test rig were as follows:

- Gas Cooler: Brazed plate heat exchanger with 30 plates, SWEP B18Hx100 as the first-stage gas cooler. Brazed plate heat exchanger with 20 plates KAORI K095C-30C-NP8M as the second-stage gas cooler.

- Evaporator: Brazed plate heat exchanger with 30 plates, SWEP B16DWHx100. The reference superheat of the evaporator, set by the Danfoss controller system, was of 8 K.

- Two internal counterflow heat exchangers to provide pure vapour phase of CO_2 in the compressors.

5.2.3 Tank

The test rig was equipped with two pressure receivers in CO_2 loop, oil tank and glycol tank:

- Liquid receiver tank: 39-litre Frigomec pressure vessel.
- Suction accumulator tank: 39-litre Frigomec pressure vessel.
- Oil accumulator tank: 21-litre Frigomec pressure vessel.
- Cold glycol tank: 200-litre IMA thermal storage tank.

5.2.4 Valve

The electronic expansion valves applied in the test facility provide a control of the pressure reduction in response to signals sent by the Danfoss system controller:

- Danfoss CCMT8 applicable for CO_2 systems, as the high-pressure valve and flash valve. Maximum working pressure of 140 bar.
- Danfoss CCM20 applicable for CO_2 systems, as the metering valve in base-load evaporator. Maximum working pressure of 90 bar.

Besides the electronic expansion valves, the rig is secured by applied shut-off and safety valves.

5.2.5 The Multi-ejector Block

Figure 5.6 presents the multi-ejector block together with Danfoss controller sensors. The aim of introducing the multi-ejector block to the standard refrigeration facility is improve the system performance, adapting to the operating conditions, which are enforced by supermarket refrigeration system. Therefore, the block has got four fixed vapour ejectors with a linearly variable capacity, designed to ensure the maximum system flexibility. This means that the smallest ejector VEJ1 has two times smaller capacity than the second ejector VEJ2 and eight times smaller than the fourth ejector VEJ4. In this thesis the largest ejector VEJ4 were omitted. The motive, suction, and outlet ports are connected with three independent collectors due to the same outer dimensions of the ejectors. The work of the ejectors is operated by solenoid valves mounted in the motive side, with the possibility fully open or closed valve. As a result of working ejectors regulation, the overall capacity of the multi-ejector block varies from 1x of the base capacity during VEJ1 to 7x of the base capacity when VEJ1, VEJ2 and VEJ3 work simultaneously.
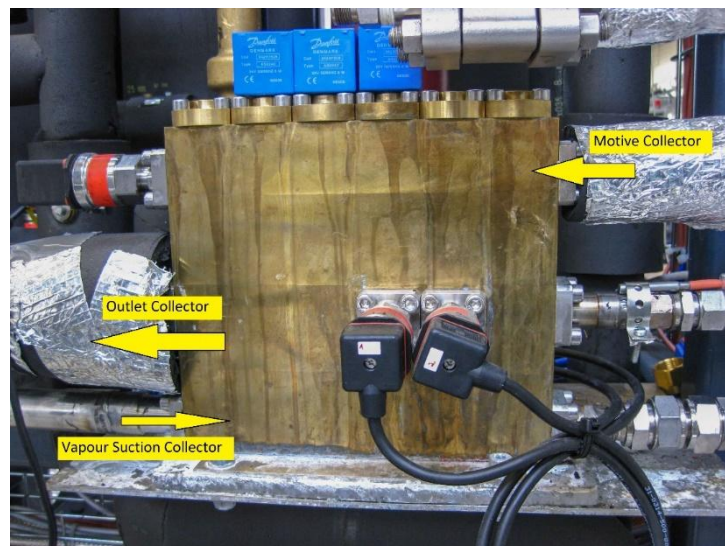
Figure 5.6:   The multi-ejector block with three utilized vapour ejectors.

5.3 Data acquisition equipment and processing

The facility is fully equipped with the pressure and temperature sensors in order to evaluate, monitor, control and safeguard the system. All sensors are connected to the Danfoss control system, thereby the test rig is fully protected during investigation. To calculate the system

performance, besides pressure and temperature sensors, the mass flow meters and the inverters are introduced. Most part of the sensors registered magnitude of pressure and temperature are used to the safeguarding of the system. Therefore, Figure 5.2 and Figure 5.3 present specific measurement to set the operating conditions and to evaluate the work characteristics of compressors, multi-ejector block and evaporator. A description of each sensor is presented below.

- The resistance thermometer Danfoss AKS 21 A PT1000 applied for R744 and glycol loop. The temperature range is from -70 $^{\circ}$C to 180 $^{\circ}$C. The resistance thermometer PT1000 consists of a metal clip made of a platinum, thereby the temperature magnitude is proportional to the value of the electrical resistance conducted along the sensor. When the temperature of fluid is equal to 0 $^{\circ}$C, the sensor gives a resistance of 1000 Ω.

- The piezoelectric transmitter Danfoss AKS 2050 as a gauge pressure applied for R744 loop. The piezoelectric transmitter converts measured pressure to a linear voltage output signal and utilizes a principle of gauge measuring for a pressure reference of 1.013 bar. The pressure ranges depends on the sensor position in the system and the range of either from 0 to 100 bar abs or 0 to 150 bar abs.

- The Coriolis type mass flow meter RHEONIK RHM06 and RHM15 applied for R744 loop and glycol loop, respectively. In the Coriolis mass flow meter the fluid flows through the curved tube, which vibrates. As a result of vibration in tube the phase shift is created. The measure of the mass flow rate is a function of angle of phase shift between the inlet and outlet of the vibrating tube.

- The frequency inverter Danfoss IP55/Type 12 from VLT FC103 Danfoss Refrigeration Drive. The inverter converts the direct current DC into a controlled alternate current with the pulse code modulation (PWM AC) waveform for a controlled variable output to the motor. The frequency ranges from 30 Hz to 60 Hz.

Set of sensors and instrumentation installed to monitor the test facility is presented in Table 5.1. Accuracy of electric power consumption is assumed as for the range of five times larger than the scale of reading, which is of $\pm$ 0.01 kW. For the frequency, the accuracy of reading is

assumed for the same range as scale of reading, which is of ± 0.1 Hz. Accuracies of temperature, pressure and mass flow rate sensors are taken from product datasheets.

Table 5.1: Sensors specifications in the R744 Multi-ejector test rig.

Variable	Transducer	Accuracy	Range
Temperature	Resistance thermometers PT1000	$\pm (0.3+0.005 \cdot t)$ t in $^{\circ}$C	-70 $^{\circ}$C ÷ 180 $^{\circ}$C
Pressure	Piezoelectric transmitter	$\pm (0.3\%)$ of reading	0 ÷ 100 bar abs 0 ÷ 150 bar abs
Mass flow rate	Coriolis type RHM06	$\pm (0.2\%)$ of reading	0 ÷ 20 kg/min
	Coriolis type RHM15	$\pm (0.2\%)$ of reading	0 ÷ 200 kg/min
Electric power consumption	Inverter IP55 Type 12	± 0.05 kW	0 ÷ 20 kW
Frequency	Inverter IP55 Type 12	± 0.1 Hz	30 ÷ 60 Hz

Output signals from all sensors are processes and transmits by the Danfoss control unit to the Danfoss Minilog system. Minilog system is a live recording software installed on the operator computer in order to set specific parameters of the system during carrying out of an experiment. The operator is able to change manually which ejector should be utilize or the system can work in automatic mode, where the system is programmed to use the maximum ability of the ejectors work. In order to improve the visibility of monitoring the key-parameter, the Minilog has a graphical representation of the selected parameters.

When during the assumed time step demands test condition was reached, the steady state operation was determined. The time step was set to nine minutes to ensure a stabilization of the temperatures, mass flow rates and the pressure and minimization of the oscillation of each parameter. Finally, the test point was recorded and data was exported from Minilog to be imported to the Microsoft Excel post processing spreadsheet. The spreadsheet used the Visual Basic environment with REFPROP 8.0 thermodynamic libraries (Lemmon et al., 2013) to automatic the post processing calculations. The equation of state for carbon dioxide was taken from Span and Wagner (1996). The calculation of each test point regarded the COP value, the exergy efficiency, the compressors efficiency for both systems and multi-ejector block parameters for R744 multi-ejector system, i.e. the mass entrainment ratio, ejector efficiency, pressure lift and pressure ratio. In addition, the post processing results contain the uncertainty analysis including both type A and B.

5.4 Uncertainty Analysis

The experimental data have many test points, where every single measurement consists of the real value and the measurement uncertainty. The calculation of the mean value together with uncertainties affected by statistical and instrumentation errors, has to be done to estimate a range, where the real value of measured parameter can be found. Moffat (1988) writes that uncertainty analysis is the process of estimation to define the influence of the effect of uncertainties in the individual measurement on the calculated result. Evaluating and expressing uncertainties given from experimental experiments were carried out based on NIST guideline (Taylor and Kuyatt, 1994). In the test rig each component can be evaluated by statistical methods and the measurement can be estimated by a standard deviation. Therefore, foregoing approach is termed standard uncertainty u_i and is equal to the positive root of the estimated variance u^2_i.

The uncertainty of the test series is evaluated by the statistical analysis for a type A evaluation of standard uncertainty. Based on type A evaluation of standard uncertainty, any valid statistical may be used to treat the data. For the evaluation of experimental test data, for a steady state condition, an estimation of input quantity X_i for n independent recorded measurement is the sample mean and expressed as:

$$x_i = \bar{X}_i = \frac{1}{n} \cdot \sum_{k=1}^{n} X_{i,k} \tag{5.2}$$

The standard uncertainty of type A denoted $u_{A,i}$, associated with input estimate, is the estimated standard deviation of the sample mean:

$$u_A(x_i) = s(\bar{X}_i) = \sqrt{\left[\frac{1}{n \cdot (n-1)} \cdot \sum_{k=1}^{n}(X_{i,k} - \bar{X}_i)^2\right]} \tag{5.3}$$

Besides type A evaluation of standard uncertainty, the evaluation by other means than the statistical analysis, termed as type B evaluation, need to be done. A type B evaluation uses all available relevant information including previous measurement data, manufacturer's specifications, calibration reports, general knowledge and/or experience of the instruments and materials behaviour and property etc.

According to Taylor and Kuyatt (1994) the probability that the estimation of the measurement value lies between lower (a_-) and upper (a_+) limits for the value of the quantity, is equal to 100%. The specific sensor accuracy given from the manufacturer's specification is used to evaluate lower and upper limits of the quantity measurement. Assumed that the value lies within these limits, the probability is modelled by a rectangular distribution. For the type B evaluation of standard uncertainty, based on Taylor and Kuyatt (1994), the best estimate for the quantity is expressed as:

$$x_i = \frac{a_+ + a_-}{2} \tag{5.4}$$

The standard uncertainty of type B denoted u_B:

$$u_B = \frac{a}{\sqrt{3}} = \frac{\frac{a_+ - a_-}{2}}{\sqrt{3}} \tag{5.5}$$

Both types of standard uncertainties describes measurement performance, but to determine uncertainty of the measurement result, the combined standard uncertainty has to be used. According to Moffat (1988) the combined uncertainty of function depending of several independent variables is defined by a room-sum-square method:

$$u_{c,j}(f) = \sqrt{\sum_{i=1}^{n}\left(\frac{\partial f}{\partial x_i} \cdot u_j(x_i)\right)^2} \tag{5.6}$$

Where the partial derivative is formulated as:

$$\frac{\partial f}{\partial x} = \frac{f(x+dx,y) - f(x,y)}{dx} \tag{5.7}$$

In Eq. (5.6) the u_j can be either type A or type B, therefore combined standard uncertainty is divided into type A $u_{c,A}$ and type B $u_{c,B}$. In this work, the foregoing approach has been used to determine the uncertainty for CO_2 thermodynamics properties such as enthalpy h(p,T) and entropy s(p,T) and all external results such as COP, exergy efficiency and compressors efficiencies.

Figure 5.7 shows the relative uncertainty of the combined type A and B standard errors for the COP, conducted for the vapour compression rack with the multi-ejector block. This figure presents the relation between type A and type B errors during the steady state conditions, when the type A uncertainty is either equal or lower than the type B uncertainty. It can be seen that few points for type A relative uncertainty are above the value of type B, but they are lower than 3% .
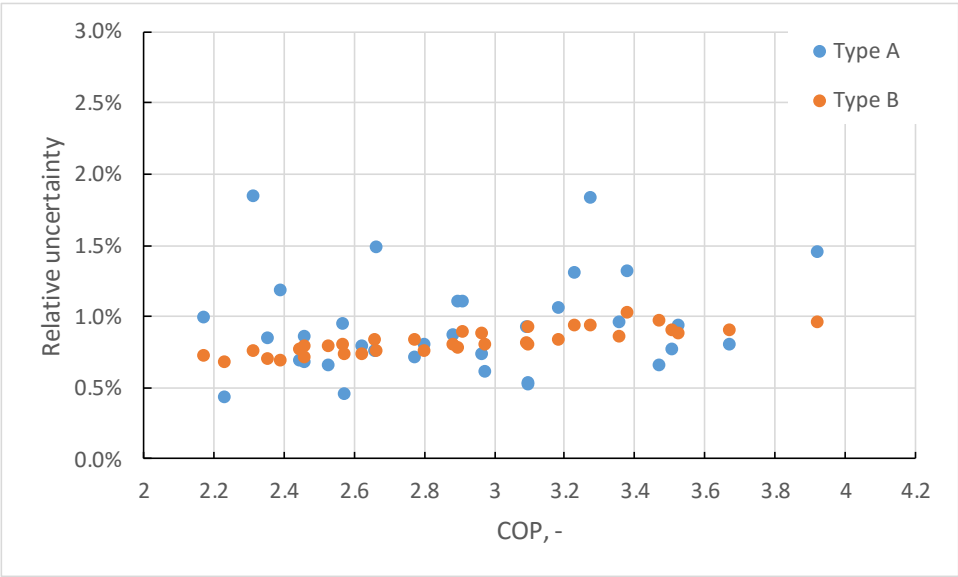
Figure 5.7: Different values for standard combined uncertainty type A and type B for the COP of the vapour compression rack with the multi-ejector block. Points taken from all investigation days.

In this thesis, the results of the experimental investigation were presented together with the standard uncertainty type B due to higher value than the uncertainty type A for all direct measurements.

5.5 Test Campaign

5.5.1 Operating Condition Settings

Aim of this thesis is to present the system performance of a R744 vapour compression system with multi-ejector expansion pack for a standard operating conditions and comparing results with commonly used the R744 refrigeration system in a supermarket. The R744 multi-ejector test rig can be operated in three specific configuration of refrigeration system:

- The R744 transcritical booster system – the vapor fraction of CO_2 from liquid separator is throttled in the flash valve. The high-pressure refrigerant is throttled in high-pressure electronic valve.
- The R744 transcritical parallel system – the vapor fraction of CO_2 from liquid separator is compressed in parallel compressors section. The high-pressure refrigerant is throttled in high-pressure electronic valve.
- The R744 transcritical parallel system with multi-ejector expansion pack – the vapor fraction of CO_2 from liquid separator is either compressed in parallel compressors section or throttled in flash valve. The high-pressure refrigerant is expanded in multi-ejector block as a main flashing device, supported by high-pressure electronic valve.

As a result of the possibility of changing the facility configuration, the baseline system was defined as both systems, which did not utilize the multi-ejector block. In situation, where the capacity for a parallel compressors section was too low, the controller unit switched automatically to the booster system.

In the literature, there is no precise information, about optimal flash-tank pressure in the R744 transcritical refrigeration system. An operator can regulate the pressure level of the liquid receiver tank during the investigation. Hence, the optimization of the liquid receiver tank pressure, based on experimental investigation was done for both operation alternatives. In addition, for the multi-ejector block, the analysis of the flash-tank pressure can present the upper limit of pressure ratio for a work of ejectors in selected operating conditions.

The experimental investigation was carried out for two different refrigeration loads. The control system of the test rig is set to obtain maximum refrigeration capacity in the evaporator. Therefore, the operator can set the CO_2 evaporation temperature $T_{0,MT}$ and the

glycol temperature outside from glycol pump T_{51} (see Figure 5.2 and Figure 5.3). The pressure difference between both tanks is expressed as:

$$\Delta p = P_{rec} - P_{evap}\left(T_{0,MT}\right) \tag{5.8}$$

where Δp is a tanks pressure lift, P_{rec} is a pressure of the liquid separator and P_{evap} is a pressure of the liquid receiver. The CO_2 evaporation temperature $T_{0,MT}$ for both refrigeration loads was fixed. Thereby, the value of the tanks pressure lift depended on the value of the pressure level in the liquid separator. Value of pressure in liquid receiver is controlled by inlet parallel compressors temperature $T_{0,par}$. The discharge pressure is calculated by set of the CO_2 exit

2nd stage gas cooler temperature T_6 to obtain the most effectiveness cooling of the CO_2 supercritical fluid. Assumptions for the experimental investigation are presented in Table 5.2.

Table 5.2: Set of operating conditions for the experimental investigation for both R744 refrigeration systems.

Name	Refrigeration load (T_{51})	CO_2 evaporation temperature/ pressure in the evaporator ($T_{0,MT}$/ P_{evap})	Tanks pressure lift (Δp)	CO_2 exit 2nd stage gas cooler temperature (T_6)
1st cooling demand	12 °C	-8 ^{0}C / 28.02 bar	2÷16 bar Step 2 bar	26÷36 °C Step 2 K
2nd cooling demand	15 °C	-8 ^{0}C / 28.02 bar	2÷16 bar Step 2 bar	26÷36 °C Step 2 K

5.5.2 Test Campaign Progress

The experimental investigation embraced wide range of the gas coolers parameters and the liquid receiver pressure for the baseline refrigeration system (parallel system) and the multi-ejector system. During the test campaign progress, many experimental points had to be

rejected due to several problems. For the R744 multi-ejector system, the multi-ejector block did not entrain the suction stream above a limit value of the tanks pressure lift. Hence, this system above the limit value of the tanks pressure lift worked as a baseline system and all of these experimental points were rejected.

For the 1st cooling demand, in the case, when the exit gas cooler temperature is of 26 ^{o}C, the multi-ejector system did not establish for any set of the tanks pressure lift. The multi-ejector module changed very often the configuration of the running ejectors, which influenced the load of the compressors. Hence, for the 1st cooling demand ($T_{51} = 12$ ^{o}C) and for the exit gas cooler temperature of 26 ^{o}C, the multi-ejector system was not able to obtain steady state conditions and the comparison of the system performances for above mentioned settings was omitted.

The rest of the rejected points did not reached established setpoint parameters due to limits of each compressors capacity, or as a result of the non-continuous switching between of the parallel compressors. For small values of the pressure tanks lift, in the multi-ejector system the capacity of the parallel compressors was of 100%, when the base-load compressor was below 50%. The limit of the minimum capacity of the base-load compressor was of 50%. Therefore, the multi-ejector system was not able to obtain the set CO_2 evaporation temperature
($T_{0,MT} = -8$ ^{o}C) and these investigation points were rejected. During decrease of the exit gas cooler temperature, the capacity of the parallel compressors decreased. The control system utilized the parallel compressors, depending on the demand capacity of the parallel compressors. In the range of 17% to 30% the parallel compressor #1 was utilized. The control system switched onto the parallel compressor #2, when the parallel compressors demand capacity was over 45%, but for the demand capacity over 70%, both parallel compressors were utilized. In the case, when the parallel compressors demand capacity decreased, the limit values were different: 60% from both parallel compressors to the parallel compressor #2 and 30% to the parallel compressors #1. Switching between the parallel compressors strongly influenced the destabilization of the system parameters. During investigation, both system configurations, for some operating conditions, demanded the capacity of the parallel compressors in the range of 30% to 40%, which caused constant switching between the

parallel compressors. Therefore, the steady state conditions for foregoing operating conditions were not able to obtain.

Tables of test campaign including investigated and rejected point are shown in Appendix B.

5.5.3 Test Facility Performance Calculations

Calculation of the system characteristics and the ejector parameters has been described in details in section 4. However, the set of equations to present results of both refrigeration system configuration of the test facility has to be shown. Every measurement parameter such as the temperature, pressure or mass flow rate are named in the same way as in Figure 5.2 and Figure 5.3.

For the steady state, it can be assumed that in the evaporator, the heat rate absorbed by the refrigerant is equal to the heat rate rejected by the second fluid. As a result of following assumption, the refrigeration capacity was calculated as the heat rate reject from the glycol stream, because the mass flow rate and both temperatures of the glycol in the base-load evaporator were measured. During investigation, the concentration of ethylene glycol of 30% in the brine loop. For the calculation of this thesis, the values of the specific heat capacity of the glycol were taken from CoolPack results (Jakobsen et al., 1999) and the values can be expressed as a linear function of the glycol temperature expressed in $^{\circ}$C.

$$c_p(t_i) = 0.0029 \cdot t_i + 3.5895 \tag{5.9}$$

where $c_p(t_i)$ is a specific heat capacity in kJ kg^{-1}K^{-1}. Hence, for the steady state conditions, the refrigeration capacity of the base-load evaporator can be calculated as the total heat rate rejected from glycol.

$$\dot{Q}_{evap} = \dot{m}_{gl,evap} \cdot \left[T_{53} \cdot c_p(t_{53}) - T_{54} \cdot c_p(t_{54})\right] \tag{5.10}$$

The overall electric power consumption is a sum of electric power of each utilized compressor. Therefore, COP for both configurations is expressed as:

$$COP = \frac{Q_{evap}}{N_{el,CD1400H} + N_{el,CD1000H} + N_{el,CD380H}} \tag{5.11}$$

The evaluation of the overall volumetric and compressors efficiencies is performed in order to present the characteristic of the rack of compressors. The overall volumetric and compressors efficiencies are defined as a weighted average of each compressor efficiency:

$$\eta_{vol} = \frac{\dot{m}_{CO2,CD1400H} + \dot{m}_{CO2,CD1000H} + \dot{m}_{CO2,CD380H}}{\dot{m}_{CO2,CD1400H,ref} + \dot{m}_{CO2,CD1000H,ref} + \dot{m}_{CO2,CD1000H,ref}} \tag{5.12}$$

$$\eta_{comp} = \frac{1}{N_{el,CD1400H} + N_{el,CD1000H} + N_{el,CD380H}} \left(N_{el,CD1400H} \cdot \eta_{comp,CD1400H} + N_{el,CD1000H} \right.$$
$$\left. \cdot \eta_{comp,CD1000H} + N_{el,CD380H} \cdot \eta_{comp,CD380H} \right) \tag{5.13}$$

For the same operating condition, the overall compressor efficiency of the multi-ejector system was different than of the parallel system. Therefore, the relative change of the overall compressor efficiency after the run of the multi-ejector block is expressed as:

$$\Delta\eta_{comp} = \frac{\eta_{comp,multi-ejector} - \eta_{comp,parallel}}{\eta_{comp,parallel}} \tag{5.14}$$

To calculate exergy efficiency, the information about total fuel and product exergy has to be known. Therefore, the total exergy output of cooling mode is defined as an exergy rate increment in the base-load evaporator.

$$\psi_{incr} = [T_{53} \cdot c_p(t_{53}) - T_{54} \cdot c_p(t_{54})] \cdot \left| 1 - \frac{T_{amb} \cdot \left(\ln\frac{T_{53}}{T_{54}} \right)}{T_{53} - T_{54}} \right| \tag{5.15}$$

$$E_{out} = \dot{m}_{gl,evap} \cdot \psi_{incr} \tag{5.16}$$

Ambient temperature used in Eq. (5.15) was recorded for every investigation day. The total exergy input is the overall electric power consumption. Finally, the second law efficiency can be defined as:

$$\eta_{ex} = \frac{E_{out}}{E_{in}} = \frac{\dot{m}_{gl,evap} \cdot \psi_{incr}}{N_{el,CD1400H} + N_{el,CD1000H} + N_{el,CD380H}} \tag{5.17}$$

6 Results and Discussion

In the current section the results of R744 vapour compression rack equipped with the multi-ejector expansion pack are presented followed by discussion.

6.1 System Working Parameters

6.1.1 Gas Cooler Pressure

Figure 6.1 shows CO_2 conditions outside the gas cooler section for both configurations. The specific enthalpy difference between the multi-ejector system and the parallel system can be seen in the exit gas cooler section. The control system was set to maximize the system energy performance. The exit gas cooler parameters influenced the value of COP, which was described in section 4.3. Therefore, the different COP functions related to the exit gas cooler parameters, for the system with and without the multi-ejector module, were implemented to the control system. The different values of specific enthalpy outside the exit gas cooler section for the multi-ejector system and the parallel system, presented in Figure 6.1, were obtained as a result of the use of the energy performance optimization functions by the control system. For the system with the multi-ejector module the specific enthalpy was lower than for the parallel system.
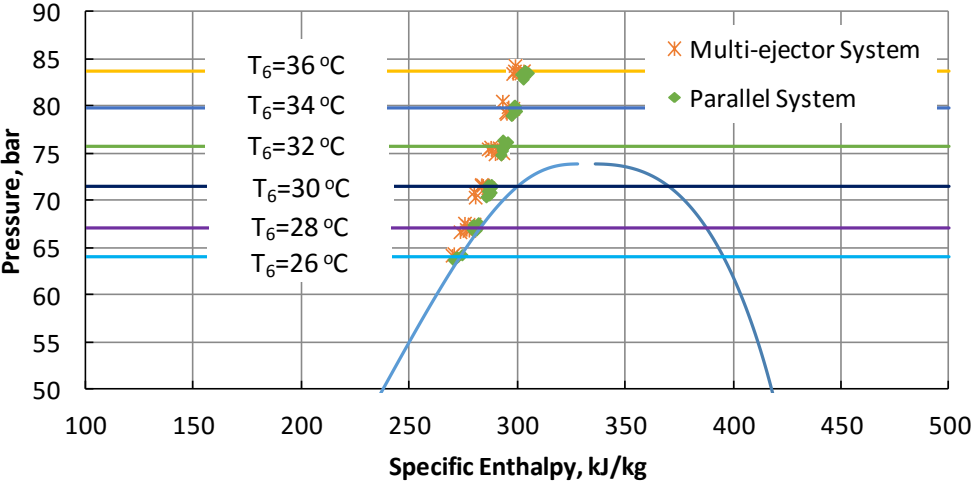
Figure 6.1:   The CO_2 gas cooler exit parameters for both cooling demands.

6.1.2 Refrigeration Capacity

The refrigeration system has to maintain the respectively low value of temperature in the chiller and freezer cabinets. The temperature close to the cabinets door is a main parameter affecting on the refrigeration load, which corresponds to the inlet evaporator temperature of glycol (T_{51}). The control system is set to obtain a maximum refrigeration capacity. Therefore, Figure 6.2 presents chart of refrigeration capacity versus tanks pressure lift (Δp) for the R744 multi-ejector system and the R744 parallel system, respectively. The value of refrigeration capacity was decreasing during the higher value of pressure lift. For the 1st cooling demand ($T_{51}= 12^{o}C$) the difference of the refrigeration capacity is in the range of 41 kW for $\Delta p= 2$ bar to 36 kW for $\Delta p= 16$ bar. Both systems obtain similar values of refrigeration capacity apart from 2nd cooling demand ($T_{51}= 15^{o}C$), where the multi-ejector system gained higher refrigeration capacity than the parallel system for the tanks pressure lift of 8 bar and 10 bar.
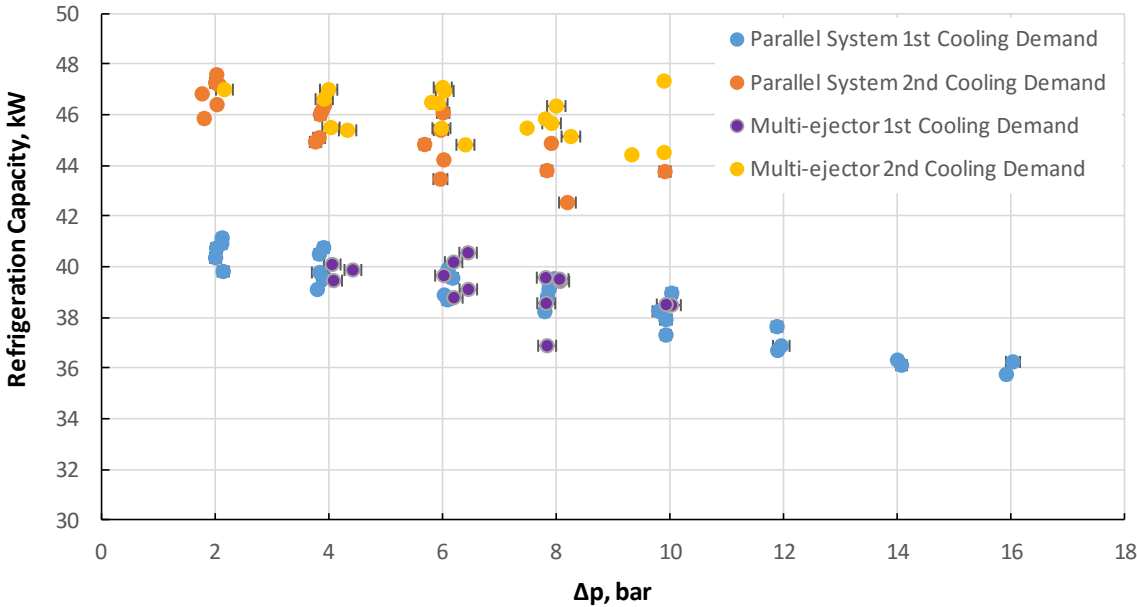
Figure 6.2:   Refrigeration capacity vs. pressure lift of the base-load evaporator for two cooling demands.

Decreasing a value of the heat transfer rate during rising of the tanks pressure lift can be caused by increasing the value of CO_2 specific enthalpy at the inlet of evaporator. The liquid CO_2 from the liquid receiver is throttled by metering valve, before it flows through the evaporator. Upraised pressure level in the separator decreases difference of specific enthalpies

in the evaporator. Hence, in order to achieve constant refrigeration capacity in the evaporator for each tank pressure lift, the mass flow rate of CO_2 should be increased.

Fluctuation of measured setpoints was able to influence on the differences between refrigeration capacities. Table 6.1 presents real measurement with uncertainties in comparison to set values for both refrigeration systems in the same operating conditions.

Table 6.1: Comparison of setpoints and the measurement of each refrigeration system.

Parameter	Setpoint	Parallel System	Multi-ejector System
		Measurement	Measurement
T_{51}	12 ^{o}C	11.87 ^{o}C ±0.42 K	11.96 ^{o}C ±0.40 K
T_6	30 ^{o}C	29.90 ^{o}C ±0.52 K	30.01 ^{o}C ±0.52 K
$T_{0,MT}$	-8 ^{o}C	-7.91 ^{o}C ±0.30 K	-8.01 ^{o}C ±0.30 K
P_{rec}	36 bar	35.89 bar ±0.13 bar	35.82 bar ±0.12 bar

6.1.3 Electric Power Consumption

Utilizing the ejectors during the experimental investigation reduced significantly capacity of the base-load compressor. The multi-ejector system indicated changeability of CO_2 mass flow rate through the base-load compressor, which is shown in Figure 6.3. The figure shows the mass flow rates, in the base-load compressor, for both cooling demands, for the exit gas cooler temperature (T_6) of 28°C ± 0.2 K. The calculation of CO_2 mass flow rate in the base-load compressor has been carried out based on data given from Dorin CD1400H catalogue (see section 5.2.1). For the tanks pressure lift of 2 bar, the mass flow rate of the multi-ejector system was almost two times smaller than the mass flow rate of the parallel system.

The reason of the stream reduction was the mass flow rate entrained in the ejectors. Based on the mass balance of the liquid receiver, the CO_2 mass flow from the evaporator was equal to the CO_2 mass flow in the base-load compressor and the mass flow in the suction nozzle of the ejectors, if the multi-ejector module worked well. During increasing of the tanks pressure lift, the mass entrainment ratio of the multi-ejector block decreased. Hence, for the tanks pressure lift of 8 bar, the difference between mass flow rates of both system is small due to low value

of mass entrainment ratio. Hence, for the tanks pressure lift of 8 bar, the difference between mass flow rates of both systems is small due to low value of the mass entrainment ratio (below 5%).
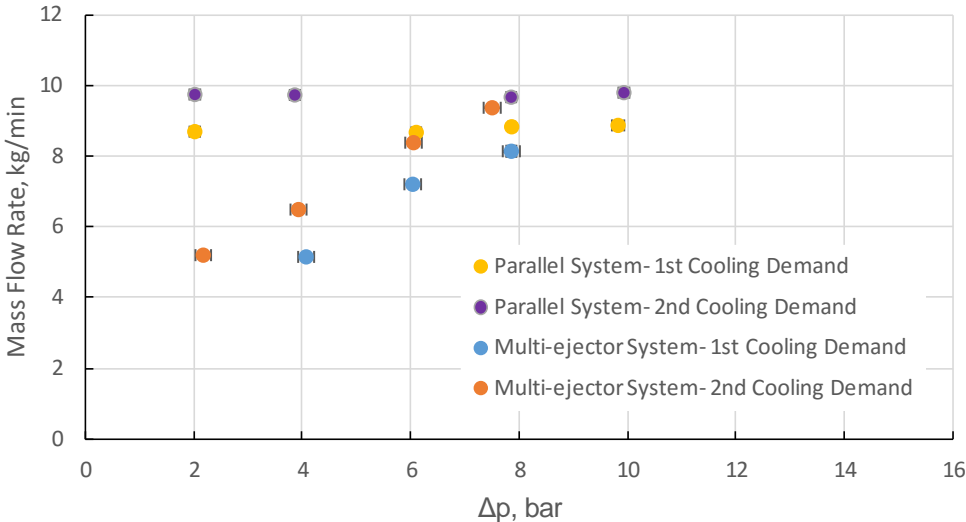
Constant parameters: T_6=28 $^{\circ}$C $\pm$ 0.2 K

Figure 6.3:   R744 mass flow rate in the base-load compressor vs. pressure lift.

The CO_2 mass flow entraining by the ejectors was able to influence on the work parameters of each compressor. Apart from the multi-ejector block parameters, volumetric and compressor efficiency of each compressors depended on tanks pressure lift and the CO_2 exit parameter of the gas cooler section. All of foregoing considerations are related with each other. During operation of the multi-ejector block, the load of the parallel compressors increases significantly, which is shown in Figure 6.4. The figure shows the share of electric power consumption of each compressor on the overall electric power consumption for both refrigeration systems at the same operating conditions. The load of the base-load compressor decreased relatively around 50%. It can be noticed that the contribution of the parallel compressors section in the multi-ejector system increased close to two times (from 35% to 66%) than in the parallel system.

Multi-ejector System

- CD 1400H Base-load Compressor
- CD 1000H Parallel Compressor
- CD 380H Parallel Compressor

34% / 42% / 24%

Parallel System

- CD 1400H Base-load Compressor
- CD 1000H Parallel Compressor

65% / 35%
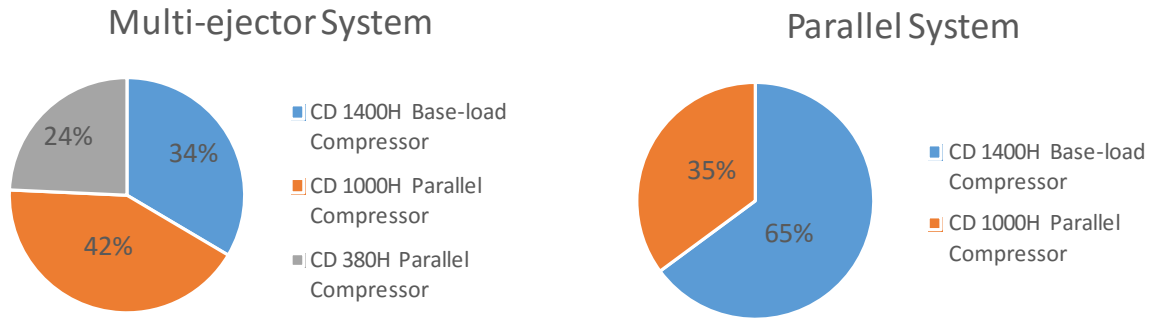
Constant parameters: T_{51}=12 $^{\circ}$C ± 0.4 K T_6=36 $^{\circ}$C ± 0.5 K Δp=6 bar ± 0.15 bar

Figure 6.4: The share of electric power consumption of each compressor on the overall electric power consumption.

The share of power consumption and individual efficiency of each compressor allows for calculation of the overall efficiency of the rack of compressors, which represents the quality of the rack work in the operating system. Figure 6.5 shows the comparison of the overall compressors and volumetric efficiency of the system with efficiency distribution for the individual compressor. The calculation compressor and volumetric efficiency, based on data given from Dorin catalogues, are described in section 5.2.1. The operating conditions were the same as in Figure 6.4, therefore the contributions of each compressor were used to calculate overall efficiencies. For the parallel system, the volumetric efficiencies for both working compressors were comparable. Growth of parallel compressors load forced to compress much more amount of the refrigerant. Therefore, in the multi-ejector system the volumetric efficiencies of both parallel compressors were relatively low. As a result of low values of volumetric efficiencies and the large load, the parallel compressors obtained the compressors efficiency lower than 60%. The individual compressor efficiencies in the parallel system were comparable to volumetric efficiency and therefore the parallel refrigeration system achieved higher value of overall compressor efficiency than the multi-ejector system. The low value of overall compressor efficiency in the multi-ejector system made the growth of overall electric power consumption, which lowered the system performance and finally the value of COP and exergy efficiency.

(a) Volumetric efficiency

(b) Compressor efficiency

Constant parameters: T_{51}=12 $^{\circ}$C ± 0.4 K T_6=36 $^{\circ}$C ± 0.5 K Δp=6 bar ± 0.15 bar

Figure 6.5:   Characteristics of the rack of compressors with comparison of both systems in the same operating condition.

6.1.4 Multi-ejector Block Measurement and Characteristics

The use of vapour ejectors in the R744 vapour compression rack influences the working condition of each compressor. Therefore, analysis of working parameters of multi-ejector has to be done in order to evaluate the best operating conditions for the system performance improvement. Evaluation of multi-ejector block characteristics has been done for two separated cooling demands.

Set of multi-ejector pack measurement, presented in Table 6.2, has been prepared for 1st cooling demand (T_{51}=12 ^{o}C). For the exit gas cooler temperature T_6 of 36 ^{o}C and 34 ^{o}C, respectively, the multi-ejector block was able to entrain suction flow up till the pressure in the liquid receiver of 38 bar (Δp =10 bar). The limit of work for multi-ejector block for the rest of exit gas cooler temperature existed for the pressure receiver of 36 bar (Δp =8 bar). It can be noticed that the outlet pressure of the ejectors was higher than set pressure in the liquid receiver, which causing additional growth of load for the parallel compressors.

The last column presented in Table 6.2, shows the ratio between the mass flow rate of the motive side $\dot{m}_{mot}$ and the total mass flow rate in the high pressure line $\dot{m}_{gc}$ of the carbon dioxide. It can be seen that during increasing of the pressure lift, the mass flow rate in the electronic expansion valve decreases. For T_6=34 ^{o}C and Δp =6 bar the ratio of motive section mass flow rate to total mass flow rate is of 97%. The change of the ejectors configuration influences on the value of the CO_2 mass flow in the motive and suction nozzle. The configuration of working ejectors can be found in the raw data in Appendix B.

Table 6.2: Multi-ejector block measurement for 1st cooling demand conditions. Type A and type B measurement uncertainties can be found in the raw data in Appendix B.

T_6	Δp	Measurement									
		p_{mot}	T_{mot}	p_{suc}	T_{suc}	p_{out}	T_{out}	$\dot{m}_{mot}$	$\dot{m}_{suc}$	$\dot{m}_{out}$	$\dfrac{\dot{m}_{mot}}{\dot{m}_{gc}}$
^{o}C	bar	bar	^{o}C	bar	^{o}C	bar	^{o}C	kg/min	kg/min	kg/min	%
	6	83.56	31.96	27.09	-0.85	35.65	1.64	14.47	4.15	18.61	93%
36	8	84.21	31.86	27.47	-0.63	37.08	3.11	14.04	3.06	17.10	92%
	10	83.54	31.71	28.07	1.24	39.07	5.05	12.99	1.42	14.41	91%
	6	79.79	30.39	27.23	-1.36	35.57	1.53	14.20	3.78	17.97	97%
34	8	80.60	29.84	27.66	0.06	37.02	3.01	12.97	2.52	15.49	92%
	10	80.00	30.12	28.21	2.62	38.95	4.93	12.53	0.82	13.36	89%
	4	75.59	28.34	26.72	-2.09	33.52	-0.71	13.58	4.52	18.10	93%
32	6	74.91	28.17	27.56	-0.85	35.36	1.23	13.35	3.15	16.49	93%
	8	75.57	28.22	28.09	1.61	36.92	2.87	11.82	1.78	13.59	91%
	4	70.40	25.96	27.16	-1.41	33.31	-1.01	12.84	4.06	16.90	93%
30	6	71.92	26.36	27.78	0.90	35.27	1.12	11.54	2.43	13.97	87%
	8	71.81	26.08	28.01	1.78	36.73	2.72	11.98	1.27	13.26	90%
	4	67.75	24.48	27.21	-0.98	33.04	-1.23	12.29	3.66	15.95	93%
28	6	67.27	24.31	28.08	0.80	35.16	1.08	11.20	1.90	13.10	89%
	8	67.69	24.04	28.13	3.64	36.69	2.62	10.31	0.42	10.72	88%

Measurement analysis gives an information only about working conditions of the multi-ejector block. Figure 6.6 shows the multi-ejector block characteristic for all operating conditions investigated for 1st cooling demand (T_{51}=12 ^{o}C). Left Y-axis represents the ejector efficiency $\eta_{ejector}$ and the mass entrainment ratio ϕ, but the right Y-axis represents pressure ratio Π. In addition, the configuration of the multi-ejector module is introduced in the Figure 6.6. The multi-ejector block efficiency decreased during rising of pressure in the liquid

receiver due to simultaneously decreasing of the mass entrainment ratio. The same impairment of the ejector efficiency can be noticed during decreasing of the exit gas cooler temperature and discharge pressure, respectively. For the tanks pressure lift of 8 bar (Δp =8 bar), the ejector efficiency was in the range of 27% to 8% for the exit gas cooler temperature T_6 from 36 $^\circ$C to 28 $^\circ$C, respectively. The value of the mass entrainment ratio decreased from 0.22 to 0.04 for the same range as the ejector efficiency.

Lowering of the exit gas cooler parameter caused a slight drop of the pressure ratio for the same set of the tank pressure lift. In the range of the exit gas cooler temperature T_6 of 36 $^\circ$C to 28 $^\circ$C and for the tank pressure lift of 8 bar (Δp =8 bar), the pressure lift is of 1.35 to 1.30, respectively. The multi-ejector block worked with the ejector efficiency over 30% for $\Delta p \leq 4$ bar, when T_6 greater than 28 $^\circ$C and for $\Delta p = 6$ bar, when T_6 greater than 34 $^\circ$C.
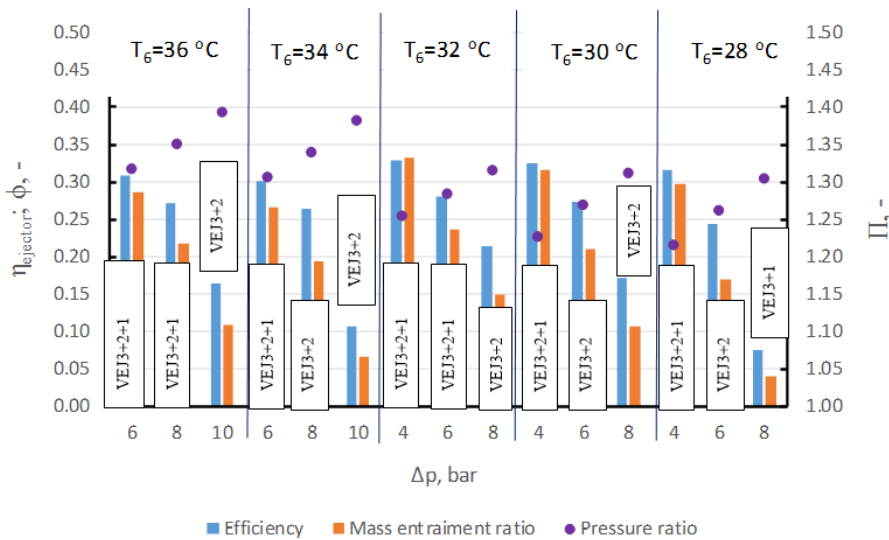
Figure 6.6:   Multi-ejector block characteristics depending on the tanks pressure lift (Δp) and exit gas cooler temperature (T_6) for 1st cooling demand conditions.

During investigation of operating conditions for the 1st cooling demand, the multi-ejector block worked at the different ejectors capacity configuration. Hence, the ejector efficiency linked to the mass entrainment ratio dropped significantly. For the 2nd cooling demand (T_{51}=12 $^\circ$C), the multi-ejector block was more stable, which can be noticed in Table 6.3. The configuration of working ejectors can be found in the raw data in Appendix B.

The mass flow rate in the motive nozzle is comparable for the same temperature T_6, with the different pressure in the liquid receiver. The maximum value of Δp, for which the multi-

ejector block can entrain the vapour CO_2 from the suction side, is of 10 bar for the T_6 temperature in the range of 36 °C to 32 °C, of 8 bar for the T_6 temperature in the range of 30 °C to 28 °C, and of 6 bar for the T_6 temperature of 26 °C, respectively. Therefore, it can be noticed that for very low average heat sink temperature, which forces the R744 system to operate in subcritical mode, the ejectors can be utilized only for the small pressure lift. The range of the ejectors work can be extended depending on the gas cooler parameters: the transcritical discharge pressure linked to exit gas cooler temperature.

The share of the motive nozzle mass flow rate in total CO_2 mass flow rate in high pressure line varied from 81% to 93% and it was not able to be found the same decreasing trend at the increase of the pressure lift. For the higher refrigeration load and more stable work of the multi-ejector pack, the highest shares of mass flow rate in the motive nozzle were for the highest values of pressure lift.

Table 6.3: Multi-ejector block measurement for 2nd cooling demand conditions. Type A and type B measurement uncertainties can be found in the raw data in Appendix B.

		Measurement									
T_6	Δp	p_{mot}	T_{mot}	p_{suc}	T_{suc}	p_{out}	T_{out}	$\dot{m}_{\text{mot}}$	$\dot{m}_{\text{suc}}$	$\dot{m}_{\text{out}}$	$\dfrac{\dot{m}_{mot}}{\dot{m}_{gc}}$
°C	bar	bar	°C	bar	°C	bar	°C	kg/min	kg/min	kg/min	%
	6	83.26	31.60	27.03	-1.13	35.62	1.48	14.96	4.22	19.18	88%
36	8	83.43	31.80	27.50	0.03	37.26	3.26	14.98	3.03	18.01	88%
	10	83.53	31.87	28.24	1.80	39.14	5.12	14.98	1.68	16.67	86%
	6	79.23	30.02	27.24	-1.17	35.26	1.11	14.09	3.99	18.08	84%
34	8	79.04	29.77	27.86	0.39	37.10	3.12	14.32	2.56	16.88	88%
	10	79.58	30.03	28.24	4.12	38.94	4.96	14.51	0.83	15.34	93%
	4	75.40	27.97	26.77	-1.96	33.48	-0.77	13.76	4.57	18.33	86%
32	6	75.25	27.91	27.54	-0.65	35.23	1.09	13.78	3.43	17.20	85%
	8	75.50	28.24	28.14	1.26	37.13	3.08	13.66	1.77	15.44	86%

	10	74.98	28.13	28.30	-1.54	38.35	4.40	13.82	0.26	14.08	93%
	4	70.95	25.83	27.00	-1.69	33.18	-1.13	13.35	4.24	17.60	87%
30	6	71.61	26.25	27.64	-0.22	35.03	0.86	13.35	2.91	16.26	86%
	8	71.37	26.36	28.22	2.74	36.84	2.80	13.17	1.09	14.26	88%
	2	66.77	24.01	26.86	-2.45	31.64	-2.94	12.58	4.92	17.50	81%
28	4	67.00	24.33	27.33	-1.40	33.11	-1.15	12.66	3.76	16.43	84%
	6	66.89	24.19	27.81	0.71	34.95	0.85	12.90	2.04	14.95	86%
	8	67.55	24.46	28.27	3.27	36.50	2.45	13.12	0.72	13.85	92%
26	4	64.40	22.74	27.44	-0.94	33.12	-1.16	13.02	3.44	16.46	89%
	6	64.22	22.22	28.04	0.64	34.91	0.79	13.05	1.95	14.99	93%

Figure 6.7 presents the multi-ejector block characteristics for the T_{51} temperature of 15 ^{o}C including the efficiency, mass entrainment ratio and pressure ratio. Left Y-axis represents the ejector efficiency $\eta_{ejector}$ and the mass entrainment ratio ϕ, but the right Y-axis represents pressure ratio Π. The highest value of the mass entrainment ratio exists for T_6 and Δp of 28 ^{o}C and 2 bar, respectively. The multi-ejector efficiency together with the mass entrainment ratio have the same decreasing trend as for results presented in Figure 6.6. It can be noticed that the value of the multi-ejector efficiency for T_6 and Δp of 28 ^{o}C and 2 bar, respectively, is comparable with the values obtained for Δp =4 bar and T_6 = 30 ^{o}C, or 32 ^{o}C.

For Δp of 8 bar, the ejector efficiency is in the range of 26% to 9% for the exit gas cooler temperature T_6 of 36 ^{o}C to 28 ^{o}C, respectively. The value of the mass entrainment ratio decreases from 0.20 to 0.06 for the same range as the ejector efficiency. For Δp of 6 bar the mass entrainment ratio and the ejector efficiency was stable for T_6 in the range of 36 ^{o}C to 34 ^{o}C and also in the range of 28 ^{o}C to 26 ^{o}C. The same stabilization of both parameters was for Δp of 4 bar and for T_6 in the range of 32 ^{o}C to 28 ^{o}C.

The pressure ratio had the slightly decreasing trend during decreasing of the T_6 temperature. In the range of the exit gas cooler temperature from 36 ^{o}C to 28 ^{o}C and for the tanks pressure lift of 8 bar, the pressure ratio is in the range of 1.36 to 1.29, respectively. The very low drop of the pressure ratio confirmed that during the decrease of the exit gas cooler temperature, the

small difference between the ejector outlet pressure and the liquid separator pressure was reduced.

The multi-ejector block worked with the ejector efficiency over 30% for $\Delta p \leq 4$ bar, when $T_6 > 26$ °C and for $\Delta p = 6$ bar, when $T_6 > 34$ °C.

Figure 6.7:   Multi-ejector block characteristics depending on the tanks pressure lift (Δp) and exit gas cooler temperature (T_6) for 2nd cooling demand conditions.

It can be observed that the similar range of values for the multi-ejector efficiency, mass entrainment ratio and pressure ratio for both cooling demands was obtained. Increase of refrigeration load stabilizes the multi-ejector work, but it does not influence on the vapour ejectors performance improvement.

6.2 Multi-ejector System Performance Improvement

To compare the system performance in the mode of the R744 transcritical parallel system, defined as the baseline system, and the R744 transcritical multi-ejector system, evaluation of the first law and the second law efficiencies has to be done. In addition, as both refrigeration configurations utilize the same rack of compressors, value of the overall compressors efficiency has to be known. For the data points, maintained for both system in the same operating conditions, were carried out for the calculations of the COP and exergy efficiency

improvements of the multi-ejector system (equations of each improvement have been defined in section 5.5.3).

6.2.1 First Cooling Demand

Figure 6.8 shows the system performances characteristics for 1st cooling demand ($T_{51}=12^{o}$C) and the exit gas cooler temperature T_6 of 36°C. During increasing the pressure level in the liquid receiver tank, the COP and the exergy efficiency increased. The multi-ejector systems gained the higher COP and exergy efficiency for the tanks pressure lift of 8 bar. Hence, for $\varDelta p$ in the range of 8 bar to 10 bar, the multi-ejector module improved the system energy performance, in despite of worse compressors work.

The parallel system worked for the overall compressors efficiency in the range of 68% to 70%, when the lowest and highest values of the efficiency for the multi-ejector system gained 60% and 65%, respectively. For $\varDelta p$ of 6 bar, the parallel system obtained almost 10% higher compressors efficiency than the multi-ejector, as a result of significant load of the parallel compressors.

The highest values of COP 2.46 and the exergy efficiency 11.9% were gained by the multi-ejector system for $\varDelta p$= 10 bar. The parallel system reached the highest COP of 2.38 and the exergy efficiency of 11.1% for the same tanks pressure lift as the multi-ejector system.
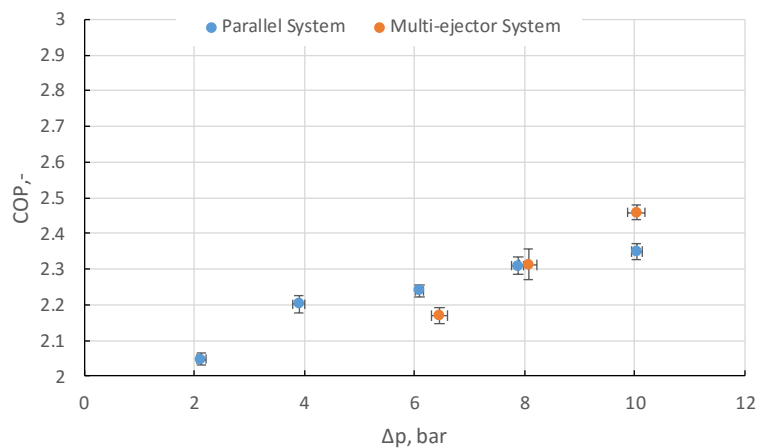
(a) Coefficient of Performance
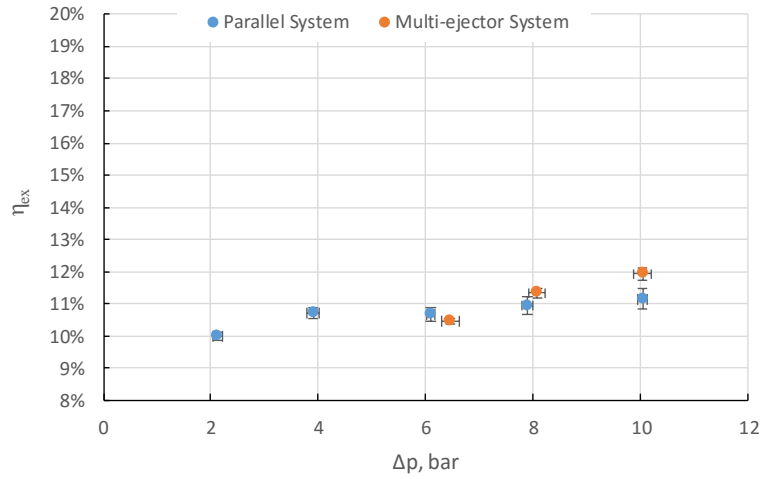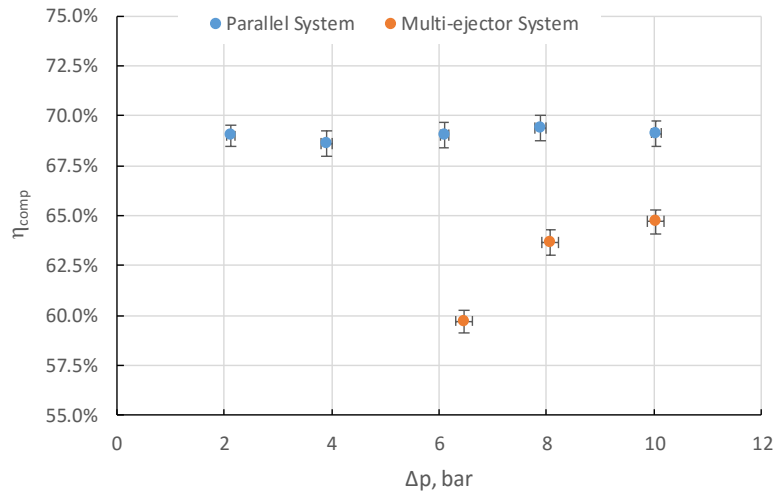
(b) Exergy efficiency

(c) The overall compressors efficiency

Constant parameters: $T_{51}=12\ ^{o}C \pm 0.4\ K$ $T_6=36\ ^{o}C \pm 0.5\ K$

Figure 6.8:   System performance characteristics vs. the tanks pressure lift (Δp) for the parallel system and the multi-ejector system for T_{51} of 12 ^{o}C and T_6 of 36 ^{o}C: (a) COP, (b) exergy efficiency and (c) overall compressors efficiency

The same increasing trends of COP and exergy efficiency value depending on the tanks pressure lift as in Figure 6.8, can be seen for T_6 of 34°C. These results are shown in Figure 6.9. In these operating conditions, the same behaviour can be noticed as for the higher exit gas

cooler temperature. During the experimental investigation for *Δp* of 10 bar, the parallel system was not able to achieve steady state conditions, thereby the system performance characteristic for selected tanks pressure lift were omitted. The multi-ejector system improved the performance for *Δp* of 8 bar. For the tanks pressure lift ranging from 12 bar to 16 bar, the overall compressors efficiency of the parallel system dropped by approximately 2.5% in comparison to points reached for smaller pressure difference. Hence, the parallel system, for the same tanks pressure lift range, obtained lower values of COP, or even smaller, than it was able to appear out of trend created by the points for the tanks pressure lift ranging from 2 bar to 8 bar. The results of the smaller overall compressors efficiency for the higher pressure in the liquid separator were caused by switch of the parallel compressor #1 (Dorin CD1000H) into the parallel compressor #2 (Dorin CD380H).

The highest values of COP 2.66 and the exergy efficiency 12.2% were gained by the multi-ejector system for *Δp*= 10 bar. In the case of the parallel system, the highest COP was equal to 2.6 for *Δp*= 16 bar and the exergy efficiency was equal to 11.8% for *Δp*= 6 bar. The value of the highest exergy efficiency for the parallel system was related to the highest overall compressors efficiency of 70%.
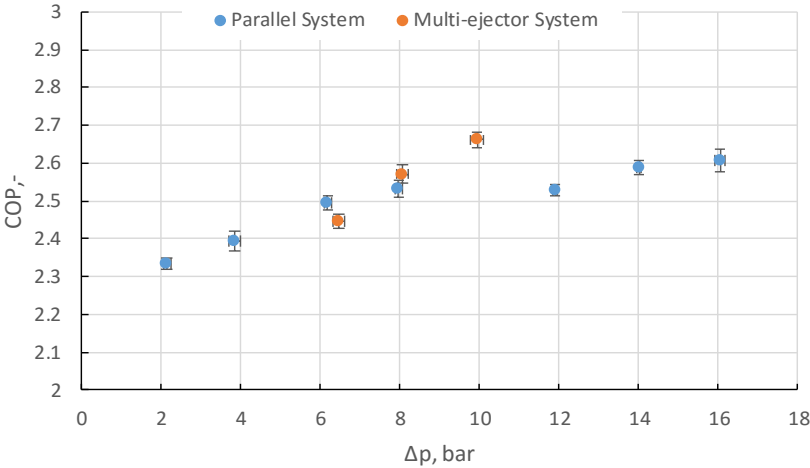
(a) Coefficient of Performance
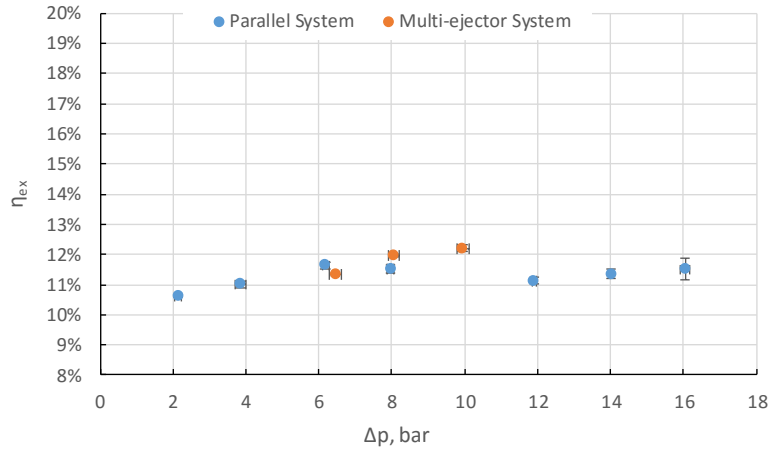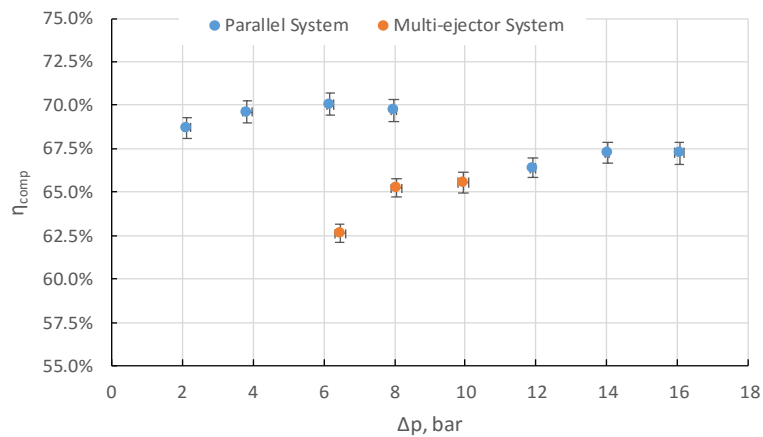
(b) Exergy efficiency

(c) The overall compressors efficiency

Constant parameters: T_{51}=12 $^{\text{o}}$C ± 0.4 K T_6=34 $^{\text{o}}$C ± 0.5 K

Figure 6.9: System performance characteristics vs. the tanks pressure lift (Δp) for the parallel system and the multi-ejector system for T_{51} of 12 $^{\text{o}}$C and T_6 of 34 $^{\text{o}}$C: (a) COP, (b) exergy efficiency and (c) overall compressors efficiency

Figure 6.10 shows system performance characteristics for 1$^{\text{st}}$ cooling demand (T_{51}=12$^{\text{o}}$C) and the exit gas cooler temperature T_6 of 32$^{\text{o}}$C. During the experimental investigation for Δp of 8 bar, the parallel system was not able to achieve steady state conditions, thereby the system performance characteristic for selected tanks pressure lift were omitted. The multi-ejector system gained higher COP for the tanks pressure lift of 6 bar. The parallel system worked

better than the multi-ejector for the *Δp* of 6 bar based on the second law analysis. In these operating conditions, the same relationship can be noticed between the overall compressors efficiency and the COP, or exergy efficiency, value for the high pressure in the liquid separator in the range of 38 bar to 44 bar.

The highest values of COP 2.91 and the exergy efficiency 13.5% were gained by the multi-ejector system for *Δp* of 8 bar. The parallel system reached the highest COP of 2.82 for *Δp* of 16 bar and the exergy efficiency of 11.1% for *Δp* of 6 bar. The highest value of the exergy efficiency of the parallel system was related to the highest value of the overall compressors efficiency of 70.2%.

(a) Coefficient of Performance
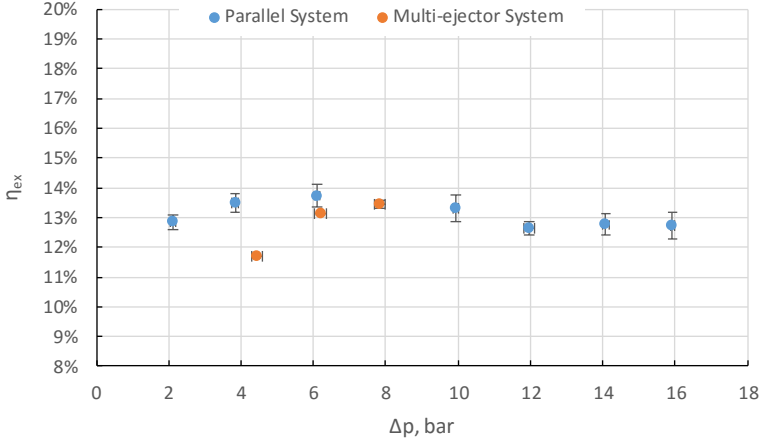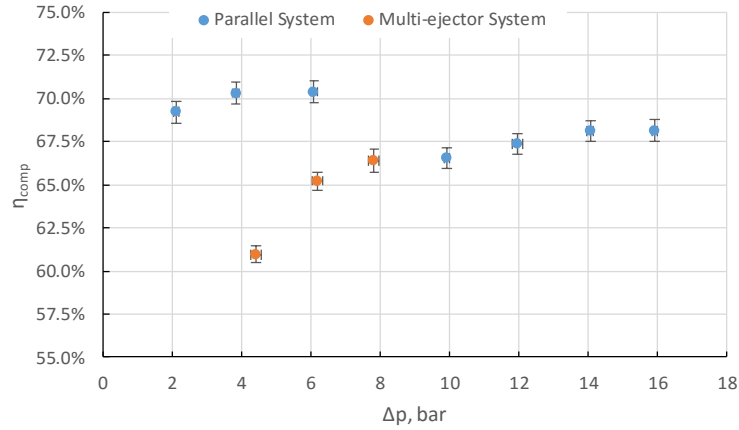
(b) Exergy efficiency

(c) The overall compressors efficiency

Constant parameters: T_{51}=12 ^{o}C ± 0.4 K T_6=32 ^{o}C ± 0.5 K

Figure 6.10:   System performance characteristics vs. the tanks pressure lift (Δp) for the parallel system and the multi-ejector system for T_{51} of 12 ^{o}C and T_6 of 32 ^{o}C: (a) COP, (b) exergy efficiency and (c) overall compressors efficiency

In the subcritical mode, COP and the exergy efficiency, depending on the tanks pressure lift, have the same increasing trends as in the transcritical mode. Furthermore, the multi-ejector system reaches much better system performance as the parallel system, which is shown in Figure 6.11. The figure presents the system performance characteristics depending on the tanks pressure lift, for the 1st cooling demand (T_{51}=12°C) and the exit gas cooler temperature T_6 of 30°C. During the experimental investigation for Δp of 6 bar, the parallel system was not able to achieve steady state conditions, thereby the system performance characteristic for selected tanks pressure lift were omitted.

The highest values of COP 3.23 and the exergy efficiency 15.3% were gained by the multi-ejector system for Δp of 8 bar. For the same operating conditions, the multi-ejector system gains slightly higher value of the overall compressors efficiency than the parallel system. In the case of the parallel system, the highest COP was equal to 3.11 for Δp= 12 bar and the exergy efficiency was equal to 15.1% for Δp= 10 bar. In the subcritical mode, the small pressure ratio in the parallel compressors section has more influence on the exergy efficiency than the high value of the overall compressors efficiency.

(a) Coefficient of Performance
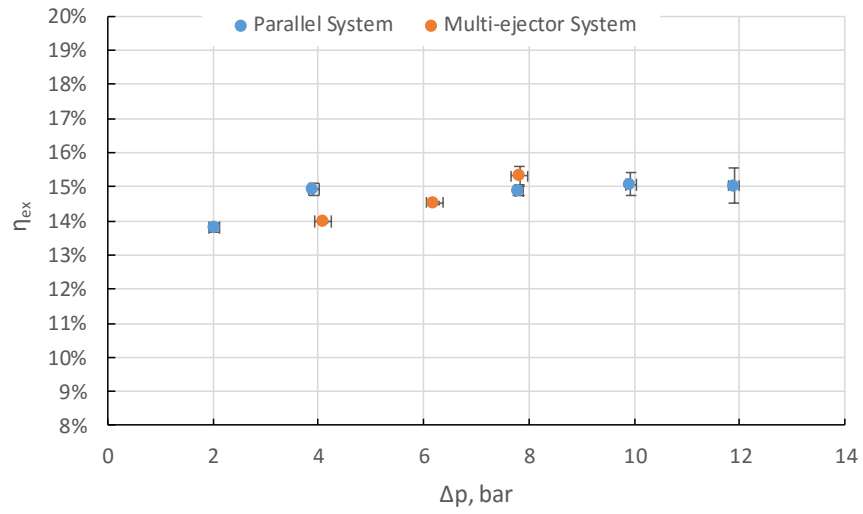
(b) Exergy efficiency
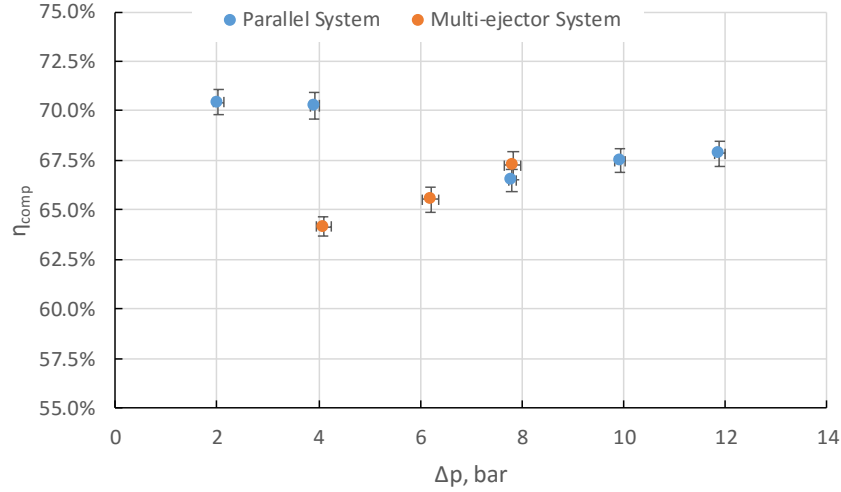
(c) The overall compressors efficiency

Constant parameters: T_{51}=12 °C ± 0.4 K T_6=30 °C ± 0.5 K

Figure 6.11:   System performance characteristics vs. the tanks pressure lift (Δp) for the parallel system and the multi-ejector system for T_{51} of 12 °C and T_6 of 30 °C: (a) COP, (b) exergy efficiency and (c) overall compressors efficiency

Figure 6.12 shows the system performance characteristic for the 1st cooling demand and the last exit gas cooler temperature T_6 set to 28°C. During the experimental investigation for Δp of 4 bar, the parallel system was not able to achieve steady state conditions, thereby the system performance characteristic for selected tanks pressure lift were omitted. The multi-ejector module improved the system energy performance for Δp of 6 bar. In the multi-ejector system, COP and the exergy efficiency decreased more rapidly for Δp=8 bar in comparison to the values reached for Δp= 6 bar. The drop of the energy performance characteristics was caused by the drop of the overall compressors efficiency and by the very low CO_2 mass flow in the suction nozzle. The multi-ejector block for Δp of 6 bar reached the mass entrainment ratio below 0.05, which is shown in Figure 6.6 As the result of low value of the mass entrainment ratio and high ejector capacity (see Appendix B), the multi-ejector module had the requested capacity too high than the real capacity.

The highest values of COP 3.53 and the exergy efficiency 16.6% are gained by the multi-ejector system for Δp= 6 bar. The parallel system reached the highest COP of 3.4 and the exergy efficiency of 16.4% for Δp of 10 bar.
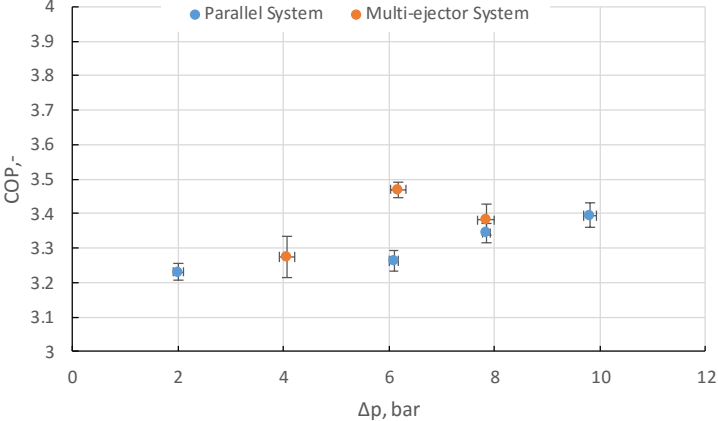
(a) Coefficient of Performance
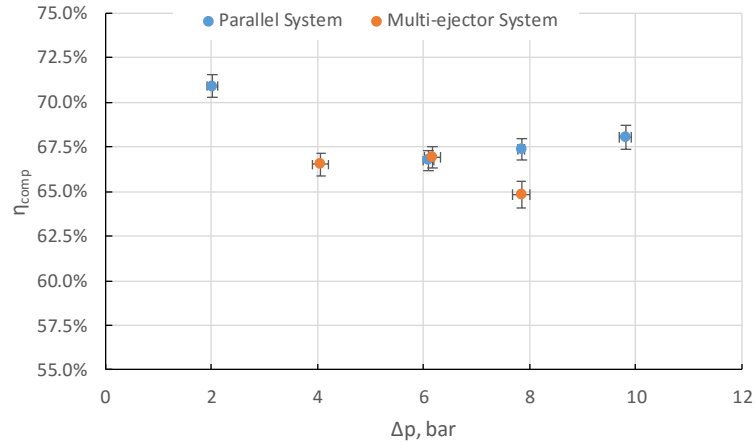
(b) Exergy efficiency

(c) The overall compressors efficiency

Constant parameters: T_{51}=12 ^{o}C ± 0.4 K T_6=28 ^{o}C ± 0.5 K

Figure 6.12: System performance characteristics vs. the tanks pressure lift (Δp) for the parallel system and the multi-ejector system for T_{51} of 12 ^{o}C and T_6 of 28 ^{o}C: (a) COP, (b) exergy efficiency and (c) overall compressors efficiency

Set of foregoing figures present the relationship between the system performance characteristics and the tanks pressure lift together with exit gas cooler parameter for the 1st cooling demand. For some operating conditions, the values of COP and the exergy efficiency were reached for both systems, therefore it can be calculated the multi-ejector performance improvement.

Table 6.4 presents a set of COP and the exergy efficiency improvements of the multi-ejector system for the 1st cooling demand (T_{51}=12°C). The highest COP improvements were obtained for T_6= 28°C and Δp= 6.1 bar up to 4.67%, whereas the highest COP degradation were obtained for T_6= 32°C and Δp= 4.1 bar up to -6.46%. It can be noticed that for the small value of tanks pressure lift, the multi-ejector system gained worse performance than the baseline, which was able to be caused by the low value of the overall compressors efficiency. The multi-ejector system obtained the best exergy performance for T_6=36 ^{o}C and Δp= 10.0 bar due to the high overall efficiency and over 15% of the work recovery by the multi-ejector block, which is shown in Figure 6.6. The exergy improvement for foregoing operating conditions was of 7.05%. The worst degradation of the second law efficiency, the multi-ejector system

reached for T_6 of 32°C and Δp of 4.1 bar up to -13.24%, what was strongly dependent on the poor work of the rack of compressors.

For $\Delta\eta_{comp}$ > -8.25% the multi-ejector system improved COP and the exergy efficiency. Therefore, the combination of the multi-ejector block efficiency of 24.39% and the relative change of the overall compressor efficiency of 0.28% reached the best COP improvement for Δp = 6.1 bar and for T_6 =28 ^{o}C.

Based on results presented in Table 6.4, the use of the multi-ejector module improved the energy performance for Δp > 6 bar, when $T_6 \leq 32$ ^{o}C and also for Δp > 8 bar, when $T_6 > 32$ ^{o}C. The exergy improvement of the multi-ejector system related to the parallel system was for Δp > 8 bar, when $T_6 \leq 36$ ^{o}C.

Table 6.4: COP and exergy efficiency improvement of the R744 multi-ejector system relative to the R744 parallel system, the multi-ejector block efficiency (η_{ej}) and the relative change of the overall compressors efficiency ($\Delta\eta_{comp}$) for the 1st cooling demand (T_{51}= 12°C), related to the exit gas cooler temperature (T_6) and the tanks pressure lift (Δp).

T_6	Δp	$COP_{improvement}$	$\eta_{ex,improvement}$	η_{ej}	$\Delta\eta_{comp}$
36 ^{o}C ± 0.1 K	6.3 bar ± 0.1 bar	-3.12% ± 0.04%	-2.04% ± 0.05%	30.83% ± 0.75% VEJ3+VEJ2+VEJ1	-13.50% ± 0.15%
36 ^{o}C ± 0.2 K	8.0 bar ± 0.1 bar	0.14% ± 0.01%	3.60% ± 0.11%	27.16% ± 0.37% VEJ3+VEJ2+VEJ1	-8.25% ± 0.11%
36 ^{o}C ± 0.1 K	10.0 bar ± 0.1 bar	4.67% ± 0.06%	7.05% ± 0.25%	16.51% ± 0.23% VEJ3+VEJ2	-6.4% ± 0.08%
34 ^{o}C ± 0.1 K	6.3 bar ± 0.1 bar	-1.98% ± 0.02%	-2.56% ± 0.02%	30.13% ± 0.50% VEJ3+VEJ2+VEJ1	-10.60% ± 0.12%
34 ^{o}C ± 0.1 K	8.0 bar ± 0.1 bar	1.51% ± 0.02%	3.96% ± 0.05%	26.42% ± 0.34% VEJ3+VEJ2	-6.43% ± 0.07%
32 ^{o}C ± 0.1 K	4.1 bar ± 0.1 bar	-6.46% ± 0.06%	-13.24% ± 0.26%	32.90% ± 0.44% VEJ3+VEJ2+VEJ1	-13.32% ± 0.14%
32 ^{o}C ± 0.1 K	6.2 bar ± 0.1 bar	0.70% ± 0.01%	-4.33% ± 0.11%	28.16% ± 0.50% VEJ3+VEJ2+VEJ1	-7.33% ± 0.08%
30 ^{o}C ± 0.1 K	4.0 bar ± 0.1 bar	-0.82% ± 0.01%	-6.29% ± 0.08%	32.44% ± 0.56% VEJ3+VEJ2+VEJ1	-8.69% ± 0.09%
30 ^{o}C ± 0.1 K	7.8 bar ± 0.1 bar	6.98% ± 0.01%	2.94% ± 0.06%	17.18% ± 0.21% VEJ3+VEJ2	1.11% ± 0.01%

| 28 °C ± 0.1 K | 6.1 bar ± 0.1 bar | 8.07% ± 0.11% | 5.07% ± 0.10% | 24.39% ± 0.29% VEJ3+VEJ2 | 0.28% ± 0.01% |
| 28 °C ± 0.1 K | 7.9 bar ± 0.1 bar | 1.11% ± 0.02% | -0.46% ± 0.02% | 7.51% ± 0.09% VEJ3+VEJ1 | -3.78% ± 0.01% |

6.2.2 Second Cooling Demand

Figure 6.13 shows system performance characteristics, depending on the tanks pressure lift (Δp) of both systems for the 2nd cooling demand (T_{51}=15°C) and the exit gas cooler temperature (T_6) of 36°C. During the experimental investigation, both refrigeration systems were able to be compared only for Δp of 6 bar. The parallel system obtained higher COP and the exergy efficiency due to over 6% higher value of the overall compressors efficiency than that of the multi-ejector system.

The multi-ejector system gained the maximum value of COP 2.39 for Δp of 10 bar. In comparison with the maximum COP for the 1st cooling demand and the same exit gas cooler temperature, which is shown in Figure 6.8, the highest COP value dropped due to the higher refrigeration load. The multi-ejector system for Δp= 8 bar reached the highest value of the exergy efficiency of 9.4%, which was over 1.7% lower than in Figure 6.8. The parallel system worked for the overall compressors efficiency of over 65%, in contrast to the multi-ejector system, which gained the overall compressors efficiency ranging from 59% to 63%.
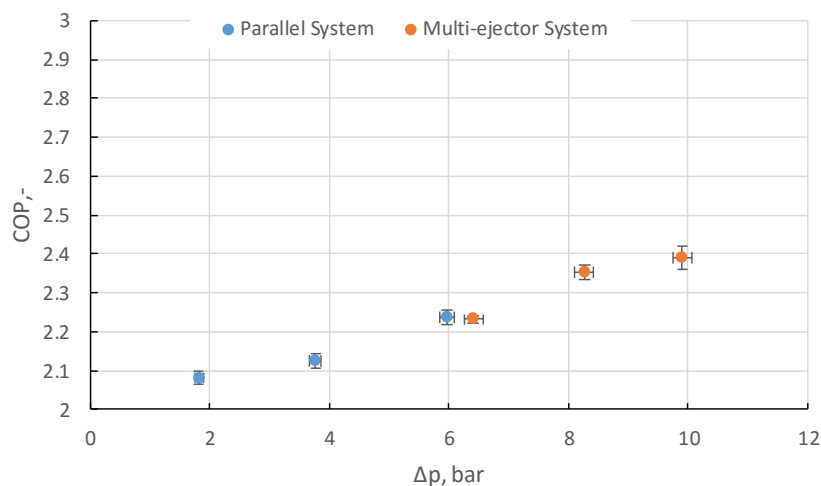
(a) Coefficient of Performance
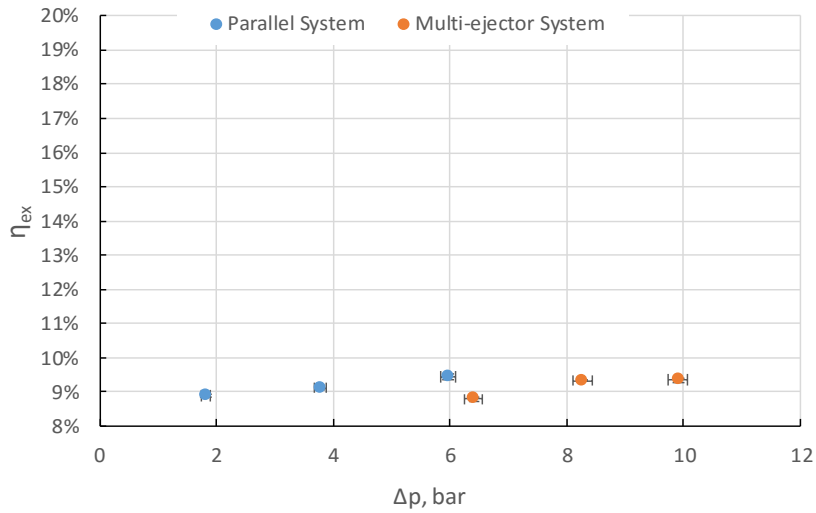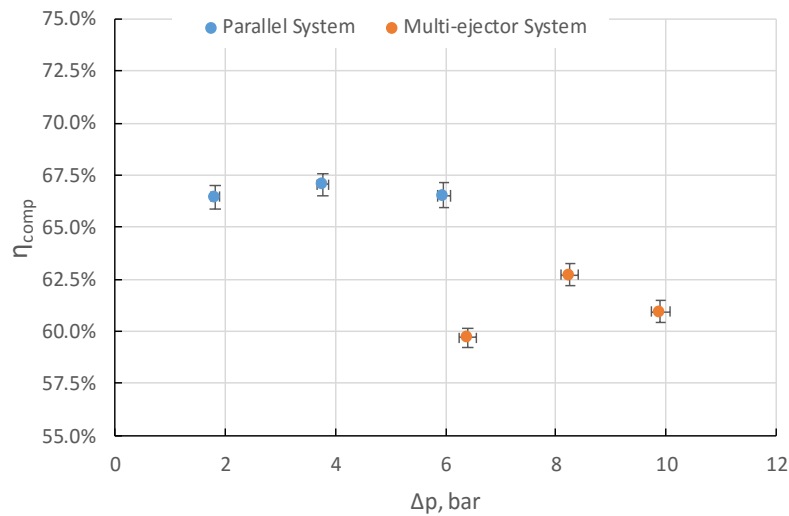
(b) Exergy efficiency

(c) The overall compressors efficiency

Constant parameters: T_{51}=15 ^{o}C ± 0.4K T_6=36 ^{o}C ± 0.5K
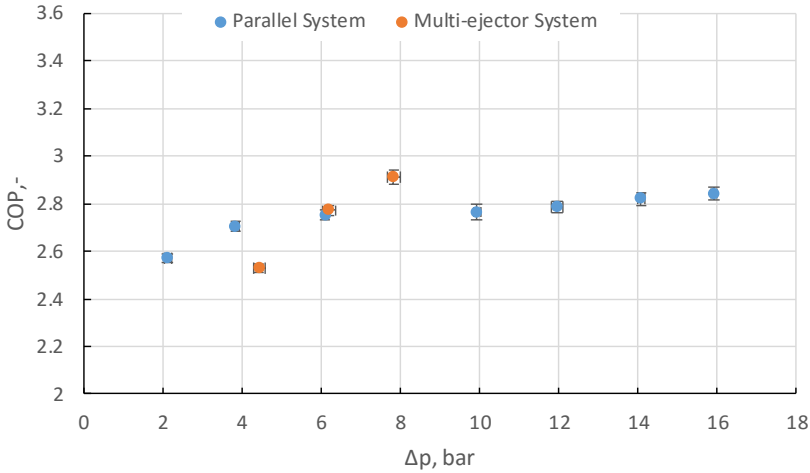
Figure 6.13:   System performance characteristics vs. the tanks pressure lift (Δp) for the parallel system and the multi-ejector system for T_{51} of 15 ^{o}C and T_6 of 36 ^{o}C: (a) COP, (b) exergy efficiency and (c) overall compressors efficiency.

Simultaneously as in Figure 6.13, the same comparison of both refrigeration systems, for T_{51}=15°C and T_6=34°C, can be done only for Δp= 6 bar, which is shown in Figure 6.14. As a

result of significant difference between the overall compressors efficiencies of approximately 5%, COP and the exergy efficiency of the multi-ejector system were smaller than the values of the parallel system. The highest values of COP 2.66 and the exergy efficiency 10.4% were gained by the multi-ejector system for $\Delta p = 10$ bar.

The overall compressors efficiency for the multi-ejector system did not cross the level of 65%. The parallel system gained the overall compressors efficiency ranging from 66% to 67%.
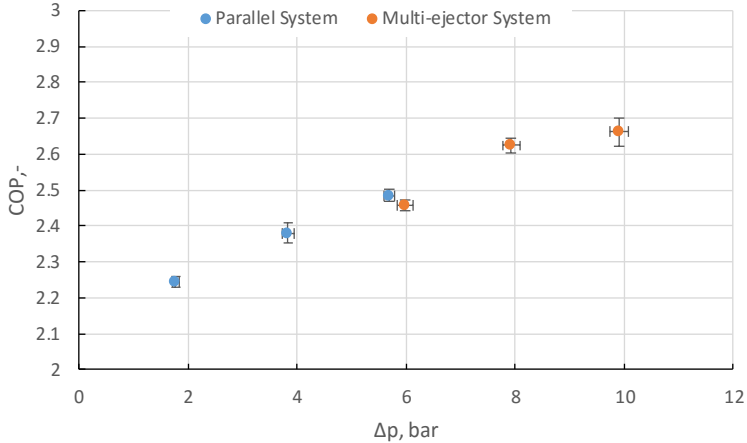
(a) Coefficient of Performance
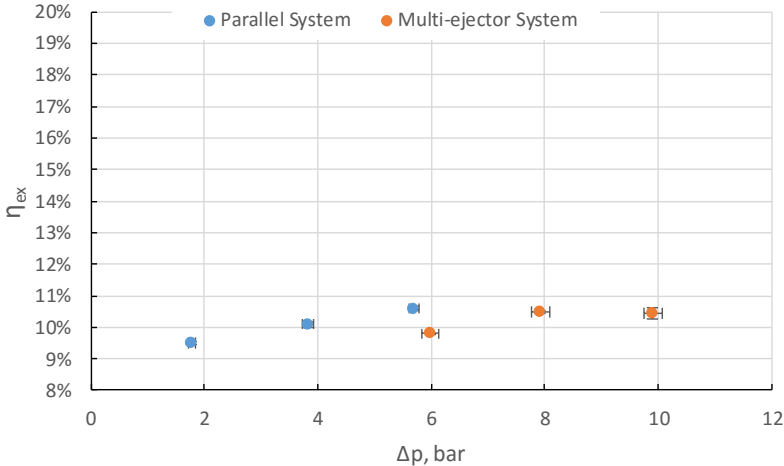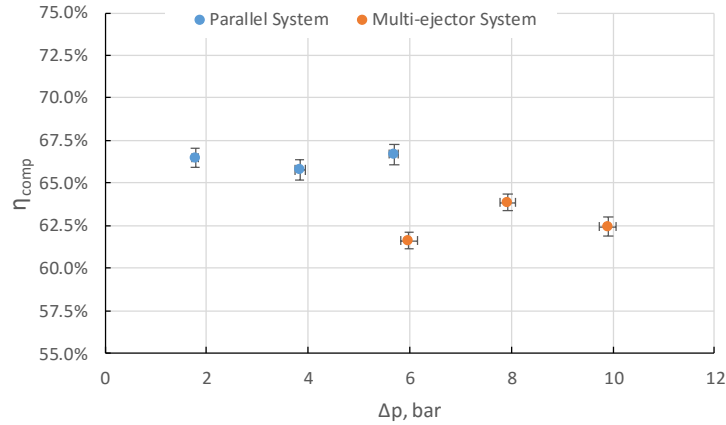
(b) Exergy efficiency

(c) The overall compressors efficiency

Constant parameters: T_{51}=15 ^{o}C ± 0.4 K T_{6}=34 ^{o}C ± 0.5 K

Figure 6.14:   System performance characteristics vs. the tanks pressure lift (Δp) for the parallel system and the multi-ejector system for T_{51} of 15 ^{o}C and T_{6} of 34 ^{o}C: (a) COP, (b) exergy efficiency and (c) overall compressors efficiency.

Figure 6.15 shows the system performance characteristics for 2nd cooling demand (T_{51}=15°C) and the exit gas cooler temperature T_{6} of 32°C. The multi-ejector system gained better performance for Δp= 6 bar due to decreased difference of the overall compressors efficiency of both configurations (below 3%). For Δp= 4 bar, the exergy efficiency of the multi-ejector system is higher than that of the baseline system, despite that the parallel system reaches the higher COP. In addition, the overall compressor efficiency of the multi-ejector system is much smaller than of the parallel system. The exergy improvement of the multi-ejector system is caused by the drop of the irreversibility losses created in the multi-ejector expansion pack due to stabilization of multi-ejector block work during higher refrigeration load (T_{51}=15°C).

The highest values of COP 2.90 and the exergy efficiency 12.8% were gained by the multi-ejector system for Δp= 8 bar. The overall compressors efficiency for the multi-ejector system was obtained in the range of 61% to 65%, in contrast to the parallel system, for which the overall compressors efficiency values was over 66%.
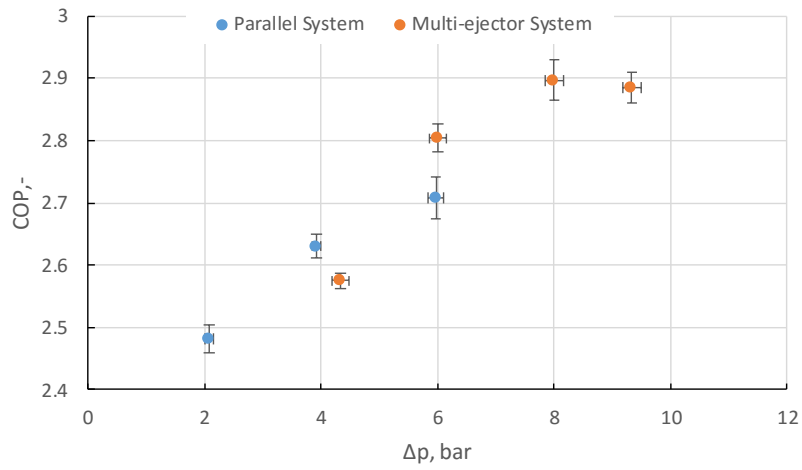
(a) Coefficient of Performance
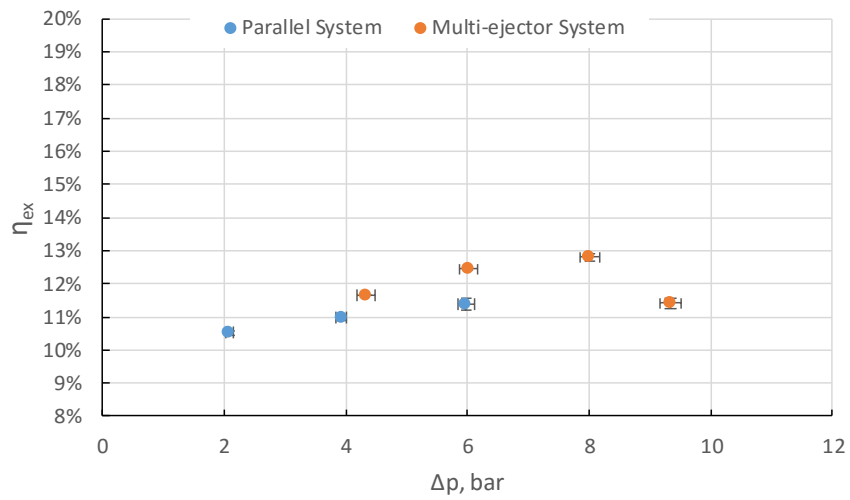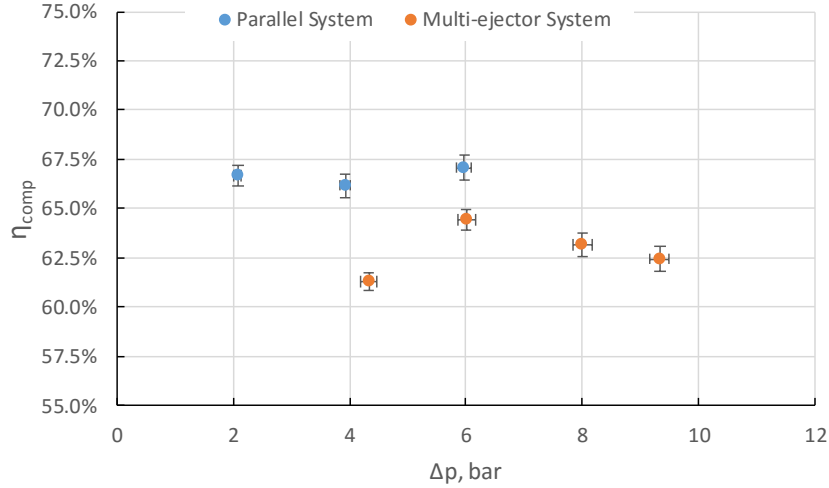
(b) Exergy efficiency

(c) The overall compressors efficiency

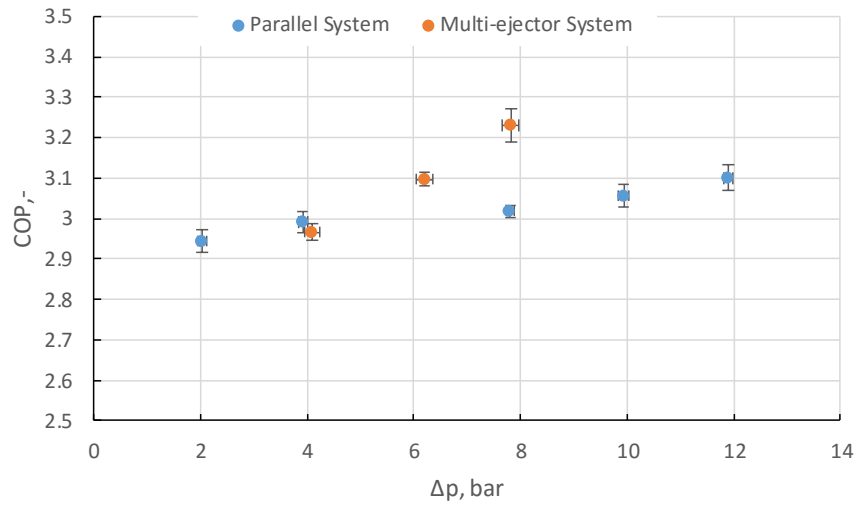Constant parameters: T_{51}=15 ^{o}C ± 0.4 K T_{6}=32 ^{o}C ± 0.5 K

Figure 6.15:   System performance characteristics vs. the tanks pressure lift (Δp) for the parallel system and the multi-ejector system for T_{51} of 15 ^{o}C and T_{6} of 32 ^{o}C: (a) COP, (b) exergy efficiency and (c) overall compressors efficiency.

Figure 6.16 shows system performance characteristics, depending on the tanks pressure lift (Δp), of both systems for the 2nd cooling demand (T_{51}=15 ^{o}C) and the exit gas cooler temperature (T_{6}) of 30 ^{o}C. In these operating conditions, the COP and the exergy efficiency improvements of the multi-ejector system can be noticed for every reached conditions.

The highest value of COP 3.19 was gained by the multi-ejector system for Δp of 8 bar. In addition, the overall compressors efficiency for the multi-ejector system was slightly smaller than that of the parallel system. The multi-ejector system for Δp of 6 bar reached the highest exergy efficiency of 13.8%, as a result of the value of the overall compressors efficiency over 65%. The parallel system gained the highest value of COP 3.10 and the exergy efficiency 12.9% for Δp of 6 bar.
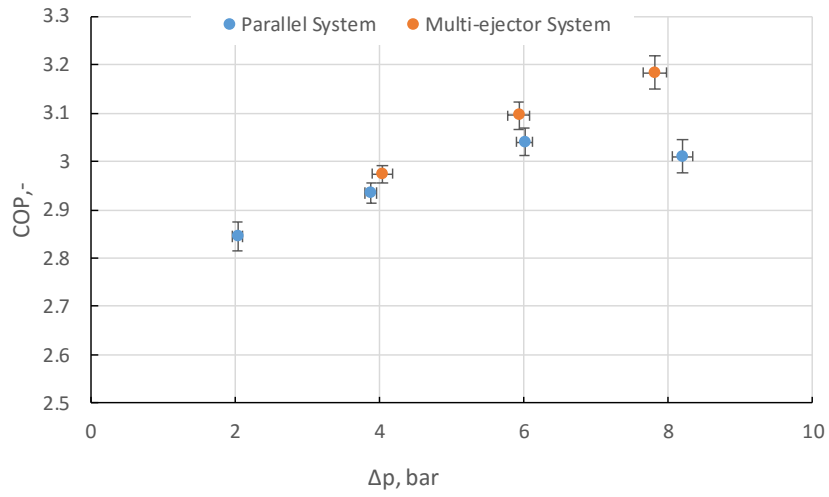
(a) Coefficient of Performance
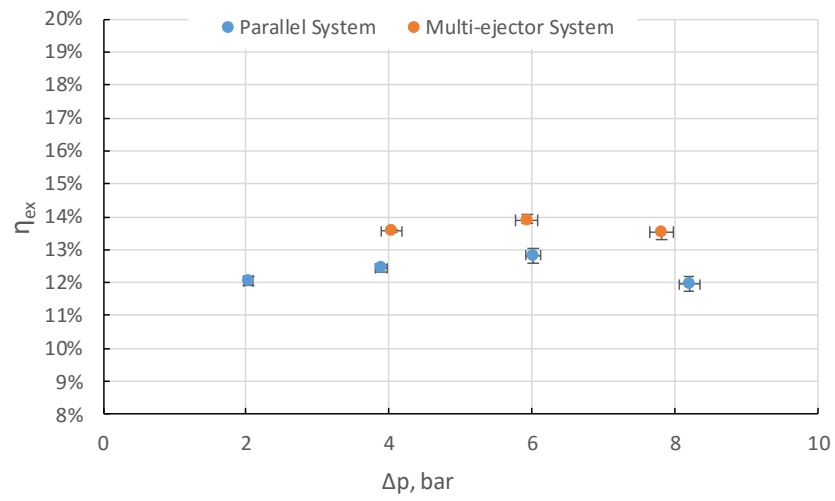
(b) Exergy efficiency
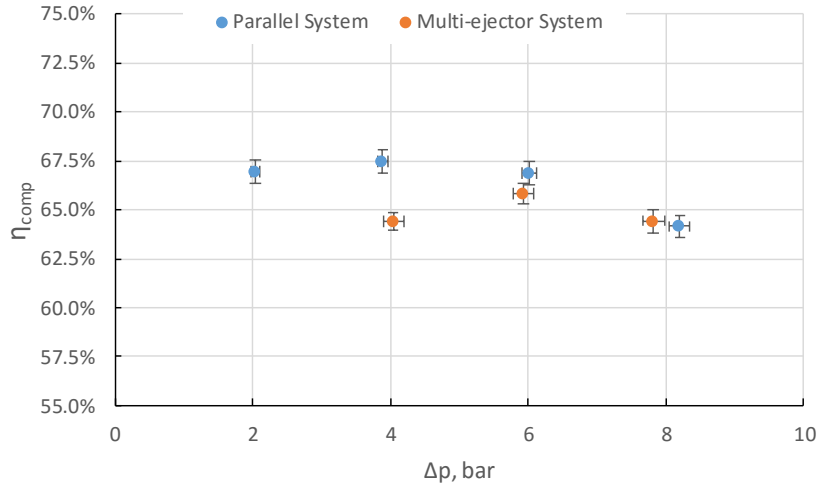
(c) The overall compressors efficiency

Constant parameters: T_{51}=15 $^{\circ}$C ± 0.4 K T_6=30 $^{\circ}$C ± 0.5 K

Figure 6.16:   System performance characteristics vs. the tanks pressure lift (Δp) for the parallel system and the multi-ejector system for T_{51} of 15 $^{\circ}$C and T_6 of 30 $^{\circ}$C: (a) COP, (b) exergy efficiency and (c) overall compressors efficiency.

For the exit gas cooler temperature of 28 $^{\circ}$C and the 2nd cooling demand (T_{51}=15°C), the system performance characteristics, depending on the tanks pressure lift, of compared refrigeration systems are shown in Figure 6.17. During the experimental investigation for Δp of 6 bar, the parallel system was not able to achieve steady state conditions, thereby the system performance characteristic for selected tanks pressure lift were omitted. The multi-ejector reached better the energy and the exergy performance above Δp= 4 bar. The parallel system gained higher values of COP and exergy efficiency for Δp of 2 bar as the result of the approximately 5% higher value of the overall compressors efficiency than that the multi-ejector system. The highest values of COP and the exergy efficiency were gained by the multi-ejector system for Δp= 6 bar and of 3.53 and 15.4%, respectively.

Comparing the overall compressors efficiency for both systems, showed in Figure 6.17, it can be noticed that for the multi-ejector system, the efficiency values were over or close to 65%, apart from the case of Δp= 2 bar as a result of significant share of the parallel compressor section in the overall power consumption. The rapid drop of the overall compressors

efficiency for the parallel system was caused by switch of the parallel compressor #1 (Dorin CD1000H) into the parallel compressor #2 (Dorin CD380H), which was characterized much worse compressor and volumetric efficiency.
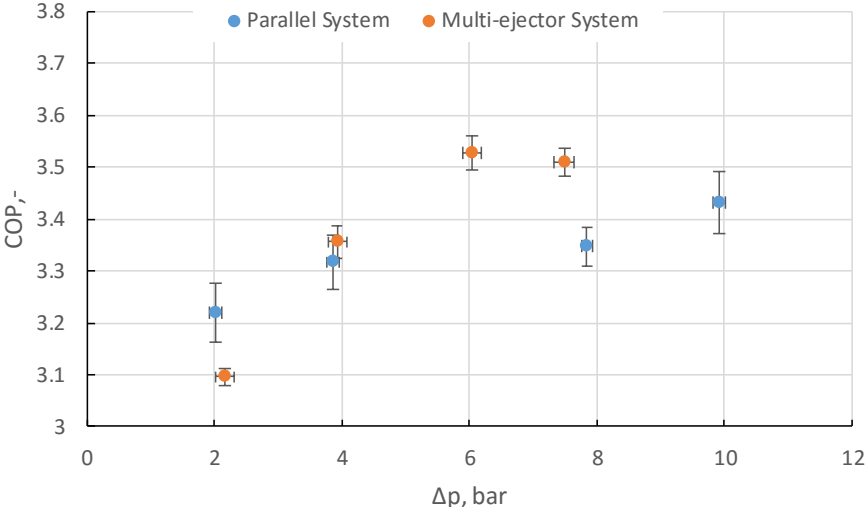
(a) Coefficient of Performance
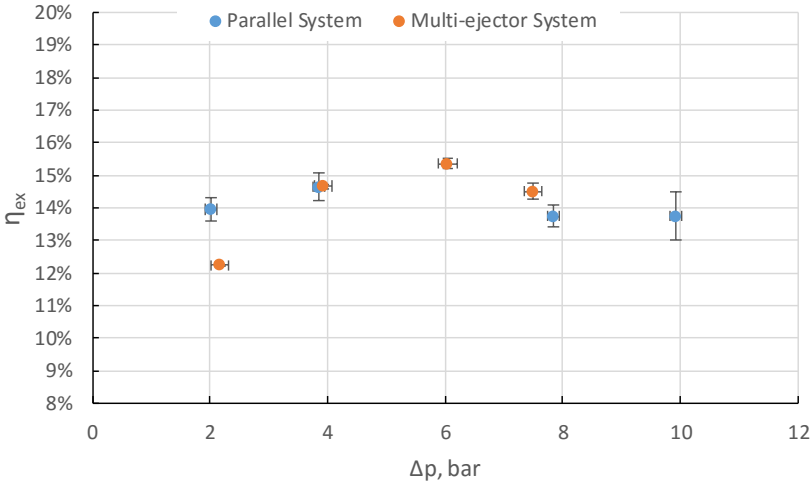
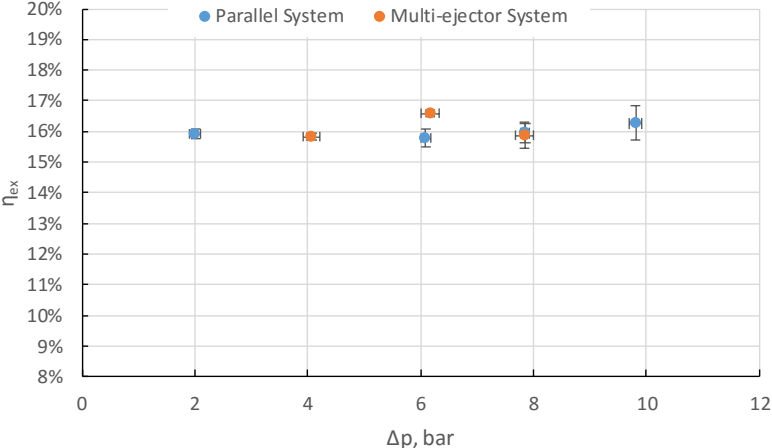(b) Exergy efficiency
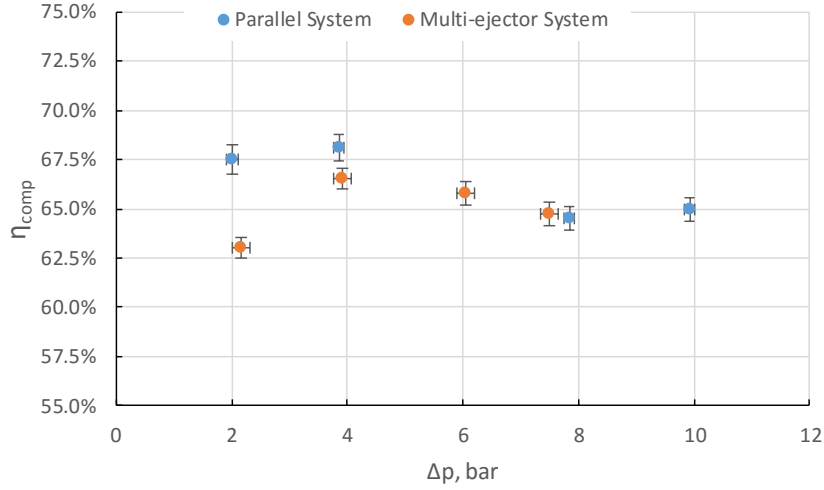
(c) The overall compressors efficiency

Constant parameters: T_{51}=15 $^{\circ}$C ± 0.4 K T_6=28 $^{\circ}$C ± 0.5 K

Figure 6.17:   System performance characteristics vs. the tanks pressure lift ($\mathit{\Delta p}$) for the parallel system and the multi-ejector system for T_{51} of 15 $^{\circ}$C and T_6 of 28 $^{\circ}$C: (a) COP, (b) exergy efficiency and (c) overall compressors efficiency.

Figure 6.18 presents the system performance characteristics, depending on the tanks pressure lift (Δp) of both refrigeration systems for the 2nd cooling demand (T_{51}=15 $^{\circ}$C) and for the exit gas cooler temperature (T_6) of 26°C. The highest values of COP 3.92 and the exergy efficiency 17.0% were gained by the multi-ejector system for $\mathit{\Delta p}$= 6 bar. For the same operating conditions, the multi-ejector system worked with the higher overall compressors efficiency than the parallel system. The parallel system reached the highest value of COP 3.7 and the exergy efficiency 16.1% for $\mathit{\Delta p}$ of 8 bar.
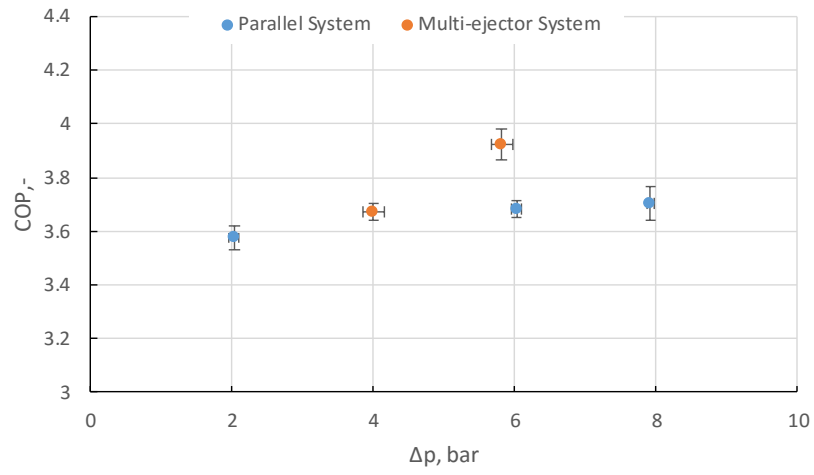
(a) Coefficient of Performance
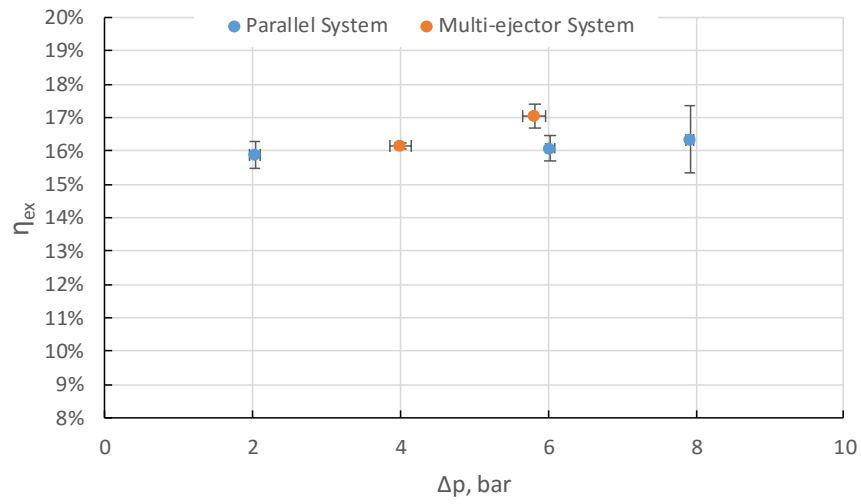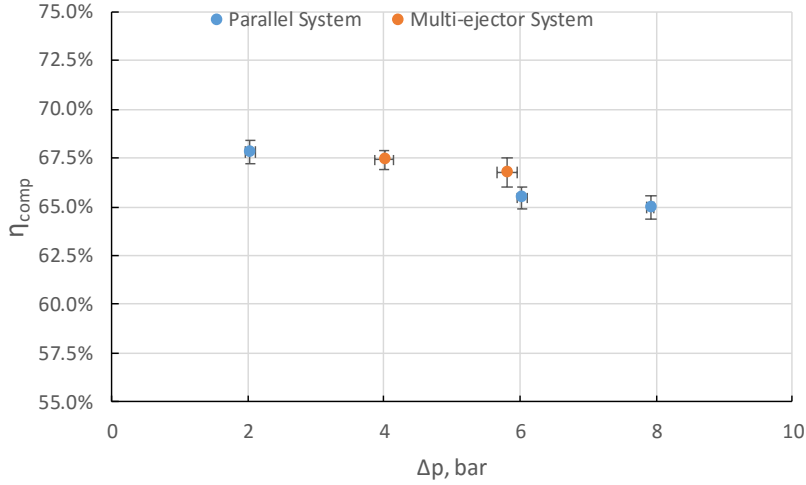
(b) Exergy efficiency

(c) The overall compressors efficiency

Constant parameters: $T_{51}=15\ ^{o}C \pm 0.4\ K$ $T_6=26\ ^{o}C \pm 0.5\ K$

Figure 6.18:   System performance characteristics vs. the tanks pressure lift (Δp) for the parallel system and the multi-ejector system for T_{51} of 15 ^{o}C and T_6 of 26 ^{o}C: (a) COP, (b) exergy efficiency and (c) overall compressors efficiency.

Similarly to the results for the 1st cooling demand, the COP and the exergy improvements of the-multi ejector system results are calculated and presented in Table 6.5. In addition, the multi-ejector module efficiency η_{ej} and the relative change of the overall compressor efficiency after the run of the multi-ejector block $\Delta\eta_{comp}$ are set. It can be noticed that for the higher Δp, the multi-ejector gains the best improvements. For the small tanks pressure lift, the overall compressor efficiency of the multi-ejector system is relatively low, which significantly influences the values of energy and exergy improvements. Hence, the smallest cooling effectiveness of the multi-ejector system is for $\Delta p = 2$ bar and $T_6 =28\ ^{o}$C. The multi-ejector system improves the COP by up to 6.52% for $T_6 =26\ ^{o}$C and $\Delta p=6$ bar in comparison to the reference system. The highest exergy improvement of the multi-ejector system is reached for $T_6 = 30\ ^{o}$C and $\Delta p = 8$ bar up to 13.17% due to comparable value of the overall compressors efficiency between both systems. For the same operating condition COP improvement is of 5.77%, as the highest improvement for the exit gas cooler temperature $T_6 = 30\ ^{o}$C.

It can be noticed that the energy performance improvement of the multi-ejector system was strongly related to the relative change of the overall compressor efficiency. For $\Delta\eta_{comp} > -5\%$ the multi-ejector system improved COP and the exergy efficiency. Therefore, the combination of the multi-ejector block efficiency of 23.27% and the relative change of the overall compressor efficiency of 1.99% reached the best COP improvement for $\Delta p = 6.1$ bar and for $T_6 = 26\ ^{o}C$.

Based on results presented in Table 6.5, the use of the multi-ejector module improved the energy performance for $\Delta p > 4$ bar, when $T_6 < 32\ ^{o}C$ and for $\Delta p = 6$ bar, when $T_6 = 32\ ^{o}C$. The exergy improvement of the multi-ejector system related to the parallel system was for $\Delta p > 4$ bar, when $T_6 \leq 32\ ^{o}C$.

Table 6.5: COP and exergy efficiency improvement of the R744 multi-ejector system relative to the R744 parallel system, the multi-ejector block efficiency (η_{ej}) and the relative change of the overall compressors efficiency ($\Delta\eta_{comp}$) for the 2nd cooling demand ($T_{51} = 15^{o}C$), related to the exit gas cooler temperature T_6 and the tanks pressure lift Δp.

T_6	Δp	$COP_{improvement}$	$\eta_{ex,improvement}$	η_{ej}	$\Delta\eta_{comp}$
$36\ ^{o}C \pm 0.1$ K	6.2 bar $\pm$ 0.1 bar	-0.18% $\pm$ 0.01%	-6.93% $\pm$ 0.07%	30.98% $\pm$ 0.33% VEJ3+VEJ2+VEJ1	-10.26% $\pm$ 0.11%
$34\ ^{o}C \pm 0.1$ K	5.8 bar $\pm$ 0.1 bar	-1.07% $\pm$ 0.01%	-7.52% $\pm$ 0.05%	31.23% $\pm$ 0.38% VEJ3+VEJ2+VEJ1	-7.61% $\pm$ 0.05%
$32\ ^{o}C \pm 0.2$ K	4.1 bar $\pm$ 0.1 bar	-2.1% $\pm$ 0.02%	5.98% $\pm$ 0.05%	33.07% $\pm$ 0.42% VEJ3+VEJ2+VEJ1	-7.35% $\pm$ 0.05%
$32\ ^{o}C \pm 0.1$ K	6.3 bar $\pm$ 0.1 bar	3.52% $\pm$ 0.05%	9.37% $\pm$ 0.16%	29.68% $\pm$ 0.49% VEJ3+VEJ2+VEJ1	-3.94% $\pm$ 0.05%
$30\ ^{o}C \pm 0.1$ K	4.0 bar $\pm$ 0.1 bar	1.35% $\pm$ 0.01%	8.94% $\pm$ 0.97%	32.82% $\pm$ 0.41% VEJ3+VEJ2+VEJ1	-4.52% $\pm$ 0.05%
$30\ ^{o}C \pm 0.2$ K	6.0 bar $\pm$ 0.1 bar	1.80% $\pm$ 0.02%	8.24% $\pm$ 0.16%	27.69% $\pm$ 0.35% VEJ3+VEJ2+VEJ1	-1.57% $\pm$ 0.02%
$30\ ^{o}C \pm 0.1$ K	8.0 bar $\pm$ 0.2 bar	5.77% $\pm$ 0.10%	13.17% $\pm$ 0.35%	13.11% $\pm$ 0.17% VEJ3+VEJ2+VEJ1	0.44% $\pm$ 0.01%
$28\ ^{o}C \pm 0.1$ K	2.1 bar $\pm$ 0.1 bar	-3.84% $\pm$ 0.07%	-12.37% $\pm$ 0.27%	33.36% $\pm$ 0.40% VEJ3+VEJ2+VEJ1	-6.62% $\pm$ 0.08%
$28\ ^{o}C \pm 0.2$ K	3.9 bar $\pm$ 0.1 bar	1.16% $\pm$ 0.02%	0.14% $\pm$ 0.01%	31.48% $\pm$ 0.39% VEJ3+VEJ2+VEJ1	-2.29% $\pm$ 0.03%

| 28 °C ± 0.2 K | 7.7 bar ± 0.1 bar | 4.84% ± 0.07% | 5.54% ± 0.17% | 9.51% ± 0.12% VEJ3+VEJ2+VEJ1 | 0.34% ± 0.01% |
| 26 °C ± 0.2 K | 6.1 bar ± 0.1 bar | 6.52% ± 0.12% | 5.98% ± 0.20% | 23.27% ± 0.26% VEJ3+VEJ2+VEJ1 | 1.99% ± 0.03% |

6.2.3 Influence of The Overall Compressors Efficiency on The System Energy Performance

For the same working conditions, the significant difference of the overall compressors efficiency between both refrigeration systems has an essential influence on the system performance. The sum of electric power consumption of each compressor can be calculated as the overall isentropic power of compressors divided by the overall compressors efficiency.

$$\sum_{i=1}^{n} N_{el,i} = \frac{N_{is}}{\eta_{comp}} \tag{6.1}$$

Therefore, COP of each refrigeration system, assuming that the refrigeration heat capacity ($\dot{Q}_{evap}$) and the overall isentropic power (N_{is}) are constant for the specific operating conditions, dependent only on the thermodynamic parameters (temperature, pressure, mass flow rate), can be defined as a function of the variable overall compressors efficiency.

$$COP(\eta_{comp}) = \eta_{comp} \cdot \left(\frac{\dot{Q}_{evap}}{N_{is}}\right) \tag{6.2}$$

Where:

$$\begin{aligned} \eta_{comp} &\in \langle 0; 1 \rangle \\ \dot{Q}_{evap} &= const \\ N_{is} &= const \end{aligned} \tag{6.3}$$

The linear function of COP depending on the overall compressors efficiency allows to compare the value of COP of both systems for the same overall compressors efficiency. Figure 6.19 shows COP functions of the multi-ejector and the parallel systems, depending on the overall compressors efficiency, relating to constant working conditions. Both functions presented in Figure 6.19 were performed based on the experimental results for T_{51} of 12 °C, T_6 of 34 °C, and Δp of 6 bar. It can be noticed that at the same value of the overall compressors efficiency, the multi-ejector system obtained higher value of COP. As an example for $\eta_{comp} = 70\%$, the COP improvement of the multi-ejector block was equal to 9%.
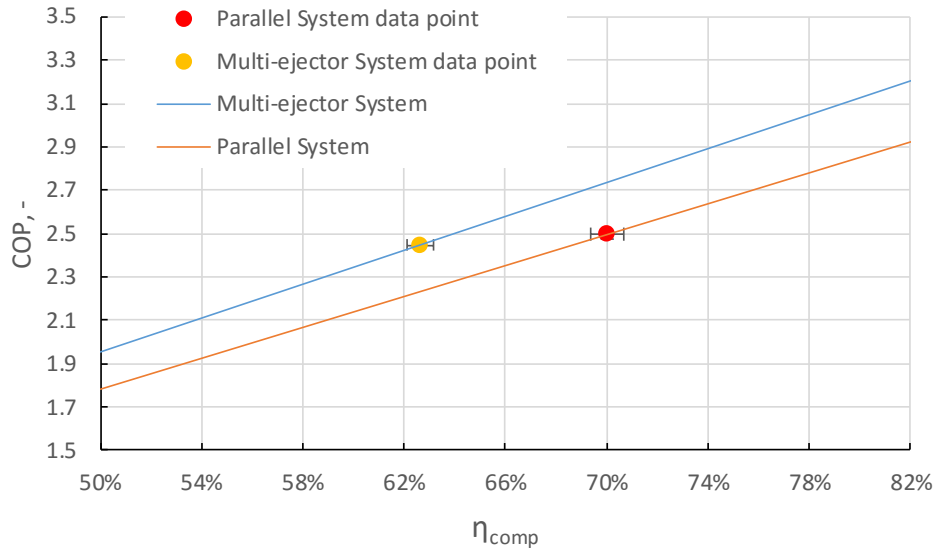
Constant parameters: T_{51}=12 $^{\circ}$C $\pm$ 0.4 K T_6=34 $^{\circ}$C $\pm$ 0.5 K Δp=6 bar $\pm$ 0.14 bar

Figure 6.19:   COP vs. the overall compressors efficiency (η_{comp}).

Figure 6.20 shows COP functions of the multi-ejector system, depending on the overall compressors efficiency, for each tanks pressure lift achieved for the experimental investigation. In addition, the experimental results for each pressure lift were added. It can be seen that for the same overall compressors efficiency, the multi-ejector refrigeration system obtains the highest COP for the possible highest pressure lift in the multi-ejector pack. As an example for η_{comp} = 70%, the COP improvement of the multi-ejector system for Δp=8 bar $\pm$ 0.2 bar in comparison to Δp=2 bar $\pm$ 0.2 bar is of 10%. Therefore, the pressure level in liquid receiver should be set on relatively high value in order to improve energy performance of the multi-ejector system.
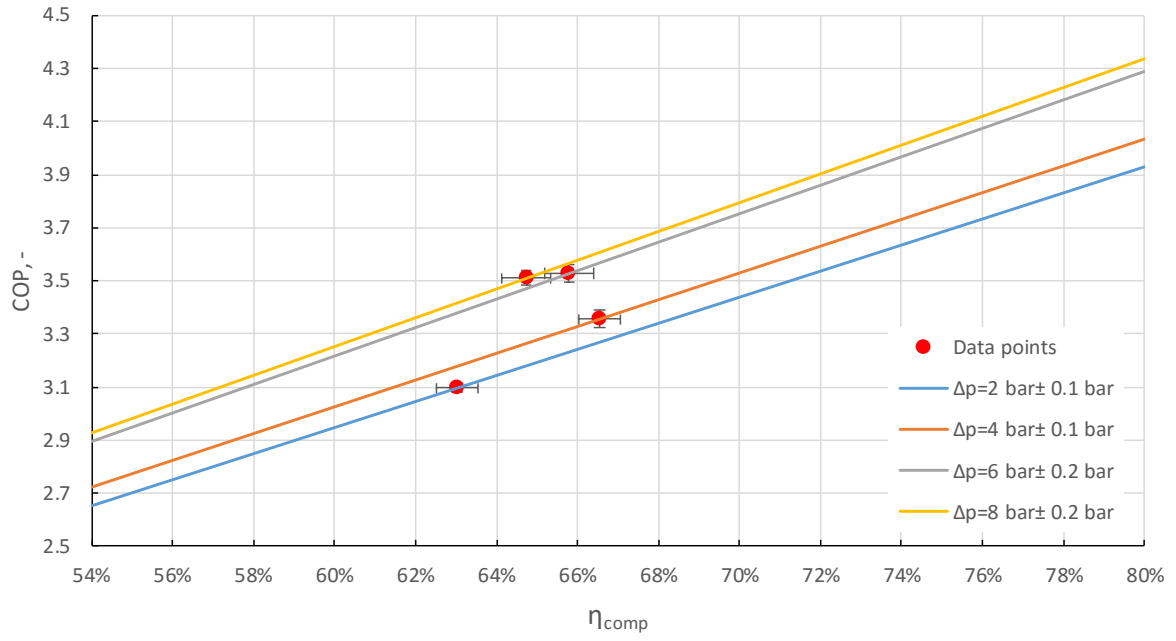
Constant parameters: $T_{51}=15\ ^{o}C \pm 0.4\ K$ $T_6=28\ ^{o}C \pm 0.5\ K$

Figure 6.20: COP vs. the overall compressors efficiency (η_{comp}) of the multi-ejector system.

7 Conclusion

Experimental investigation of R744 vapour compression rack, equipped with the multi-ejector expansion pack, was performed, based on the first law and the second law analysis. The results were compared to the R744 vapour compression rack with high-pressure electronic expansion valve, as an expansion device. The test facility was designed to operate in both alternative configurations. Comparison was carried out for two refrigeration loads and both refrigeration systems were operated in transcritical and subcritical mode. Apart from the system performance comparison, influence of the pressure level in the flash tank on the system performance for both alternatives was analysed.

The experimental results indicated the maximum COP improvement of the CO_2 multi-ejector system of up to 7% for the working conditions around the critical point and the upper limit of the flash gas pressure, for which the multi-ejector pack can be utilized. The range of pressure lift in the configuration with the multi-ejector block was smaller than for the reference system due to the significantly decreased mass entrainment ratio and the ejectors efficiency. The range of the flash tank pressure level for the R744 multi-ejector system was dependent of the motive side parameters of the ejectors (temperature, pressure). For every gas cooler working condition, investigated in this thesis, the maximum COP of the R744 multi-ejector system was obtained for relatively high pressure in the flash tank, close to the upper limit of the multi-ejector pack utilization. During decreasing of the gas cooler/ condenser exit parameters, the value of COP increased for both configurations.

The second law analysis reported that the utilization of the multi-ejector expansion pack in the R744 vapour compression rack improved exergy efficiency up to 13% for the working conditions around the critical point and the same upper limit of the flash tank as for the first law analysis. Similarly to the COP evaluation of the R744 multi-ejector system, the maximum exergy efficiency was indicated for the relatively high value of the flash tank pressure, close to upper limit of the multi-ejector pack utilization and relatively low exit gas cooler/ condenser parameters.

The evaluation of the performance improvement of the R744 multi-ejector system was strongly related to the utilized compressors efficiencies. The high load and low-effective compression of the parallel compressors caused growth of electric power consumption and

decrease of the COP and exergy efficiency. Therefore, the significant work degradation of the rack of compressors did not provide the improvement of the R744 multi-ejector system for respectively low pressure lift. The comparable overall compressors efficiency of both configurations may indicate the COP and the second law improvement for all working range of the flash tank pressure. It was also noticed that the comparable high-efficiency of the rack of compressors obtained the best performance of the R744 vapour compression rack with the multi-ejector expansion pack, for the upper limit of the pressure lift.

The multi-ejector block worked more steadily for the relatively high refrigeration load. The experimental results reported the multi-ejector block efficiency of up to 33% depending on motive and suction side parameters, and the pressure lift. The highest efficiencies of the ejectors were obtained for relatively low pressure lift. During decreasing of the gas cooler parameters, the multi-ejector block efficiency decreased too due to drop of the CO_2 motive mass flow rate and simultaneously decreased of the mass entrainment ratio. The multi-ejector block reached wider range of the pressure lift for the higher refrigeration load.

The significant difference between the efficiencies of the rack of compressors for each refrigeration systems influenced negatively the energy and exergy performance improvements of the R744 refrigeration system with the ejectors expansion pack. Therefore, the evaluation of system performance with the ejectors expansion pack for the comparable high-efficiently rack of compressors need to be done for further works. In addition, the rack of compressors in the test facility should be adapted to significantly increase of the parallel compressors load during the utilization of the ejectors pack.

References

AHAMED, J. U., SAIDUR, R. & MASJUKI, H. H. 2011. A review on exergy analysis of vapor compression refrigeration system. *Renewable and Sustainable Energy Reviews,* 15**,** 1593-1600.

BANASIAK, K., HAFNER, A. & ANDRESEN, T. 2012. Experimental and numerical investigation of the influence of the two-phase ejector geometry on the performance of the R744 heat pump. *International Journal of Refrigeration,* 35**,** 1617-1625.

BANSAL, P. 2012. A review – Status of CO2 as a low temperature refrigerant: Fundamentals and R&D opportunities. *Applied Thermal Engineering,* 41**,** 18-29.

CHAIWONGSA, P. & WONGWISES, S. 2007. Effect of throat diameters of the ejector on the performance of the refrigeration cycle using a two-phase ejector as an expansion device. *International Journal of Refrigeration,* 30**,** 601-608.

CHESI, A., ESPOSITO, F., FERRARA, G. & FERRARI, L. 2014. Experimental analysis of R744 parallel compression cycle. *Applied Energy,* 135**,** 274-285.

DA SILVA, A., BANDARRA FILHO, E. P. & ANTUNES, A. H. P. 2012. Comparison of a R744 cascade refrigeration system with R404A and R22 conventional systems for supermarkets. *Applied Thermal Engineering,* 41**,** 30-35.

DENG, J. Q., JIANG, P. X., LU, T. & LU, W. 2007. Particular characteristics of transcritical CO2 refrigeration cycle with an ejector. *Applied Thermal Engineering,* 27**,** 381-388.

ELBEL, S. 2011. Historical and present developments of ejector refrigeration systems with emphasis on transcritical carbon dioxide air-conditioning applications. *International Journal of Refrigeration-Revue Internationale Du Froid,* 34**,** 1545-1561.

ELBEL, S. & HRNJAK, P. 2008. Experimental validation of a prototype ejector designed to reduce throttling losses encountered in transcritical R744 system operation. *International Journal of Refrigeration-Revue Internationale Du Froid,* 31**,** 411-422.

FANG, G., XING, L., YANG, F. & LI, H. 2005. Exergy analysis of a dual-mode refrigeration system for ice storage air conditioning. *International Journal of Architectural Science,* 6**,** 6.

GE, Y. T. & TASSOU, S. A. 2011. Thermodynamic analysis of transcritical CO2 booster refrigeration systems in supermarket. *Energy Conversion and Management,* 52**,** 1868-1875.

GETU, H. M. & BANSAL, P. K. 2008. Thermodynamic analysis of an R744–R717 cascade refrigeration system. *International Journal of Refrigeration,* 31**,** 45-54.

GIROTTO, S., MINETTO, S. & NEKSA, P. 2004. Commercial refrigeration system using CO2 as the refrigerant. *International Journal of Refrigeration,* 27**,** 717-723.

HAFNER, A., FORSTERLING, S. & BANASIAK, K. 2014. Multi-ejector concept for R-744 supermarket refrigeration. *International Journal of Refrigeration-Revue Internationale Du Froid,* 43**,** 1-13.

JAKOBSEN, A., RASMUSSEN, B. D. & ANDERSEN, S. E. 1999. CoolPack – Simulation tools for refrigeration systems. *Scanref,* 28**,** 7-10.

KIM, M. H., PETTERSEN, J. & BULLARD, C. W. 2004. Fundamental process and system design issues in CO2 vapor compression systems. *Progress in Energy and Combustion Science,* 30**,** 119-174.

KORNHAUSER, A. A. 1990. The Use of an Ejector as a Refrigerant Expander. *International Refrigeration and Air Conditioning Conference.* Purdue University: Purdue e-Pubs.

LAMBERS, K. J. 2008. Isentropic and Volumetric Efficiencies for Compressors with Economizer Port. *International Compressor Engineering Conference.* Purdue.

LAWRENCE, N. & ELBEL, S. 2013. Theoretical and practical comparison of two-phase ejector refrigeration cycles including First and Second Law analysis. *International Journal of Refrigeration-Revue Internationale Du Froid,* 36**,** 1220-1232.

LEMMON, E. W., HUBER, M. L. & MCLINDEN, M. O. 2013. NIST Standard Reference Database 23: Reference Fluid Thermodynamic and Transport Properties-REFPROP. *Standard Reference Data Program.* 9.1 ed. Gaithersburg: National Institute of Standards and Technology.

LI, D. & GROLL, E. A. 2005. Transcritical CO2 refrigeration cycle with ejector-expansion device. *International Journal of Refrigeration,* 28**,** 766-773.

LIAO, S. M., ZHAO, T. S. & JAKOBSEN, A. 2000. A correlation of optimal heat rejection pressures in transcritical carbon dioxide cycles. *Applied Thermal Engineering,* 20**,** 831-841.

LORENTZEN, G. 1990. Trans-critical vapour compression cycle device. Google Patents.

MENEGAY, P. & KORNHAUSER, A. A. Improvements to the ejector expansion refrigeration cycle. Energy Conversion Engineering Conference, 1996. IECEC 96., Proceedings of the 31st Intersociety, 11-16 Aug 1996 1996. 702-706 vol.2.

MOBLEY, K. 1999. Glossary. *In:* MOBLEY, K. (ed.) *Root Cause Failure Analysis.* Burlington: Butterworth-Heinemann.

MOFFAT, R. J. 1988. Describing the uncertainties in experimental results. *Experimental Thermal and Fluid Science,* 1**,** 3-17.

PEARSON, A. 2005. Carbon dioxide—new uses for an old refrigerant. *International Journal of Refrigeration,* 28**,** 1140-1148.

SARKAR, J. 2009. Performance characteristics of natural-refrigerants-based ejector expansion refrigeration cycles. *In:* DEPARTMENT OF MECHANICAL ENGINEERING, I. O. T., BHU, VARANASI 221005, INDIA (ed.). Varanasi.

SARKAR, J. & AGRAWAL, N. 2010. Performance optimization of transcritical CO2 cycle with parallel compression economization. *International Journal of Thermal Sciences,* 49**,** 838-843.

SAWALHA, S. 2008. Theoretical evaluation of trans-critical CO2 systems in supermarket refrigeration. Part I: Modeling, simulation and optimization of two system solutions. *International Journal of Refrigeration,* 31**,** 516-524.

SAWALHA, S., KARAMPOUR, M. & ROGSTAM, J. 2015. Field measurements of supermarket refrigeration systems. Part I: Analysis of CO2 trans-critical refrigeration systems. *Applied Thermal Engineering,* 87**,** 633-647.

SCHÖNENBERGER, J. 2014. *New Bench Mark in CO2 Technology* [Online]. Bern: Frigo Consulting LTD. Available: http://www.frigoconsulting.ch/en/news/new_bench_mark_in_co2_technology.html.

SHARMA, V., FRICKE, B. & BANSAL, P. 2014. Comparative analysis of various CO2 configurations in supermarket refrigeration systems. *International Journal of Refrigeration-Revue Internationale Du Froid,* 46**,** 86-99.

SPAN, R. & WAGNER, W. 1996. A New Equation of State for Carbon Dioxide Covering the Fluid Region from the Triple-Point Temperature to 1100 K at Pressures up to 800 MPa. *Journal of Physical and Chemical Reference Data,* 25**,** 87.

SUMERU, K., NASUTION, H. & ANI, F. N. 2012. A review on two-phase ejector as an expansion device in vapor compression refrigeration cycle. *Renewable & Sustainable Energy Reviews,* 16**,** 4927-4937.

TAYLOR, B. N. & KUYATT, C. E. 1994. Guidelines for Evaluating and Expressing the Uncertainty of NIST Measurement Results. *In:* TECHNOLOGY, N. I. O. S. A. (ed.). U.S. Department of Commerce Technology.

UNITED, N. Kyoto Protocol. 1997 New York. United Nations.

UNITED NATIONS ENVIRONMENT, P. & OZONE, S. 1987. Handbook for the Montreal Protocol on Substances that Deplete the Ozone Layer.

WANG, C.-C., HAFNER, A., KUO, C.-S. & HSIEH, W.-D. 2012. An overview of the effect of lubricant on the heat transfer performance on conventional refrigerants and natural refrigerant R-744. *Renewable and Sustainable Energy Reviews,* 16**,** 5071-5086.

WIEDENMANN, E., SCHÖNENBERGER, J., HAFNER, A., BANASIAK, K. & GIROTTO, S. 2014. Effiziente Kälteerzeugung im Supermarkt mittels CO2-Booster-Kälteanlage und Ejektor. *Deutscher Kälte- und Klimatechnischer Verein e.V.* Düsseldorf: AA.

YUMRUTAŞ, R., KUNDUZ, M. & KANOĞLU, M. 2002. Exergy analysis of vapor compression refrigeration systems. *Exergy, An International Journal,* 2**,** 266-272.

A Research Paper

Experimental analysis of the R744 vapour compression rack equipped with the multi-ejector expansion work recovery module

Abstract

A test facility for experimental investigation of the R744 vapour compression rack equipped with the multi-ejector expansion work recovery module was designed and manufactured. Comparison of the R744 multi-ejector refrigeration system with the R744 parallel compression system on the same test facility was carried out based on energy performance characteristics: refrigeration capacity, power consumption, COP, and exergy efficiency. Apart from the system performance comparison, influence of the pressure level in the flash tank on the system performance for both alternatives was analysed. The experimental results indicated COP and exergy efficiency improvement of the multi-ejector refrigeration system up to 7% and 13.7%, respectively. The highest values of COP and the exergy efficiency were obtained by the multi-ejector refrigeration system for the tanks pressure lift value close to the limit value. The values of the overall compressor efficiencies were significantly differentiated, dependent on the operation module (cooling load and heat rejection conditions), which strongly influenced the values of COP and the exergy efficiency.

Keywords: multi-ejector, expansion work recovery, R744, parallel compression, COP, exergy efficiency

Nomenclature

Roman Letter

c_p	Specific heat capacity	kJ kg^{-1} K^{-1}
$\dot{E}$	Exergy rate	kW

h	Specific enthalpy	kJ kg^{-1}
s	Specific entropy	kJ kg^{-1} K^{-1}
$\dot{m}$	Mass flow rate	kg s^{-1}
N	Power	kW
p	Pressure	bar
T, t	Temperature	K, $^{\circ}$C
W	Work rate	kW

Greek Letters

η	Efficiency	
Φ	Mass entrainment ratio	
Π	Pressure Ratio	
ρ	Density	kg m^{-3}
ψ	Specific exergy	kJ kg^{-1}

Subscripts

comp	Compressor
ej	Ejector
el	Electric power
evap	Evaporator
ex	Exergy
gc	Gas cooler
gl	Glycol
hp	High pressure
in	Inlet
incr	Increment

is	Isentropic
max rec	Maximum work recovery
me	Electric-mechanical motor
motive	The motive parameter
multi-ejector	The multi-ejector system
parallel	The parallel system
suction	The suction parameter
vol	Volumetric

Abbreviations

CD1400H	Base-load Compressor Dorin CD1400H
CD1000H	Parallel Compressor Dorin CD1000H
CD380H	Parallel Compressor Dorin CD380H
COP	Coefficient of performance
HPV	High-pressure electronic expansion valve
IHX	Internal Heat Exchanger
MT	Medium-temperature level
VEJ	Vapour Ejector number

1. Introduction

Increase of using the refrigeration system, based on the natural refrigerant, in the commercial refrigeration is related to the restrictive political regulations about environment protection. environmentally friendly carbon dioxide (denoted as R744), well known natural refrigerant in the first half of twentieth century, has been commonly used in recent refrigeration systems thanks to Prof Gustav Lorentzen activities to revival of the CO_2 use in refrigeration (Pearson, 2005). In 1990 Prof Lorentzen patented the transcritical carbon dioxide system for automotive air-conditioning, what let to design and manufacture rival refrigeration systems with CO_2 as a main working fluid (Lorentzen, 1990).Carbon dioxide has the low critical temperature and the

high critical pressure. Therefore, for the surrounding temperature above the critical temperature, the refrigeration system has to reject the heat from the R744 cycle in the transcritical mode, which influences on the degradation of the system performance (Kim et al., 2004). As a result of the ambient temperature influence on energy efficiency, the R744 transcritical refrigeration systems are located most frequently in the cold climate regions. Although the development of CO_2 transcritical system configuration and the development of devices included in the system let to introduce the CO_2 commercial refrigeration system in a warm climates.

The performance of the CO_2 system depends on the surrounding temperature, which determines working condition of CO_2 in transcritical, or subcritical mode. To reduce high pressure ratio in the transcritical mode, the booster system is divided into four pressure levels: low-temperature, medium-temperature, high pressure and intermediate pressure. The additional receiver on the intermediate pressure level collects R744 after the heat rejection in the gas cooler and expands the saturated refrigerant liquid into the MT and LT evaporators (Sharma et al., 2014). The saturated vapor of CO_2 from the receiver, named flash gas, is throttled to the medium-temperature pressure level, before it enters to the high-stage compressors. Girotto et al. (2004) stated that in hot climate region, the annual electric energy consumption of R744 transcritical booster system can be higher than a conventional R404A system, but in cold climate it consumed less electric energy than R404A systems during the year due to operation in subcritical mode for the higher number of hours. Therefore, R744 transcritical booster system is located mostly in Northern Europe countries (Sawalha et al., 2015).

The booster configuration with flash tank reduces the throttling losses by increase of the specific enthalpy difference in evaporator. Although, throttled flash gas to the MT level do not provide any useful effect. In order to advantageously use of the flash gas, it can be done by means of an auxiliary compressor. The parallel compression concept allows to compression the saturated CO_2 gas phase from the flask tank with a lower pressure ratio (Chesi et al., 2014). This system is applied to increase energy performance of a refrigeration system during summertime in hot climates (Bansal, 2012). Sarkar and Agrawal (2010) compared performance of three different parallel compression configuration. Authors determined that the parallel compression economized system (flash gas directly compressed by the parallel compressors section) achieves 47% COP improvement over the basis CO_2

transcritical refrigeration cycle for the chosen ranges of operating conditions. Chesi et al. (2014) investigated experimental analysis of the R744 parallel compression system, based on energy performance analysis for different compressors discharge pressures, exit gas cooler temperatures and evaporation pressures. In addition, the influence of the flash tank separation capacity and the compressors volumetric flow ratio were analysed. According to Chesi et al. (2014), the ideal parallel compression cycle can reach COP improvements of over 65% and over 30% in terms of negligible pressure loss, considered perfect liquid-vapour separator and certain controlled value of the superheating. Authors identified the influence of compressors volumetric flow ratio closely linked to the flash tank pressure and the separator efficiency on the system performance.

Experimental and theoretical analysis indicates that replacing the expansion valve by the ejector in CO_2 transcritical vapour compression cycle improves energy performance and reduces exergy losses of the cycle (Sumeru et al., 2012). Therefore, the evaluation of system performance for new, or existing R744 refrigeration system equipped with the ejector expansion pack in the supermarket has to be carried out.

Hafner et al. (2014) presented ejector technology for supermarket applications and carried out analysis of simulation model of the multi-ejector system and the reference CO_2 transcritical booster system for the selected operating conditions like load profiles, controls concept and climate data. The transient simulations were performed based on the annual variable ambient temperature and annual variable load profiles for heating and cooling mode, for three different climate regions: North European, Middle European and Mediterranean. In addition, experimental analysis of both foregoing refrigeration systems was presented. To simplify the refrigeration systems, calculations were done for only medium-temperature evaporation level due to fact that for both systems less than 20% of the overall cooling capacity is provided for the low-temperature cabinets (Hafner et al., 2014). According to (Hafner et al., 2014), for a steady-state analysis, the COP of the R744 multi-ejector refrigeration system improved in comparison to the reference system by up to 10% and 20% at the ambient temperature 15 $^{\circ}$C and 45 $^{\circ}$C, respectively. The transient simulations indicated significant COP improvement of the multi-ejector system for cooling and heating mode. For selected climate zone, the COP for cooling mode increased between 20% and 30% during the winter and 17% in Mediterranean, 16% in Middle European, and 5% in Northern European countries during the summer.

Wiedenmann et al. (2014) presented work of R744 transcritical parallel compression refrigeration system in Migros Bulle supermarket after the integration of the ejectors. Wiedenmann et al. (2014) stated that the annual energy power consumption, depending on the climate region, of the refrigeration system with integrated ejectors was in the range of 12% to 20% less than the reference system.

Applying multi-ejector module in CO_2 transcritical refrigeration system could reduce the power consumption of overall system in supermarket as has already been proved by Hafner et al. (2014), Wiedenmann et al. (2014). As a result of high-efficiency work, the CO_2 refrigeration system equipped with the ejector pack can be much more competitive solution in throughout climate regions (Sumeru et al., 2012). However, there are still small number of papers interested in the modern R744 transcritical refrigeration system equipped with the ejector expansion module. Hence, the study on the ejector technology in commercial CO_2 refrigeration system is required.

2. Test facility

Figure 21 illustrates the pipeline and instrumentation diagram of R744 loop of the test rig, which includes all main components For the experimental investigation, the peak-load evaporator was not utilized, because the base-load evaporator had enough refrigeration capacity for set loads. The multi-ejector test rig has only medium temperature evaporator in order to simplify the system. The pressure level in the evaporator is controlled by the metering expansion valve. The suction accumulator tank (liquid receiver in Figure 21) delivers saturated, or superheated vapour to the compressor and to the suction side of the vapor ejectors (VEJ) in multi-ejector block. In addition, it can supply liquid phase of CO_2 to the suction side of liquid ejector (LEJ), which enables to utilize the evaporator in flooded mode. In thermodynamic point of view the decrease of the evaporation temperature in the flooded mode improves the performance of the system. However, during the experimental investigation the liquid ejectors were omitted and the evaporator had set the superheat in order to investigate the system performance improvement of the R744 vapour compression system with the vapour ejectors.

The vapor phase of CO_2 from suction accumulator is delivered to medium temperature compressor, where it is compressed to set discharge pressure. The compressor rack consists of

medium temperature compressor and two parallel compressors that compressed the gas from the liquid separator (denoted also as the pressure receiver tank or the flash tank). The liquid separator has to deliver saturated liquid to the evaporator. The system has a flash valve to throttle the vapor from the pressure receiver tank if the parallel compressors do not have to be utilized. The pressure level in the receiver is governed by either parallel compressors or flash valve. The vapor phase of CO_2 from the both receivers flows through the additional internal heat exchangers and absorbs the heat from the high-pressure CO_2, after the gas coolers section, in order to safety of the compressors. After the compression, stream flows through the two gas cooler stages. The high-pressure of CO_2 behind the gas cooler section can be reduced either by high-pressure electronic expansion valve (HPV), or by the multi-ejector pack, with assistance of HPV. During the investigation, the largest vapour ejector number 4 (VEJ4) was omitted due to too high capacity of the ejector module. The test rig has a separate loop of lubricant. The oil receiving loop contains the high-pressure separator, behind the compressor rack, and the receivers installed together with the CO_2 tanks. Integration of lubricant separators results in the heat transfer improvement in heat exchangers and the minimization of an annual leakage of the lubricant (Wang et al., 2012).
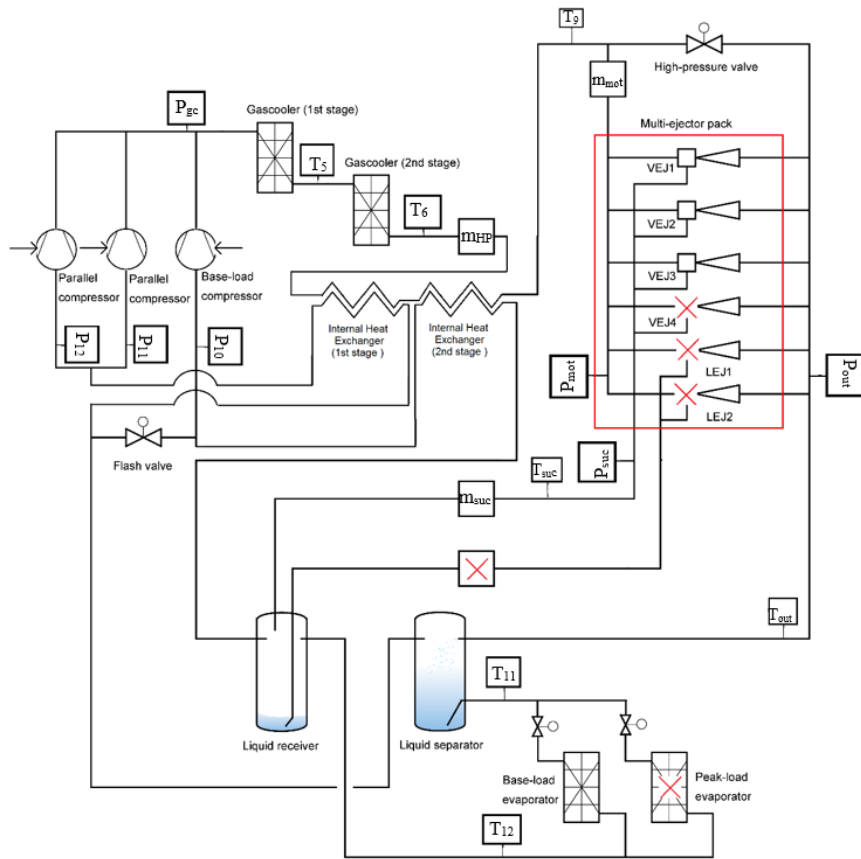
Figure 21- P&ID diagram of CO_2 loop in R744 multi-ejector refrigeration test rig, with omitted the peak-load evaporator, the vapour ejector VEJ4 and both liquid ejector during the experimental investigation.

In order to provide cooling and heating in the gas cooler section and in the evaporator, the test facility has got an auxiliary glycol loop and additional cooling water loop. Simplified schema of auxiliary loops is shown in Figure 22. The glycol unit consists of the glycol tank and two separated evaporator and gas cooler loops, respectively. Aim of both coolant loops was to absorb the heat from first stage of the gas cooler and reject the heat in evaporator. The glycol is delivered to heat exchangers by two pumps manufactured by Grundfos. The cooling water cycle decreases the temperature of CO_2 in the second stage of the gas cooler until R744 expands to pressure receiver tank. Therefore, the exit gas cooler temperature of R744 is regulated by mass flow rate of cooling water. The glycol stream flowed through the gas cooler can be cooled by additional cooling water network loop, but for presented investigations was not utilized.

Figure 22- P&ID diagram of auxiliary loops in R744 multi-ejector refrigeration test rig, with omitted the peak-load evaporator and additional cooling water network during the experimental investigation.

The main components, utilized in the test facility, have been set in Table 6.The R744 multi-ejector test rig can be operated in three specific configuration of refrigeration system:

- The R744 transcritical booster system – the vapor fraction of CO_2 from liquid separator is throttled in the flash valve. The high-pressure refrigerant is throttled in high-pressure electronic valve.
- The R744 transcritical parallel system – the vapor fraction of CO_2 from liquid separator is compressed in parallel compressors section. The high-pressure refrigerant is throttled in high-pressure electronic valve.
- The R744 transcritical parallel system with multi-ejector expansion pack – the vapor fraction of CO_2 from liquid separator is either compressed in parallel compressors section or throttled in flash valve. The high-pressure refrigerant is expanded in multi-ejector block as a main flashing device, supported by high-pressure electronic valve.

As a result of the possibility of changing the facility configuration, the baseline system was defined as both systems, which did not utilize the multi-ejector block. In situation, where the

capacity for a parallel compressors section was too low, the controller unit switched automatically to the booster system. The aim of introducing the multi-ejector module to the standard refrigeration facility is improve the system performance, adapting to the operating conditions, which are enforced by supermarket refrigeration system. The multi-ejector module has got four fixed vapour ejectors with a linearly variable capacity, designed to ensure the maximum system flexibility. The motive, suction, and outlet ports are connected with three independent collectors due to the same outer dimensions of the ejectors. The work of the ejectors is operated by solenoid valves mounted in the motive side, with the possibility fully open or closed valve.

Table 6 –Set of the main system components of the R744 multi-ejector test rig.

System Component	Model	Type
Base-load compressor	Dorin CD 1400H	Semi-heretic reciprocating
Parallel compressor #1	Dorin CD 1000H	Semi-heretic reciprocating
Parallel compressor #2	Dorin CD 380H	Semi-heretic reciprocating
First-stage gas cooler	SWEP B18Hx100	30 brazed plates heat exchanger
Second-stage gas cooler	KAORI K095C-30C-NP8M	20 brazed plates heat exchanger
Base-load evaporator	SWEP B16DWHx100	30 brazed plates heat exchanger
Liquid receiver tank Liquid separator tank	Frigomec 39-litre	Pressure vessel
Oil accumulator tank	Frigomec 21-litre	Pressure vessel
Cold glycol tank	IMA 200-litre	Thermal storage tank
High-pressure valve Flash valve	Danfoss CCMT8	Electronic expansion valve
Base-load evaporator metering valve	Danfoss CCM20	Electronic expansion valve

The facility is fully equipped with the pressure and temperature sensors in order to evaluate, monitor, control and safeguard the system. To calculate the system performance, besides pressure and temperature sensors, the mass flow meters and the inverters are introduced. Most part of the sensors registered magnitude of pressure and temperature are used to the safeguarding of the system. Therefore, Figure 21 and Figure 22 present specific measurement to set the operating conditions and to evaluate the work characteristics of compressors, multi-ejector block and evaporator. Set of sensors and instrumentation installed to monitor the test facility is presented in Table 7. Accuracy of electric power consumption is assumed as for the

range of five times larger than the scale of reading, which is of ± 0.01 kW. For the frequency, the accuracy of reading is assumed for the same range as scale of reading, which is of ± 0.1 Hz. Accuracies of temperature, pressure and mass flow rate sensors are taken from product datasheets. Output signals from all sensors are processes and transmits by the Danfoss control unit to the Danfoss Minilog system (live recording software). When during the assumed time step demands test condition was reached, the steady state operation was determined. The time step was set to nine minutes to ensure a stabilization of the temperatures, mass flow rates and the pressure and minimization of the oscillation of each parameter. Finally, the test point was recorded and data was exported from Minilog to be imported to the Microsoft Excel post processing spreadsheet. The spreadsheet used the Visual Basic environment with REFPROP 8.0 thermodynamic libraries (Lemmon et al., 2013) to automatic the post processing calculations. The equation of state for carbon dioxide was taken from Span and Wagner (1996). The calculation of each test point regarded the COP value, the exergy efficiency, the compressors efficiency for both systems and multi-ejector block parameters for R744 multi-ejector system, i.e. the mass entrainment ratio, ejector efficiency, pressure lift and pressure ratio.

Table 7 - Sensors specifications in the R744 multi-ejector test rig.

Variable	Transducer	Accuracy	Range
Temperature	Resistance thermometers PT1000	$\pm (0.3+0.005 \cdot t)$ t in $^{\circ}$C	-70 $^{\circ}$C ÷ 180 $^{\circ}$C
Pressure	Piezoelectric transmitter	$\pm (0.3\%)$ of reading	0 ÷ 100 bar abs 0 ÷ 150 bar abs
Mass flow rate	Coriolis type RHM06	$\pm (0.2\%)$ of reading	0 ÷ 20 kg/min
	Coriolis type RHM15	$\pm (0.2\%)$ of reading	0 ÷ 200 kg/min
Electric power consumption	Inverter IP55 Type 12	± 0.05 kW	0 ÷ 20 kW
Frequency	Inverter IP55 Type 12	± 0.1 Hz	30 ÷ 60 Hz

The experimental investigation was carried out for two different refrigeration loads. The control system of the test rig is set to obtain maximum refrigeration capacity in the evaporator. Therefore, the operator can set the CO_2 evaporation temperature $T_{0,MT}$ and the glycol temperature outside from glycol pump T_{51} (see Figure 22). The pressure difference between both tanks is expressed as:

$$\Delta p = P_{rec} - P_{evap}\left(T_{0,MT}\right) \tag{4}$$

where Δp is a tanks pressure lift in bar, P_{rec} is a pressure of the liquid separator in bar and P_{evap} is a pressure of the liquid receiver in bar. The discharge pressure is calculated by set of the CO_2 exit 2nd stage gas cooler temperature T_6 to obtain the most effectiveness cooling of the CO_2 supercritical fluid. Assumptions for the experimental investigation are presented in Table 8.

Table 8 - Set of operating conditions for the experimental investigation for both R744 refrigeration systems.

Name	Refrigeration load (T_{51})	CO_2 evaporation temperature/ pressure in the evaporator ($T_{0,MT}$/ P_{evap})	Tanks pressure lift (Δp)	CO_2 exit 2nd stage gas cooler temperature (T_6)
1st cooling demand	12 ^{o}C	-8 ^{0}C / 28.02 bar	2÷16 bar Step 2 bar	26÷36 ^{o}C Step 2 K
2nd cooling demand	15 ^{o}C	-8 ^{0}C / 28.02 bar	2÷16 bar Step 2 bar	26÷36 ^{o}C Step 2 K

3. System performance calculations

3.1. First Law Analysis

For the steady state, it can be assumed that in the evaporator, the heat rate absorbed by the refrigerant is equal to the heat rate rejected by the second fluid. As a result of following assumption, the refrigeration capacity was calculated as the heat rate reject from the glycol stream, because the mass flow rate and both temperatures of the glycol in the base-load evaporator were measured. During investigation, the concentration of ethylene glycol of 30% in the brine loop. For the calculation of this thesis, the values of the specific heat capacity of the glycol were taken from CoolPack results (Jakobsen et al., 1999) and the values can be expressed as a linear function of the glycol temperature expressed in ^{o}C.

$$c_p(t_i) = 0.0029 \cdot t_i + 3.5895 \tag{5}$$

where $c_p(t_i)$ is a specific heat capacity in kJ kg^{-1}K^{-1}. Hence, for the steady state conditions, the refrigeration capacity of the base-load evaporator can be calculated as the total heat rate rejected from glycol.

$$\dot{Q}_{evap} = \dot{m}_{gl,evap} \cdot \left[T_{53} \cdot c_p(t_{53}) - T_{54} \cdot c_p(t_{54}) \right] \tag{6}$$

where $\dot{Q}_{evap}$ is the base-load refrigeration capacity, $\dot{m}_{gl,evap}$ is the glycol mass flow rate, T_{53} and T_{54} are inlet and outlet temperature of the glycol in the base-load evaporator. The overall electric power consumption is a sum of electric power of each utilized compressor. Therefore, COP for both configurations is expressed as:

$$COP = \frac{\dot{Q}_{evap}}{N_{el,CD1400H} + N_{el,CD1000H} + N_{el,CD380H}} \tag{7}$$

where $N_{el,CD1400H}$, $N_{el,CD1000H}$, and $N_{el,CD380H}$ are the electric power consumption of each compressor.

3.2. Volumetric and compressor efficiency

Effectiveness of individual compressor was expressed by the volumetric and compressor efficiency. According to Lambers (2008), volumetric efficiency is a ratio of the real inlet gas mass flow to the inlet gas mass flow in reference process. The reference mass flow of R744 can be defined as positive displacement of compressor multiplied by the density at the CO_2 suction parameters. The positive displacement compressor is a device that confines successive volumes of fluid within a closed space in with the pressure of the fluid is increased as the volume of the closed space is decreased (Mobley, 1999). Therefore, the positive displacement can be defined as the most possible volume flow rate of the fluid that can be discharged in the selected compressor.

$$\eta_{vol} = \frac{\dot{m}_{CO_2}}{\dot{V}_{displ} \cdot \rho(T_{suction}, p_{suction})} \tag{8}$$

where, $\dot{m}_{CO2}$ is a CO_2 mass flow rate, $\dot{V}_{displ}$ is the positive displacement of the individual compressor (information about value of the positive displacement is given by the supplier) in m^{3}s^{-1}, ρ is the density of CO_2 in the suction side of the compressor in kg m^{-3}.

The compressor efficiency is a ratio between isentropic internal power of compression and the electric power consumption of the compressor.

$$\eta_{comp} = \frac{N_{is}}{N_{el}} \tag{9}$$

where isentropic internal power of compression N_{is} of each compressor is expressed as:

$$N_{is} = h_{out,isen}(s_{suction}; P_{discharge}) - h_{in}(T_{suction}; P_{suction}) \tag{10}$$

where $s_{suction} = s(T_{suction}; P_{suction})$ is the specific entropy at the suction side of the compressor in kJ kg^{-1}K^{-1}, h_{in} is the specific enthalpy at the suction side of the compressor in kJ kg^{-1}, $h_{out,isen}$ is the isentropic specific enthalpy at the discharge side of the compressor in kJ kg^{-1}.

The evaluation of the overall volumetric and compressors efficiencies is performed in order to present the characteristic of the rack of compressors. The overall volumetric efficiency is defined as a sum of the CO_2 mass flow rates in each compressor divided by a sum of the maximum possible CO_2 mass flow rates in each compressor at the suction parameters.

$$\eta_{vol} = \frac{\sum_i \dot{m}_{CO2,i}}{\sum_i \dot{V}_{displ,i} \cdot \rho(T_{suction,i}; P_{suction,i})} \tag{11}$$

where i = CD1400H, CD1000H, and CD380H. The overall compressors efficiency is expressed as a ratio between sum of the each compressor isentropic internal power and a sum of electric power consumption of the each compressor.

$$\eta_{comp} = \frac{\sum_i N_{is,i}}{\sum_i N_{el,i}} \tag{12}$$

For the same operating condition, the overall compressor efficiency of the multi-ejector system was different than of the parallel system. Therefore, the relative change of the overall compressor efficiency after the run of the multi-ejector block is expressed as:

$$\Delta\eta_{comp} = \frac{\eta_{comp,multi-ejector} - \eta_{comp,parallel}}{\eta_{comp,parallel}} \tag{13}$$

3.3. Second Law Analysis

During experimental investigation, presented in this thesis, the temperature T of heat source, or heat sink changed from T_1 to T_2. According to Fang et al. (2005), the exergy increment can be defined as:

$$\psi_{incr} = q \cdot \left| 1 - \frac{T_{amb} \cdot \ln\left(\frac{T_1}{T_2}\right)}{(T_1 - T_2)} \right| \tag{14}$$

where ψ_{incr} in kJ kg^{-1}, q is an amount of heat The positive sign of the exergy increment is set due to negative sign of the removed heat from the evaporator, where the temperature of refrigerant is below the ambient temperature ($T < T_{amb}$). To calculate exergy efficiency, the information about total fuel and product exergy has to be known. Therefore, the total exergy output of cooling mode is defined as an exergy rate increment in the base-load evaporator.

$$\psi_{incr} = \left[T_{53} \cdot c_p(t_{53}) - T_{54} \cdot c_p(t_{54}) \right] \cdot \left| 1 - \frac{T_{amb} \cdot \left(\ln \frac{T_{53}}{T_{54}} \right)}{T_{53} - T_{54}} \right| \tag{15}$$

$$E_{out} = \dot{m}_{gl,evap} \cdot \psi_{incr} \tag{16}$$

where E_{out} is a total exergy rate output in kW. Ambient temperature T_{amb} was recorded for every investigation day. The total exergy input is the overall electric power consumption. Finally, the second law efficiency can be defined as:

$$\eta_{ex} = \frac{E_{out}}{E_{in}} = \frac{\dot{m}_{gl,evap} \cdot \psi_{incr}}{N_{el,CD1400H} + N_{el,CD1000H} + N_{el,CD380H}} \tag{17}$$

3.4. The ejector parameters

The multi-ejector module can be described by three specific parameters: pressure ratio (or pressure lift), mass entrainment ratio and the ejector efficiency. Pressure ratio a division of the outlet pressure level to the suction nozzle pressure level.

$$\Pi = \frac{P_{outlet}}{P_{suction}} \tag{18}$$

The mass entrainment ratio shows the ratio between mass flow rate of the entrainment fluid and mass flow rate of the motive fluid, which is expressed as:

$$\phi = \frac{\dot{m}_{suction}}{\dot{m}_{motive}} \tag{19}$$

The ejector efficiency is defined as the ejector efficiency definition proposed by Elbel and Hrnjak (2008). The one of the benefit to use foregoing definition is that it can be applied for an experimental investigation, because it avoids the measured static pressure in the mixing chamber. The ejector efficiency is the amount of expansion work recovered divided by the maximum potential to recover expansion work rate by the ejector.

$$\eta_{ejector} = \frac{W_{rec}}{\dot{W}_{max,rec}} = \frac{\dot{m}_{suction}}{\dot{m}_{motive}} \cdot \frac{[h_C(s=s_{suction},P=P_{outlet})-h_D(s=s_{suction},P=P_{suction})]}{[h_A(h=h_{motive},P=P_{outlet})-h_B(s=s_{motive},P=P_{outlet})]} \tag{20}$$

where $\dot{W}_{rec}$ is an expansion work rate recovered in kW, $\dot{W}_{max,rec}$ is a maximum potential to recover expansion work rate in kW. Finally, the ejector efficiency can be expressed as:

$$\eta_{ejector} = \phi \cdot \frac{(h_C - h_D)}{(h_A - h_B)} \tag{21}$$

3.5. The R744 multi-ejector system improvement

Evaluation of the refrigeration system performance result after introducing the multi-ejector module to the standard parallel system can be expressed by COP and exergy efficiency improvement.

$$COP_{improvement} = \frac{COP_{multi-ejector} - COP_{parallel}}{COP_{parallel}} \cdot 100\% \tag{22}$$

$$\eta_{ex\,improvement} = \frac{\eta_{ex\,multi-ejector} - \eta_{ex\,parallel}}{\eta_{ex\,parallel}} \cdot 100\% \tag{23}$$

4. Results

4.1. The multi-ejector module parameters

Figure 23 shows the multi-ejector block characteristic for all operating conditions investigated for 1st cooling demand (T_{51}=12°C). Left Y-axis represents the ejector efficiency $\eta_{ejector}$ and the mass entrainment ratio ϕ, but the right Y-axis represents pressure ratio Π. In addition, the configuration of the multi-ejector module is introduced in the Figure 23. The multi-ejector block efficiency decreased during rising of pressure in the liquid receiver due to simultaneously decreasing of the mass entrainment ratio. The same impairment of the ejector efficiency can be noticed during decreasing of the exit gas cooler temperature and discharge

pressure, respectively. For the tanks pressure lift of 8 bar (Δp =8 bar), the ejector efficiency was in the range of 27% to 8% for the exit gas cooler temperature T_6 from 36°C to 28°C, respectively. The value of the mass entrainment ratio decreased from 0.22 to 0.04 for the same range as the ejector efficiency.

Lowering of the exit gas cooler parameter caused a slight drop of the pressure ratio for the same set of the tank pressure lift. In the range of the exit gas cooler temperature T_6 of 36°C to 28°C and for the tank pressure lift of 8 bar (Δp =8 bar), the pressure lift is of 1.35 to 1.30, respectively. The multi-ejector block worked with the ejector efficiency over 30% for $\Delta p \le 4$ bar, when $T_6 > 28$ °C and for $\Delta p = 6$ bar, when $T_6 > 34$ °C. During investigation of operating conditions for the 1st cooling demand, the multi-ejector block worked at the different ejectors capacity configuration. Hence, the ejector efficiency linked to the mass entrainment ratio dropped significantly
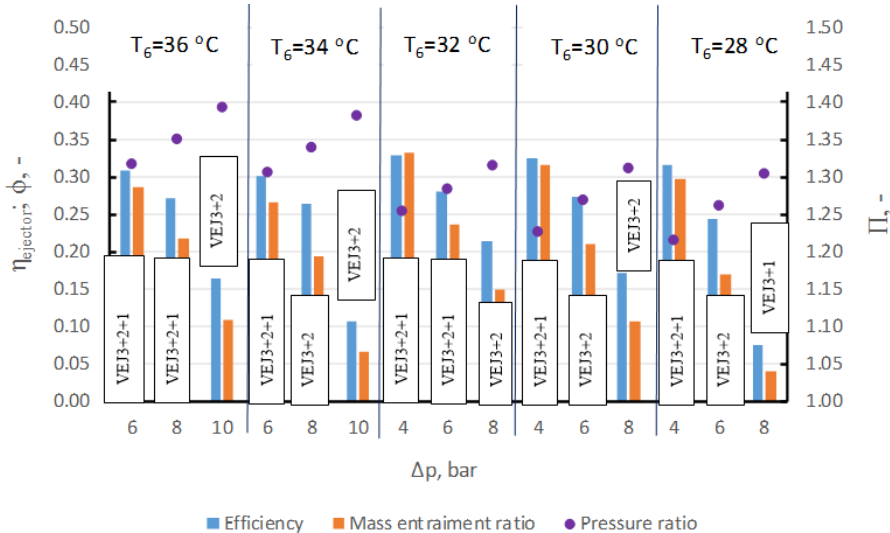
Figure 23 - Multi-ejector block characteristics depending on the tanks pressure lift (Δp) and exit gas cooler temperature (T_6) for 1st cooling demand conditions.

Figure 24 presents the multi-ejector block characteristics for the T_{51} temperature of 15 °C including the efficiency, mass entrainment ratio and pressure ratio. Left Y-axis represents the ejector efficiency $\eta_{ejector}$ and the mass entrainment ratio ϕ, but the right Y-axis represents pressure ratio Π. The highest value of the mass entrainment ratio exists for T_6 and Δp of 28 °C and 2 bar, respectively. The multi-ejector efficiency together with the mass entrainment ratio

have the same decreasing trend as for results presented in Figure 23. It can be noticed that the value of the multi-ejector efficiency for T_6 and Δp of 28 °C and 2 bar, respectively, is comparable with the values obtained for Δp =4 bar and $T_6 = 30$ °C, or 32 °C.

For Δp of 8 bar, the ejector efficiency is in the range of 26% to 9% for the exit gas cooler temperature T_6 of 36 °C to 28 °C, respectively. The value of the mass entrainment ratio decreases from 0.20 to 0.06 for the same range as the ejector efficiency. For Δp of 6 bar the mass entrainment ratio and the ejector efficiency was stable for T_6 in the range of 36 °C to 34 °C and also in the range of 28 °C to 26 °C. The same stabilization of both parameters was for Δp of 4 bar and for T_6 in the range of 32 °C to 28 °C.

The pressure ratio had the slightly decreasing trend during decreasing of the T_6 temperature. In the range of the exit gas cooler temperature from 36 °C to 28 °C and for the tanks pressure lift of 8 bar, the pressure ratio is in the range of 1.36 to 1.29, respectively. The very low drop of the pressure ratio confirmed that during the decrease of the exit gas cooler temperature, the small difference between the ejector outlet pressure and the liquid separator pressure was reduced.

The multi-ejector block worked with the ejector efficiency over 30% for $\Delta p \leq 4$ bar, when $T_6 > 26$ °C and for $\Delta p = 6$ bar, when $T_6 > 34$ °C.
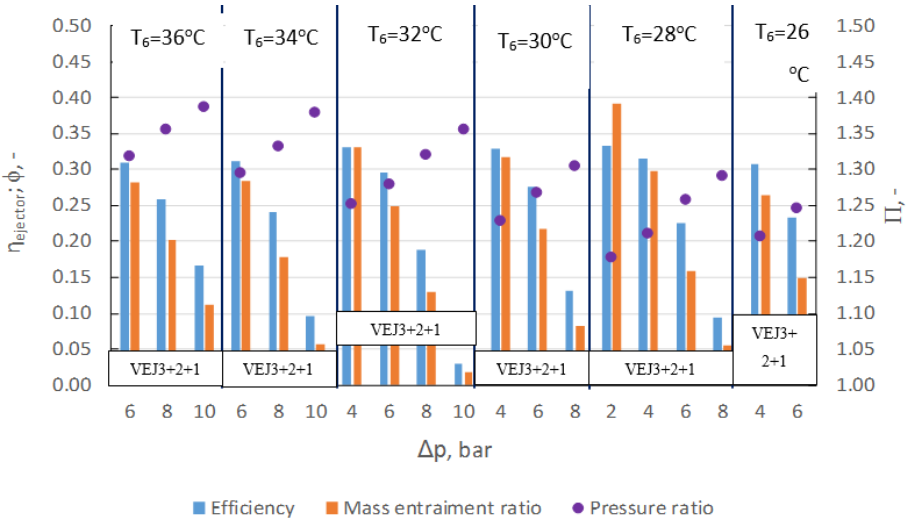
Figure 24 - Multi-ejector block characteristics depending on the tanks pressure lift (Δp) and exit gas cooler temperature (T_6) for 2nd cooling demand conditions.

It can be observed that the similar range of values for the multi-ejector efficiency, mass entrainment ratio and pressure ratio for both cooling demands was obtained. Increase of refrigeration load stabilizes the multi-ejector work, but it does not influence on the vapour ejectors performance improvement.

4.2. Electric Power Consumption

Utilizing the ejectors during the experimental investigation reduced significantly capacity of the base-load compressor. The multi-ejector system indicated changeability of CO_2 mass flow rate through the base-load compressor, which is shown in Figure 25. The figure shows the mass flow rates, in the base-load compressor, for both cooling demands, for the exit gas cooler temperature (T_6) of $28^oC \pm 0.2K$. The calculation of CO_2 mass flow rate in the base-load compressor has been carried out based on data given from Dorin CD1400H catalogue. For the tanks pressure lift of 2 bar, the mass flow rate of the multi-ejector system was almost two times smaller than the mass flow rate of the parallel system.

The reason of the stream reduction was the mass flow rate entrained in the ejectors. Based on the mass balance of the liquid receiver, the CO_2 mass flow from the evaporator was equal to the CO_2 mass flow in the base-load compressor and the mass flow in the suction nozzle of the ejectors, if the multi-ejector module worked well. During increasing of the tanks pressure lift, the mass entrainment ratio of the multi-ejector block decreased. Hence, for the tanks pressure lift of 8 bar, the difference between mass flow rates of both system is small due to low value of mass entrainment ratio.

Constant parameters: $T_6 = 28\ ^oC \pm 0.2K$

Figure 25 - R744 mass flow rate in the base-load compressor vs. pressure lift.

The CO_2 mass flow entraining by the ejectors was able to influence on the work parameters of each compressor. Apart from the multi-ejector block parameters, volumetric and compressor efficiency of each compressors depended on tanks pressure lift and the CO_2 exit parameter of the gas cooler section. All of foregoing considerations are related with each other. During operation of the multi-ejector block, the load of the parallel compressors increases significantly, which is shown in Figure 26. The figure shows the share of electric power consumption of each compressor on the overall electric power consumption for both refrigeration systems at the same operating conditions. The load of the base-load compressor decreased relatively around 50%. It can be noticed that the contribution of the parallel compressors section in the multi-ejector system increased close to two times (from 35% to 66%) than in the parallel system.

Multi-ejector System

- CD 1400H Base-load Compressor
- CD 1000H Parallel Compressor
- CD 380H Parallel Compressor

Parallel System

- CD 1400H Base-load Compressor
- CD 1000H Parallel Compressor
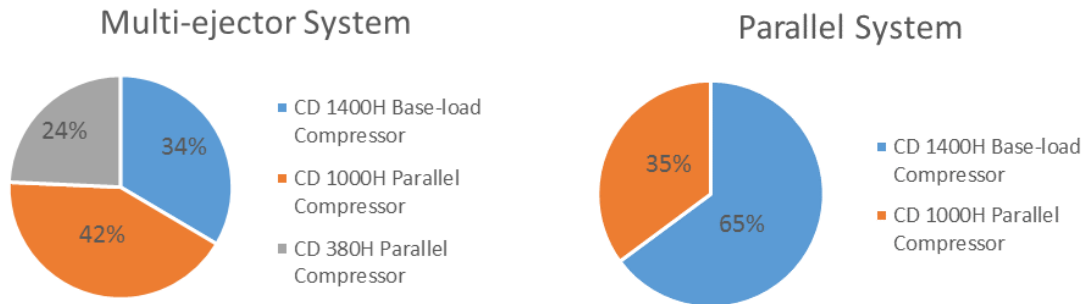
Constant parameters: $T_{51}=12\ ^{o}C \pm 0.4K$ $T_{6}=36\ ^{o}C \pm 0.5K$ $\Delta p=6$ bar $\pm$ 0.15 bar

Figure 26 - The share of electric power consumption of each compressor on the overall electric power consumption.

The share of power consumption and individual efficiency of each compressor allows for calculation of the overall efficiency of the rack of compressors, which represents the quality of the rack work in the operating system. Figure 27 shows the comparison of the overall compressors and volumetric efficiency of the system with efficiency distribution for the individual compressor. The operating conditions were the same as in Figure 26, therefore the contributions of each compressor were used to calculate overall efficiencies. For the parallel system, the volumetric efficiencies for both working compressors were comparable. Growth of parallel compressors load forced to compress much more amount of the refrigerant. Therefore, in the multi-ejector system the volumetric efficiencies of both parallel compressors were relatively low. As a result of low values of volumetric efficiencies and the large load, the parallel compressors obtained the compressors efficiency lower than 60%. The individual compressor efficiencies in the parallel system were comparable to volumetric efficiency and therefore the parallel refrigeration system achieved higher value of overall compressor efficiency than the multi-ejector system. The low value of overall compressor efficiency in the multi-ejector system made the growth of overall electric power consumption, which lowered the system performance and finally the value of COP and exergy efficiency.

(a) Volumetric efficiency

(b) Compressor efficiency

| Constant parameters: | T_{51}=12 ^{o}C ± 0.4K | T_6=36 ^{o}C ± 0.5K | Δp=6 bar ± 0.15 bar |

Figure 27 - Characteristics of the rack of compressors with comparison of both systems in the same operating condition.

4.3. Multi-ejector system performance improvement

Figure 28 shows the system performances characteristics for 1st cooling demand (T_{51}=12°C) for different values of the exit gas cooler temperature T_6 and the tanks pressure lift Δp in the range of 2 bar to 16 bar. During increasing the pressure level in the liquid receiver tank, the COP and the exergy efficiency increased. The multi-ejector systems for T_6=36 ^{o}C and T_6=34 ^{o}C gained the higher COP and the exergy efficiency for the tanks pressure lift of 8 bar. Hence, for Δp in the range of 8 bar to 10 bar, the multi-ejector module improved the system energy

performance. For the exit gas cooler temperature $T_6 \leq 32$ $^{\circ}$C, the multi-ejector system gained higher COP for the tanks pressure lift of 6 bar. The parallel system worked better than the multi-ejector for the $\varDelta p$ of 6 bar and T_6=32 $^{\circ}$C based on the second law analysis.

In the subcritical mode, COP and the exergy efficiency, depending on the tanks pressure lift, have the same increasing trends as in the transcritical mode. Furthermore, the multi-ejector system reaches much better system performance as the parallel system. The highest values of COP 3.53 and the exergy efficiency 16.6% are gained by the multi-ejector system for T_6=28 $^{\circ}$C and $\varDelta p$= 6 bar. The parallel system reached the highest COP of 3.4 and the exergy efficiency of 16.4% for T_6=28 $^{\circ}$C and $\varDelta p$ of 10 bar.
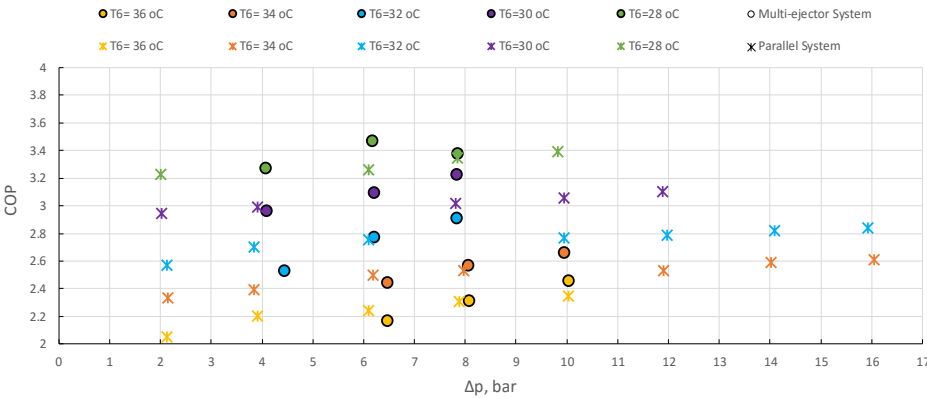
(a) COP
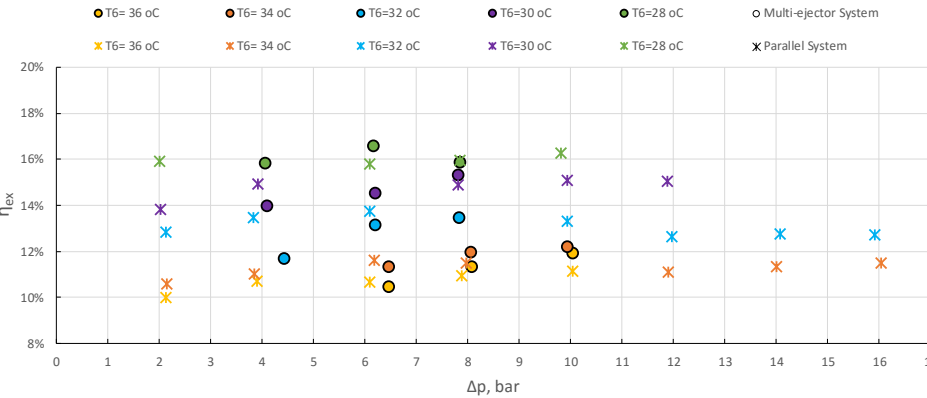
(b) Exergy efficiency

Figure 28- System performance characteristics vs. the tanks pressure lift ($\varDelta p$) for the parallel system and the multi-ejector system for 1st cooling demand (T_{51} of 12 $^{\circ}$C): (a) COP, (b) exergy efficiency.

Figure 28 shows the system performances characteristics for 1st cooling demand (T_{51}=12°C) for different values of the exit gas cooler temperature T_6 and the tanks pressure lift $\varDelta p$ in the

range of 2 bar to 10 bar. The COP improvement and the exergy efficiency improvement of the multi-ejector system was reached for $T_6 \leq 32$ $^{\mathrm{o}}$C. For the exit gas cooler temperature T_6 of 34 $^{\mathrm{o}}$C and of 36 $^{\mathrm{o}}$C, the parallel system was able to work with the tanks pressure lift $\varDelta p$ in the range of 2 bar to 6 bar, when the multi-ejector was able to work with $\varDelta p$ in the range of 6 bar to 10 bar as the result of the high refrigeration capacity and the high load of the parallel compressors. For the exit gas cooler temperature $T_6 \leq 30$ $^{\mathrm{o}}$C, the multi-ejector system gained higher COP and the exergy efficiency for the tanks pressure lift of 4 bar, but for T_6 of 32 $^{\mathrm{o}}$C the multi-ejector system improved system performance for $\varDelta p$ of 6 bar. The highest values of COP 3.92 and the exergy efficiency 17.0% were gained by the multi-ejector system for T_6=26 $^{\mathrm{o}}$C and $\varDelta p$= 6 bar. The parallel system reached the highest value of COP 3.7 and the exergy efficiency 16.1% for T_6=26 $^{\mathrm{o}}$C and $\varDelta p$ of 8 bar.
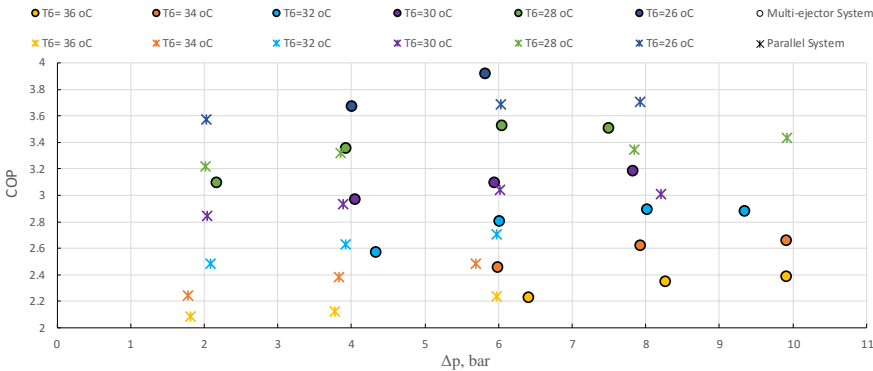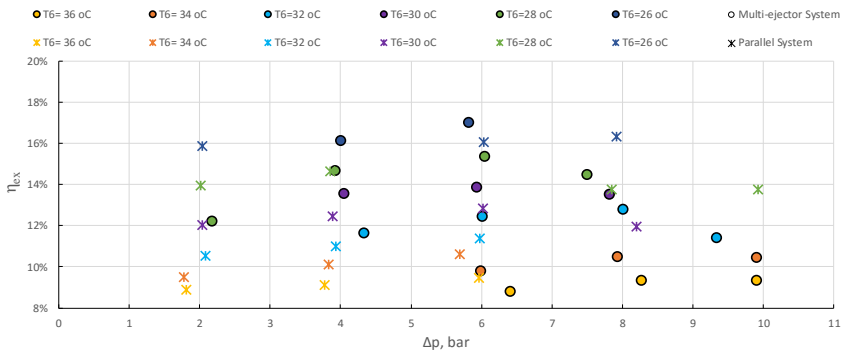
(a) COP

(a) Exergy efficiency

Figure 29 – System performance characteristics vs. the tanks pressure lift ($\varDelta p$) for the parallel system and the multi-ejector system for 2$^{\mathrm{nd}}$ cooling demand ($T_{51} = 15$ $^{\mathrm{o}}$C): (a) COP, (b) exergy efficiency.

Table 9 presents a set of COP and the exergy efficiency improvements of the multi-ejector system for the 1$^{\mathrm{st}}$ cooling demand (T_{51}=12$^{\mathrm{o}}$C). The highest COP improvements were obtained

for T_6= 28°C and Δp= 6.1 bar up to 4.67%, whereas the highest COP degradation were obtained for T_6= 32°C and Δp= 4.1 bar up to -6.46%. It can be noticed that for the small value of tanks pressure lift, the multi-ejector system gained worse performance than the baseline, which was able to be caused by the low value of the overall compressors efficiency. The multi-ejector system obtained the best exergy performance for T_6=36 °C and Δp= 10.0 bar due to the high overall efficiency and over 15% of the work recovery by the multi-ejector block, which is shown in Table 9. The exergy improvement for foregoing operating conditions was of 7.05%. The worst degradation of the second law efficiency, the multi-ejector system reached for T_6 of 32°C and Δp of 4.1 bar up to -13.24%, what was strongly dependent on the poor work of the rack of compressors.

For $\Delta\eta_{comp}$ > -8.25% the multi-ejector system improved COP and the exergy efficiency. Therefore, the combination of the multi-ejector block efficiency of 24.39% and the relative change of the overall compressor efficiency of 0.28% reached the best COP improvement for Δp = 6.1 bar and for T_6 =28 °C.

Based on results presented in Table 9, the use of the multi-ejector module improved the energy performance for Δp > 6 bar, when $T_6 \leq 32$ °C and also for Δp > 8 bar, when T_6 > 32 °C. The exergy improvement of the multi-ejector system related to the parallel system was for Δp > 8 bar, when $T_6 \leq 36$ °C.

Table 9 - COP and exergy efficiency improvement of the R744 multi-ejector system relative to the R744 parallel system, the multi-ejector block efficiency (η_{ej}) and the relative change of the overall compressors efficiency ($\Delta\eta_{comp}$) for the 1st cooling demand (T_{51}= 12°C), related to the exit gas cooler temperature (T_6) and the tanks pressure lift (Δp).

T_6	Δp	$COP_{improvement}$	$\eta_{ex,improvement}$	η_{ej}	$\Delta\eta_{comp}$
36 °C ± 0.1 K	6.3 bar ± 0.1 bar	-3.12% ± 0.04%	-2.04% ± 0.05%	30.83% ± 0.75% VEJ3+VEJ2+VEJ1	-13.50% ± 0.15%
36 °C ± 0.2 K	8.0 bar ± 0.1 bar	0.14% ± 0.01%	3.60% ± 0.11%	27.16% ± 0.37% VEJ3+VEJ2+VEJ1	-8.25% ± 0.11%
36 °C ± 0.1 K	10.0 bar ± 0.1 bar	4.67% ± 0.06%	7.05% ± 0.25%	16.51% ± 0.23% VEJ3+VEJ2	-6.4% ± 0.08%
34 °C ± 0.1 K	6.3 bar ± 0.1 bar	-1.98% ± 0.02%	-2.56% ± 0.02%	30.13% ± 0.50% VEJ3+VEJ2+VEJ1	-10.60% ± 0.12%
34 °C ± 0.1 K	8.0 bar ± 0.1 bar	1.51% ± 0.02%	3.96% ± 0.05%	26.42% ± 0.34% VEJ3+VEJ2	-6.43% ± 0.07%

32 °C ± 0.1 K	4.1 bar ± 0.1 bar	-6.46% ± 0.06%	-13.24% ± 0.26%	32.90% ± 0.44% VEJ3+VEJ2+VEJ1	-13.32% ± 0.14%
32 °C ± 0.1 K	6.2 bar ± 0.1 bar	0.70% ± 0.01%	-4.33% ± 0.11%	28.16% ± 0.50% VEJ3+VEJ2+VEJ1	-7.33% ± 0.08%
30 °C ± 0.1 K	4.0 bar ± 0.1 bar	-0.82% ± 0.01%	-6.29% ± 0.08%	32.44% ± 0.56% VEJ3+VEJ2+VEJ1	-8.69% ± 0.09%
30 °C ± 0.1 K	7.8 bar ± 0.1 bar	6.98% ± 0.01%	2.94% ± 0.06%	17.18% ± 0.21% VEJ3+VEJ2	1.11% ± 0.01%
28 °C ± 0.1 K	6.1 bar ± 0.1 bar	8.07% ± 0.11%	5.07% ± 0.10%	24.39% ± 0.29% VEJ3+VEJ2	0.28% ± 0.01%
28 °C ± 0.1 K	7.9 bar ± 0.1 bar	1.11% ± 0.02%	-0.46% ± 0.02%	7.51% ± 0.09% VEJ3+VEJ1	-3.78% ± 0.01%

Similarly to the results for the 1st cooling demand, the COP and the exergy improvements of the-multi ejector system results are calculated and presented in Table 10. In addition, the multi-ejector module efficiency η_{ej} and the relative change of the overall compressor efficiency after the run of the multi-ejector block $\Delta\eta_{comp}$ are set. It can be noticed that for the higher Δp, the multi-ejector gains the best improvements. For the small tanks pressure lift, the overall compressor efficiency of the multi-ejector system is relatively low, which significantly influences the values of energy and exergy improvements. Hence, the smallest cooling effectiveness of the multi-ejector system is for $\Delta p = 2$ bar and $T_6 = 28$ °C. The multi-ejector system improves the COP by up to 6.52% for $T_6 = 26$ °C and $\Delta p = 6$ bar in comparison to the reference system. The highest exergy improvement of the multi-ejector system is reached for $T_6 = 30$ °C and $\Delta p = 8$ bar up to 13.17% due to comparable value of the overall compressors efficiency between both systems. For the same operating condition COP improvement is of 5.77%, as the highest improvement for the exit gas cooler temperature $T_6 = 30$ °C.

It can be noticed that the energy performance improvement of the multi-ejector system was strongly related to the relative change of the overall compressor efficiency. For $\Delta\eta_{comp} > -5\%$ the multi-ejector system improved COP and the exergy efficiency. Therefore, the combination of the multi-ejector block efficiency of 23.27% and the relative change of the overall compressor efficiency of 1.99% reached the best COP improvement for $\Delta p = 6.1$ bar and for $T_6 = 26$ °C.

Based on results presented in Table 10, the use of the multi-ejector module improved the energy performance for $\Delta p > 4$ bar, when $T_6 < 32$ °C and for $\Delta p = 6$ bar, when $T_6 = 32$ °C. The

exergy improvement of the multi-ejector system related to the parallel system was for $\Delta p > 4$ bar, when $T_6 \leq 32\ {}^{\circ}$C.

Table 10 - COP and exergy efficiency improvement of the R744 multi-ejector system relative to the R744 parallel system, the multi-ejector block efficiency (η_{ej}) and the relative change of the overall compressors efficiency ($\Delta\eta_{comp}$) for the 2nd cooling demand ($T_{51}= 15^{\circ}$C), related to the exit gas cooler temperature T_6 and the tanks pressure lift Δp.

T_6	Δp	$COP_{improvement}$	$\eta_{ex,improvement}$	η_{ej}	$\Delta\eta_{comp}$
36 $^{\circ}$C ± 0.1 K	6.2 bar ± 0.1 bar	-0.18% ± 0.01%	-6.93% ± 0.07%	30.98% ± 0.33% VEJ3+VEJ2+VEJ1	-10.26% ± 0.11%
34 $^{\circ}$C ± 0.1 K	5.8 bar ± 0.1 bar	-1.07% ± 0.01%	-7.52% ± 0.05%	31.23% ± 0.38% VEJ3+VEJ2+VEJ1	-7.61% ± 0.05%
32 $^{\circ}$C ± 0.2 K	4.1 bar ± 0.1 bar	-2.1% ± 0.02%	5.98% ± 0.05%	33.07% ± 0.42% VEJ3+VEJ2+VEJ1	-7.35% ± 0.05%
32 $^{\circ}$C ± 0.1 K	6.3 bar ± 0.1 bar	3.52% ± 0.05%	9.37% ± 0.16%	29.68% ± 0.49% VEJ3+VEJ2+VEJ1	-3.94% ± 0.05%
30 $^{\circ}$C ± 0.1 K	4.0 bar ± 0.1 bar	1.35% ± 0.01%	8.94% ± 0.97%	32.82% ± 0.41% VEJ3+VEJ2+VEJ1	-4.52% ± 0.05%
30 $^{\circ}$C ± 0.2 K	6.0 bar ± 0.1 bar	1.80% ± 0.02%	8.24% ± 0.16%	27.69% ± 0.35% VEJ3+VEJ2+VEJ1	-1.57% ± 0.02%
30 $^{\circ}$C ± 0.1 K	8.0 bar ± 0.2 bar	5.77% ± 0.10%	13.17% ± 0.35%	13.11% ± 0.17% VEJ3+VEJ2+VEJ1	0.44% ± 0.01%
28 $^{\circ}$C ± 0.1 K	2.1 bar ± 0.1 bar	-3.84% ± 0.07%	-12.37% ± 0.27%	33.36% ± 0.40% VEJ3+VEJ2+VEJ1	-6.62% ± 0.08%
28 $^{\circ}$C ± 0.2 K	3.9 bar ± 0.1 bar	1.16% ± 0.02%	0.14% ± 0.01%	31.48% ± 0.39% VEJ3+VEJ2+VEJ1	-2.29% ± 0.03%
28 $^{\circ}$C ± 0.2 K	7.7 bar ± 0.1 bar	4.84% ± 0.07%	5.54% ± 0.17%	9.51% ± 0.12% VEJ3+VEJ2+VEJ1	0.34% ± 0.01%
26 $^{\circ}$C ± 0.2 K	6.1 bar ± 0.1 bar	6.52% ± 0.12%	5.98% ± 0.20%	23.27% ± 0.26% VEJ3+VEJ2+VEJ1	1.99% ± 0.03%

5. Conclusion

Experimental investigation of R744 vapour compression rack, equipped with the multi-ejector expansion pack, was performed, based on the first law and the second law analysis. The results were compared to the R744 vapour compression rack with high-pressure electronic expansion valve, as an expansion device. The test facility was designed to operate in both alternative configurations. Comparison was carried out for two refrigeration loads and both refrigeration systems were operated in transcritical and subcritical mode. Apart from the system performance comparison, influence of the pressure level in the flash tank on the system performance for both alternatives was analysed.

The experimental results indicated the maximum COP improvement of the CO_2 multi-ejector system of up to 7% for the working conditions around the critical point and the upper limit of the flash gas pressure, for which the multi-ejector pack can be utilized. The range of pressure lift in the configuration with the multi-ejector block was smaller than for the reference system due to the significantly decreased mass entrainment ratio and the ejectors efficiency. The range of the flash tank pressure level for the R744 multi-ejector system was dependent of the motive side parameters of the ejectors (temperature, pressure). For every gas cooler working condition, investigated in this thesis, the maximum COP of the R744 multi-ejector system was obtained for relatively high pressure in the flash tank, close to the upper limit of the multi-ejector pack utilization. During decreasing of the gas cooler/ condenser exit parameters, the value of COP increased for both configurations.

The second law analysis reported that the utilization of the multi-ejector expansion pack in the R744 vapour compression rack improved exergy efficiency up to 13% for the working conditions around the critical point and the same upper limit of the flash tank as for the first law analysis. Similarly to the COP evaluation of the R744 multi-ejector system, the maximum exergy efficiency was indicated for the relatively high value of the flash tank pressure, close to upper limit of the multi-ejector pack utilization and relatively low exit gas cooler/ condenser parameters.

The evaluation of the performance improvement of the R744 multi-ejector system was strongly related to the utilized compressors efficiencies. The high load and low-effective compression of the parallel compressors caused growth of electric power consumption and

decrease of the COP and exergy efficiency. Therefore, the significant work degradation of the rack of compressors did not provide the improvement of the R744 multi-ejector system for respectively low pressure lift. The comparable overall compressors efficiency of both configurations may indicate the COP and the second law improvement for all working range of the flash tank pressure. It was also noticed that the comparable high-efficiency of the rack of compressors obtained the best performance of the R744 vapour compression rack with the multi-ejector expansion pack, for the upper limit of the pressure lift.

The multi-ejector block worked more steadily for the relatively high refrigeration load. The experimental results reported the multi-ejector block efficiency of up to 33% depending on motive and suction side parameters, and the pressure lift. The highest efficiencies of the ejectors were obtained for relatively low pressure lift. During decreasing of the gas cooler parameters, the multi-ejector block efficiency decreased too due to drop of the CO_2 motive mass flow rate and simultaneously decreased of the mass entrainment ratio. The multi-ejector block reached wider range of the pressure lift for the higher refrigeration load.

The significant difference between the efficiencies of the rack of compressors for each refrigeration systems influenced negative on the energy and exergy performance improvements of the R744 refrigeration system with the ejectors expansion pack. Therefore, the evaluation of system performance with the ejectors expansion pack for the comparable high-efficiently rack of compressors need to be done for further works. In addition, the rack of compressors in the test facility should be adapted to significantly increase of the parallel compressors load during the utilization of the ejectors pack.

References

BANSAL, P. 2012. A review – Status of CO2 as a low temperature refrigerant: Fundamentals and R&D opportunities. *Applied Thermal Engineering,* 41**,** 18-29.

CHESI, A., ESPOSITO, F., FERRARA, G. & FERRARI, L. 2014. Experimental analysis of R744 parallel compression cycle. *Applied Energy,* 135**,** 274-285.

ELBEL, S. & HRNJAK, P. 2008. Experimental validation of a prototype ejector designed to reduce throttling losses encountered in transcritical R744 system operation. *International Journal of Refrigeration-Revue Internationale Du Froid,* 31**,** 411-422.

FANG, G., XING, L., YANG, F. & LI, H. 2005. Exergy analysis of a dual-mode refrigeration system for ice storage air conditioning. *International Journal of Architectural Science,* 6**,** 6.

GIROTTO, S., MINETTO, S. & NEKSA, P. 2004. Commercial refrigeration system using CO2 as the refrigerant. *International Journal of Refrigeration,* 27**,** 717-723.

HAFNER, A., FORSTERLING, S. & BANASIAK, K. 2014. Multi-ejector concept for R-744 supermarket refrigeration. *International Journal of Refrigeration-Revue Internationale Du Froid,* 43**,** 1-13.

JAKOBSEN, A., RASMUSSEN, B. D. & ANDERSEN, S. E. 1999. CoolPack – Simulation tools for refrigeration systems. *Scanref,* 28**,** 7-10.

KIM, M. H., PETTERSEN, J. & BULLARD, C. W. 2004. Fundamental process and system design issues in CO2 vapor compression systems. *Progress in Energy and Combustion Science,* 30**,** 119-174.

LAMBERS, K. J. 2008. Isentropic and Volumetric Efficiencies for Compressors with Economizer Port. *International Compressor Engineering Conference.* Purdue.

LEMMON, E. W., HUBER, M. L. & MCLINDEN, M. O. 2013. NIST Standard Reference Database 23: Reference Fluid Thermodynamic and Transport Properties-REFPROP. *Standard Reference Data Program.* 9.1 ed. Gaithersburg: National Institute of Standards and Technology.

LORENTZEN, G. 1990. Trans-critical vapour compression cycle device. Google Patents.

MOBLEY, K. 1999. Glossary. *In:* MOBLEY, K. (ed.) *Root Cause Failure Analysis.* Burlington: Butterworth-Heinemann.

PEARSON, A. 2005. Carbon dioxide—new uses for an old refrigerant. *International Journal of Refrigeration,* 28**,** 1140-1148.

SARKAR, J. & AGRAWAL, N. 2010. Performance optimization of transcritical CO2 cycle with parallel compression economization. *International Journal of Thermal Sciences,* 49**,** 838-843.

SAWALHA, S., KARAMPOUR, M. & ROGSTAM, J. 2015. Field measurements of supermarket refrigeration systems. Part I: Analysis of CO2 trans-critical refrigeration systems. *Applied Thermal Engineering,* 87**,** 633-647.

SHARMA, V., FRICKE, B. & BANSAL, P. 2014. Comparative analysis of various CO2 configurations in supermarket refrigeration systems. *International Journal of Refrigeration-Revue Internationale Du Froid,* 46**,** 86-99.

SPAN, R. & WAGNER, W. 1996. A New Equation of State for Carbon Dioxide Covering the Fluid Region from the Triple-Point Temperature to 1100 K at Pressures up to 800 MPa. *Journal of Physical and Chemical Reference Data,* 25**,** 87.

SUMERU, K., NASUTION, H. & ANI, F. N. 2012. A review on two-phase ejector as an expansion device in vapor compression refrigeration cycle. *Renewable & Sustainable Energy Reviews,* 16**,** 4927-4937.

WANG, C.-C., HAFNER, A., KUO, C.-S. & HSIEH, W.-D. 2012. An overview of the effect of lubricant on the heat transfer performance on conventional refrigerants and natural refrigerant R-744. *Renewable and Sustainable Energy Reviews,* 16**,** 5071-5086.

WIEDENMANN, E., SCHÖNENBERGER, J., HAFNER, A., BANASIAK, K. & GIROTTO, S. 2014. Effiziente Kälteerzeugung im Supermarkt mittels CO2-Booster-Kälteanlage und Ejektor. *Deutscher Kälte- und Klimatechnischer Verein e.V.* Düsseldorf: AA.

B Raw Data

Set of all parameters for investigated points, as a raw data, gives more information about each single test point. Each parameter has been presented together with uncertainty type A (U_A) and type B (U_B). The units are shown in Table B.1.

Table B.1: Units for the values and uncertainties presented in the Appendix.

Quantity	Ejector Parameters (η, Φ, Π)	Frequency	Pressure $P_{location}$	Temperature $T_{location}$	Mass Flow Rate	Electric Power Consumption $N_{el, comp.}$
Unit	-	Hz	bar	^{o}C	kg min^{-1}	kW

The evaluation of the compressors parameters such as volumetric efficiency and compressor efficiency based on experimental investigation was performed and presented in section 5.2.1. Unfortunately, the evaluation was possible only for the base-load compressor Dorin CD 1400H. Therefore, the experimental results were compared to the theoretical results calculated with the use of the polynomial functions given from Dorin supplier. Table B.2 presents the raw data of the experimental investigation of the base-load compressor parameters.

Table B.2: Raw data of the compressor Dorin CD 1400H parameters for the evaluation of compressor efficiency and volumetric efficiency presented in section 5.2.1.

ID Name		MT_1		MT_2		MT_3		MT_4	
						Dorin CD 1400H			
η_{comp}	u_A	0.6553	0.0073	0.6369	0.0076	0.6558	0.0078	0.6520	0.0073
	u_B		0.0078		0.0076		0.0078		0.0078
η_{vol}	u_A	0.7534	0.0053	0.7425	0.0060	0.7504	0.0057	0.7665	0.0071
	u_B		0.0019		0.0019		0.0019		0.0020
N_{el}	u_A	10.53	0.1042	12.95	0.1328	9.730	0.1020	10.53	0.0864
	u_B		0.1216		0.1495		0.1124		0.1215
Frequency	u_A	48.80	0.2329	59.10	0.3241	45.56	0.2268	51.95	0.2680
	u_B		0.0564		0.0682		0.0526		0.0600
$T_{comp. suction}$	u_A	-4.714	0.0843	-4.753	0.0454	-4.867	0.0559	-5.708	0.0593
	u_B		0.3192		0.3190		0.3183		0.3135
$T_{0,MT}$	u_A	-5.836	0.0896	-5.883	0.0464	-5.949	0.0675	-6.900	0.0776
	u_B		0.3127		0.3124		0.3121		0.3066
$P_{discharge}$	u_A	85.88	0.5207	85.76	0.2909	85.51	0.2744	79.23	0.2715
	u_B		0.2975		0.2971		0.2962		0.2745
m_{CO2}	u_A	9.291	0.0482	11.08	0.0662	8.613	0.0488	9.733	0.0748
	u_B		0.0215		0.0256		0.0199		0.0225

T_{51}	u_A	6.885	0.0982	8.896	0.0322	5.953	0.0631	6.940	0.0449
	u_B		0.3862		0.3978		0.3808		0.3865
T_6	u_A	34.95	0.2407	35.12	0.1579	34.97	0.0449	31.93	0.0865
	u_B		0.5482		0.5492		0.5483		0.5308

Table B.3 presents the set of coefficients used in the polynomial function for each compressor installed in the test facility defined in Eq. (5.1). According to Dorin supplier, the validity of the polynomials is limited to the application envelope of the compressor and is according to the standard conditions of EN12900.

Table B.3:   Set of polynomial coefficients for the evaluation of compressor efficiency and volumetric efficiency for nominal frequency of 50Hz.

	CD 1400H		CD 1000H		CD 380H	
Parameter	Mass Flow	Power	Mass Flow	Power	Mass Flow	Power
Unit	kg/s	W	kg/s	W	kg/s	W
C_1	0.2436384	-11206.18	0.1515211	-6897.5	0.08435603	-3929.08
C_2	0.0066928	-414.001	0.0042987	-269.84	0.00238595	-156.067
C_3	-0.000926	454.4165	-0.000601	280.963	-0.0003948	162.7711
C_4	6.266E-05	-4.569558	4.116E-05	-3.3767	2.2606E-05	-1.98566
C_5	-5.22E-06	6.017386	-4.883E-06	4.05552	-3.174E-06	2.398034
C_6	2.735E-06	-3.039822	1.587E-06	-1.8893	1.0344E-06	-1.10325
C_7	0	-0.01238	0	-0.0136	0	-0.00823
C_8	0	0.015474	0	0.01499	0	0.009257
C_9	0	-0.015835	0	-0.0108	0	-0.0063
C_{10}	0	0.008581	0	0.00503	0	0.002907

The experimental investigation of the system performance was carried out based on the prepared test campaign. The test campaign considered experimental points specified to the setpoints. Figure B.1 shows the test campaign carried out on the R744 transcritical multi-ejector refrigeration test facility for the operating conditions presented in Table 5.2.

Multi-ejector System		CO_2 exit gas cooler temperature (T_6)							
P_{rec}	Pressure Tank Lift (Δp)	36	34	32	30	28	26	^{o}C	
30	2.0	1_1	1_9	1_17	1_25	1_33	1_41		
32	4.0	1_2	1_10	1_18	1_26	1_34	1_42		
34	6.0	1_3	1_11	1_19	1_27	1_35	1_43		Legend
36	8.0	1_4	1_12	1_20	1_28	1_36	1_44	1_0	Investigated
38	10.0	1_5	1_13	1_21	1_29	1_37	1_45	1_0	Rejected
40	12.0	1_6	1_14	1_22	1_30	1_38	1_46		
42	14.0	1_7	1_15	1_23	1_31	1_39	1_47		
44	16.0	1_8	1_16	1_24	1_32	1_40	1_48		
	bar								

(a) Test campaign of the R744 Multi-ejector System for the 1st cooling demand.

| Parallel System | | CO$_2$ exit gas cooler temperature (T$_6$) | | | | | | |
P_{rec}	Pressure Tank Lift (Δp)	36	34	32	30	28	26	°C
30	2.0	2_1	2_9	2_17	2_25	2_33	~~2_41~~	
32	4.0	2_2	2_10	2_18	2_26	~~2_34~~	~~2_42~~	
34	6.0	2_3	2_11	2_19	~~2_27~~	2_35	~~2_43~~	Legend
36	8.0	2_4	2_12	~~2_20~~	2_28	2_36	~~2_44~~	1_0 Investigated
38	10.0	2_5	~~2_13~~	2_21	2_29	2_37	~~2_45~~	~~1_0~~ Rejected
40	12.0	~~2_6~~	2_14	2_22	2_30	~~2_38~~	~~2_46~~	
42	14.0	~~2_7~~	2_15	2_23	~~2_31~~	~~2_39~~	~~2_47~~	
44	16.0	~~2_8~~	2_16	2_24	~~2_32~~	~~2_40~~	~~2_48~~	
	bar							

(b) Test campaign of the R744 Parallel System for the 1st cooling demand.

| Multi-ejector System | | CO$_2$ exit gas cooler temperature (T$_6$) | | | | | | |
P_{rec}	Pressure Tank Lift (Δp)	36	34	32	30	28	26	°C
30	2.0	~~1_49~~	~~1_57~~	~~1_65~~	~~1_73~~	1_81	~~1_89~~	
32	4.0	~~1_50~~	~~1_58~~	1_66	1_74	1_82	1_90	
34	6.0	1_51	1_59	1_67	1_75	1_83	1_91	Legend
36	8.0	1_52	1_60	1_68	1_76	1_84	~~1_92~~	1_0 Investigated
38	10.0	1_53	1_61	1_69	~~1_77~~	~~1_85~~	~~1_93~~	~~1_0~~ Rejected
40	12.0	~~1_54~~	~~1_62~~	~~1_70~~	~~1_78~~	~~1_86~~	~~1_94~~	
42	14.0	~~1_55~~	~~1_63~~	~~1_71~~	~~1_79~~	~~1_87~~	~~1_95~~	
44	16.0	~~1_56~~	~~1_64~~	~~1_72~~	~~1_80~~	~~1_88~~	~~1_96~~	
	bar							

(c) Test campaign of the R744 Multi-ejector System for the 2nd cooling demand.

| Parallel System | | CO$_2$ exit gas cooler temperature (T$_6$) | | | | | | |
P_{rec}	Pressure Tank Lift (Δp)	36	34	32	30	28	26	°C
30	2.0	2_49	2_57	2_65	2_73	2_81	2_89	
32	4.0	2_50	2_58	2_66	2_74	2_82	~~2_90~~	
34	6.0	2_51	2_59	2_67	2_75	~~2_83~~	2_91	Legend
36	8.0	~~2_52~~	~~2_60~~	~~2_68~~	2_76	2_84	2_92	1_0 Investigated
38	10.0	~~2_53~~	~~2_61~~	~~2_69~~	~~2_77~~	2_85	~~2_93~~	~~1_0~~ Rejected
40	12.0	~~2_54~~	~~2_62~~	~~2_70~~	~~2_78~~	~~2_86~~	~~2_94~~	
42	14.0	~~2_55~~	~~2_63~~	~~2_71~~	~~2_79~~	~~2_87~~	~~2_95~~	
44	16.0	~~2_56~~	~~2_64~~	~~2_72~~	~~2_80~~	~~2_88~~	~~2_96~~	
	bar							

(d) Test campaign of the R744 Parallel System for the 2nd cooling demand.

Figure B.1: The experimental investigation of the R744 multi-ejector refrigeration system and the R744 parallel refrigeration system for the both refrigeration demands presented in Table 5.2.

Table B.4:   Raw data of the multi-ejector block parameters for experimental points presented in Figure B.1. Units are shown in Table B.1.

ID name	U	1_3		1_4		1_5		1_11		1_12		1_13		1_18		1_19		1_20	
η_{ej}	U_A	0.308	0.007	0.272	0.012	0.165	0.007	0.301	0.005	0.264	0.007	0.108	0.008	0.329	0.004	0.282	0.005	0.214	0.007
	U_B		0.004		0.004		0.002		0.004		0.003		0.001		0.004		0.004		0.003
Φ	U_A	0.287	0.007	0.218	0.009	0.109	0.005	0.266	0.004	0.195	0.005	0.066	0.005	0.332	0.004	0.236	0.004	0.150	0.005
	U_B		0.001		0.001		0.000		0.001		0.001		0.000		0.001		0.001		0.000
Π	U_A	1.316	0.010	1.350	0.009	1.392	0.004	1.306	0.004	1.338	0.007	1.381	0.003	1.255	0.003	1.283	0.002	1.314	0.002
	U_B		0.006		0.007		0.007		0.006		0.007		0.007		0.006		0.006		0.006
P_{lift}	U_A	8.566	0.251	9.608	0.224	10.998	0.089	8.344	0.103	9.356	0.170	10.741	0.081	6.802	0.074	7.797	0.048	8.825	0.053
	U_B		0.155		0.160		0.167		0.155		0.160		0.167		0.149		0.155		0.161
P_{motive}	U_A	83.556	0.757	84.213	0.504	83.536	0.274	79.795	0.313	80.599	0.245	79.999	0.171	75.594	0.155	74.908	0.172	75.574	0.244
	U_B		0.289		0.292		0.289		0.276		0.279		0.277		0.262		0.259		0.262
T_{motive}	U_A	31.959	0.242	31.857	0.515	31.715	0.109	30.387	0.184	29.839	0.087	30.120	0.068	28.344	0.084	28.175	0.092	28.216	0.167
	U_B		0.531		0.530		0.530		0.522		0.519		0.520		0.510		0.509		0.509
$P_{suction}$	U_A	27.089	0.093	27.471	0.115	28.071	0.066	27.227	0.059	27.660	0.123	28.212	0.052	26.721	0.046	27.559	0.030	28.091	0.035
	U_B		0.094		0.095		0.097		0.094		0.096		0.098		0.093		0.095		0.097
$T_{suction}$	U_A	-0.848	0.234	-0.625	0.142	1.238	0.030	-1.358	0.139	0.065	0.051	2.624	0.068	-2.093	0.117	-0.849	0.071	1.612	0.051
	U_B		0.342		0.343		0.354		0.339		0.347		0.362		0.334		0.342		0.356
P_{outlet}	U_A	35.654	0.233	37.078	0.192	39.069	0.059	35.571	0.084	37.015	0.117	38.954	0.062	33.522	0.058	35.356	0.037	36.916	0.040
	U_B		0.124		0.128		0.135		0.123		0.128		0.135		0.116		0.122		0.128
T_{outlet}	U_A	1.635	0.216	3.113	0.201	5.048	0.046	1.530	0.097	3.014	0.100	4.927	0.059	-0.706	0.035	1.233	0.042	2.870	0.020
	U_B		0.356		0.364		0.376		0.355		0.364		0.375		0.342		0.354		0.363
$m_{CO2,motive}$	U_A	14.467	0.308	14.039	0.493	12.990	0.104	14.195	0.165	12.970	0.176	12.534	0.091	13.583	0.126	13.346	0.171	11.817	0.113
	U_B		0.033		0.032		0.030		0.033		0.030		0.029		0.031		0.031		0.027
$m_{CO2,suction}$	U_A	4.146	0.039	3.060	0.067	1.416	0.059	3.778	0.041	2.524	0.059	0.823	0.063	4.516	0.043	3.146	0.038	1.778	0.056
	U_B		0.010		0.007		0.003		0.009		0.006		0.002		0.010		0.007		0.004
Configuration		VEJ3		VEJ3		VEJ3		VEJ3		VEJ3		VEJ3		VEJ3		VEJ3		VEJ3	
		VEJ2		VEJ2		VEJ2		VEJ2		VEJ2		VEJ2		VEJ2		VEJ2		VEJ2	
		VEJ1		VEJ1				VEJ1						VEJ1		VEJ1			

Table B.5: Raw data of the multi-ejector block parameters for experimental points presented in Figure B.1. Units are shown in Table B.1.

ID name		1_26	1_27	1_28	1_34	1_35	1_36	1_51	1_52	1_53
η_{ej}	value	0.324	0.273	0.172	0.316	0.244	0.075	0.310	0.259	0.167
	U_A	0.006	0.006	0.013	0.013	0.021	0.049	0.003	0.004	0.007
	U_B	0.004	0.003	0.002	0.004	0.003	0.001	0.004	0.004	0.002
Φ	value	0.316	0.211	0.106	0.298	0.170	0.040	0.282	0.202	0.112
	U_A	0.005	0.005	0.008	0.011	0.014	0.026	0.003	0.003	0.005
	U_B	0.001	0.001	0.000	0.001	0.001	0.000	0.001	0.001	0.000
Π	value	1.227	1.269	1.311	1.214	1.261	1.304	1.318	1.355	1.386
	U_A	0.003	0.002	0.004	0.006	0.006	0.011	0.004	0.003	0.003
	U_B	0.006	0.006	0.006	0.006	0.006	0.006	0.006	0.007	0.007
P_{lift}	value	6.159	7.485	8.719	5.831	7.279	8.552	8.593	9.752	10.905
	U_A	0.080	0.061	0.103	0.144	0.148	0.253	0.089	0.080	0.067
	U_B	0.149	0.156	0.160	0.148	0.155	0.160	0.155	0.160	0.167
P_{motive}	value	70.397	71.918	71.814	67.748	67.996	67.686	83.257	83.428	83.533
	U_A	0.162	0.188	0.265	0.256	0.334	0.611	0.274	0.214	0.174
	U_B	0.244	0.249	0.249	0.235	0.236	0.234	0.288	0.289	0.289
T_{motive}	value	25.962	26.362	26.081	24.479	24.289	24.043	31.599	31.798	31.875
	U_A	0.092	0.116	0.139	0.498	0.460	0.765	0.179	0.194	0.102
	U_B	0.496	0.499	0.497	0.488	0.487	0.485	0.529	0.530	0.530
$P_{suction}$	value	27.155	27.781	28.012	27.212	27.885	28.133	27.031	27.504	28.237
	U_A	0.044	0.035	0.076	0.066	0.131	0.211	0.047	0.049	0.051
	U_B	0.094	0.096	0.097	0.094	0.097	0.097	0.094	0.095	0.098
$T_{suction}$	value	-1.407	0.904	1.780	-0.981	0.402	3.639	-1.135	0.028	1.798
	U_A	0.102	0.201	0.212	0.055	0.079	2.652	0.027	0.061	0.069
	U_B	0.338	0.352	0.357	0.341	0.349	0.367	0.340	0.347	0.357
P_{outlet}	value	33.314	35.266	36.731	33.044	35.164	36.685	35.624	37.256	39.141
	U_A	0.066	0.050	0.070	0.128	0.070	0.139	0.076	0.063	0.044
	U_B	0.115	0.122	0.127	0.114	0.122	0.127	0.123	0.129	0.136
T_{outlet}	value	-1.007	1.117	2.717	-1.229	1.069	2.616	1.475	3.257	5.123
	U_A	0.044	0.031	0.064	0.134	0.045	0.119	0.061	0.043	0.022
	U_B	0.341	0.353	0.362	0.339	0.353	0.362	0.355	0.365	0.376
$m_{CO_2,motive}$	value	12.835	11.540	11.982	12.287	11.964	10.307	14.960	14.981	14.985
	U_A	0.189	0.180	0.274	0.433	0.323	0.370	0.110	0.110	0.126
	U_B	0.030	0.027	0.028	0.028	0.028	0.024	0.035	0.035	0.035
$m_{CO_2,suction}$	value	4.061	2.432	1.275	3.659	2.031	0.416	4.217	3.029	1.682
	U_A	0.035	0.040	0.095	0.056	0.162	0.271	0.025	0.041	0.072
	U_B	0.009	0.006	0.003	0.008	0.005	0.001	0.010	0.007	0.004
Configuration		VEJ3	VEJ3	VEJ3	VEJ3	VEJ3	VEJ3	VEJ3	VEJ3	VEJ3
		VEJ2	VEJ2	VEJ2	VEJ2	VEJ2		VEJ2	VEJ2	VEJ2
		VEJ1			VEJ1		VEJ1	VEJ1	VEJ1	VEJ1

Table B.6: Raw data of the multi-ejector block parameters for experimental points presented in Figure B.1. Units are shown in Table B.1.

ID name		1_59	1_60	1_61	1_66	1_67	1_68	1_69	1_74	1_75
η_{ej}	value	0.312	0.241	0.095	0.331	0.297	0.188	0.031	0.328	0.277
	U_A	0.004	0.008	0.009	0.004	0.005	0.006	0.005	0.005	0.007
	U_B	0.004	0.003	0.001	0.004	0.004	0.003	0.000	0.004	0.004
Φ	value	0.283	0.179	0.058	0.332	0.249	0.130	0.018	0.318	0.218
	U_A	0.003	0.006	0.005	0.004	0.004	0.004	0.003	0.005	0.006
	U_B	0.001	0.001	0.000	0.001	0.001	0.000	0.000	0.001	0.001
Π	value	1.294	1.332	1.379	1.251	1.279	1.319	1.355	1.229	1.267
	U_A	0.003	0.002	0.002	0.003	0.003	0.003	0.003	0.002	0.003
	U_B	0.006	0.007	0.007	0.006	0.006	0.006	0.007	0.006	0.006
P_{lift}	value	8.020	9.240	10.695	6.718	7.687	8.990	10.049	6.182	7.393
	U_A	0.063	0.053	0.054	0.075	0.071	0.065	0.066	0.056	0.084
	U_B	0.154	0.161	0.167	0.149	0.155	0.161	0.165	0.148	0.155
P_{motive}	value	79.225	79.041	79.577	75.403	75.250	75.504	74.980	70.948	71.610
	U_A	0.163	0.140	0.163	0.123	0.217	0.325	0.199	0.172	0.360
	U_B	0.274	0.274	0.276	0.261	0.261	0.262	0.260	0.246	0.248
T_{motive}	value	30.019	29.774	30.031	27.970	27.906	28.236	28.130	25.826	26.246
	U_A	0.066	0.157	0.063	0.070	0.150	0.242	0.119	0.087	0.135
	U_B	0.520	0.518	0.520	0.508	0.508	0.509	0.509	0.496	0.498
$P_{suction}$	value	27.237	27.863	28.240	26.767	27.539	28.137	28.305	27.001	27.639
	U_A	0.047	0.041	0.030	0.051	0.044	0.042	0.042	0.036	0.054
	U_B	0.094	0.097	0.098	0.093	0.095	0.097	0.098	0.094	0.096
$T_{suction}$	value	-1.167	0.389	4.118	-1.960	-0.646	1.259	-1.539	-1.687	-0.218
	U_A	0.098	0.042	0.152	0.043	0.028	0.052	1.204	0.091	0.024
	U_B	0.340	0.349	0.370	0.335	0.343	0.354	0.338	0.337	0.345
P_{outlet}	value	35.257	37.102	38.935	33.485	35.226	37.127	38.354	33.184	35.032
	U_A	0.042	0.035	0.045	0.055	0.055	0.050	0.051	0.042	0.065
	U_B	0.122	0.129	0.135	0.116	0.122	0.129	0.133	0.115	0.121
T_{outlet}	value	1.108	3.125	4.962	-0.769	1.086	3.085	4.405	-1.128	0.859
	U_A	0.028	0.027	0.014	0.045	0.038	0.057	0.061	0.027	0.046
	U_B	0.353	0.364	0.375	0.342	0.353	0.364	0.372	0.340	0.351
$m_{CO_2,motive}$	value	14.090	14.324	14.506	13.764	13.775	13.662	13.824	13.354	13.352
	U_A	0.099	0.212	0.128	0.136	0.156	0.158	0.120	0.178	0.162
	U_B	0.033	0.033	0.034	0.032	0.032	0.032	0.032	0.031	0.031
$m_{CO_2,suction}$	value	3.991	2.557	0.834	4.567	3.429	1.774	0.255	4.244	2.907
	U_A	0.040	0.069	0.078	0.035	0.038	0.049	0.044	0.032	0.065
	U_B	0.009	0.006	0.002	0.011	0.008	0.004	0.001	0.010	0.007
Configuration		VEJ3	VEJ3	VEJ3	VEJ3	VEJ3	VEJ3	VEJ3	VEJ3	VEJ3
		VEJ2	VEJ2	VEJ2	VEJ2	VEJ2	VEJ2	VEJ2	VEJ2	VEJ2
		VEJ1	VEJ1	VEJ1	VEJ1	VEJ1	VEJ1	VEJ1	VEJ1	VEJ1

Table B.7: Raw data of the multi-ejector block parameters for experimental points presented in Figure B.1. Units are shown in Table B.1.

ID name		1_76	1_81	1_82	1_83	1_84	1_90	1_91
η_{ej}	U_A	0.131	0.334	0.315	0.226	0.095	0.308	0.233
		0.011	0.007	0.007	0.008	0.009	0.008	0.010
	U_B	0.002	0.004	0.004	0.003	0.001	0.004	0.003
Φ	U_A	0.083	0.391	0.297	0.158	0.055	0.264	0.149
		0.007	0.008	0.006	0.005	0.005	0.007	0.006
	U_B	0.000	0.001	0.001	0.001	0.000	0.001	0.000
Π	U_A	1.305	1.178	1.211	1.257	1.291	1.207	1.245
		0.002	0.005	0.002	0.003	0.004	0.003	0.005
	U_B	0.006	0.006	0.006	0.006	0.006	0.006	0.006
P_{lift}	U_A	8.620	4.779	5.772	7.142	8.227	5.676	6.871
		0.054	0.116	0.061	0.081	0.088	0.067	0.116
	U_B	0.161	0.144	0.149	0.155	0.160	0.149	0.155
P_{motive}	U_A	71.372	66.765	67.002	66.890	67.548	64.397	64.224
		0.253	0.188	0.164	0.245	0.193	0.225	0.232
	U_B	0.247	0.231	0.232	0.232	0.234	0.223	0.222
T_{motive}	U_A	26.359	24.008	24.326	24.188	24.462	22.745	22.220
		0.079	0.170	0.127	0.120	0.097	0.109	0.445
	U_B	0.499	0.485	0.487	0.486	0.488	0.478	0.475
$P_{suction}$	U_A	28.222	26.859	27.333	27.805	28.274	27.445	28.042
		0.033	0.065	0.038	0.041	0.059	0.040	0.092
	U_B	0.098	0.093	0.095	0.096	0.098	0.095	0.097
$T_{suction}$	U_A	2.738	-2.453	-1.403	0.713	3.267	-0.938	0.643
		0.118	0.071	0.050	0.057	0.021	0.013	0.065
	U_B	0.362	0.332	0.338	0.351	0.365	0.341	0.350
P_{outlet}	U_A	36.842	31.639	33.105	34.947	36.501	33.120	34.913
		0.042	0.097	0.047	0.069	0.065	0.053	0.071
	U_B	0.128	0.110	0.115	0.121	0.126	0.115	0.121
T_{outlet}	U_A	2.804	-2.941	-1.150	0.848	2.453	-1.164	0.795
		0.028	0.092	0.024	0.048	0.037	0.030	0.052
	U_B	0.363	0.329	0.340	0.351	0.361	0.340	0.351
$m_{CO2,motive}$	U_A	13.169	12.575	12.664	12.904	13.122	13.021	13.050
		0.166	0.246	0.201	0.252	0.245	0.286	0.311
	U_B	0.030	0.029	0.029	0.030	0.030	0.030	0.030
$m_{CO2,suction}$	U_A	1.090	4.922	3.761	2.043	0.724	3.444	1.945
		0.093	0.030	0.056	0.056	0.065	0.039	0.065
	U_B	0.003	0.011	0.009	0.005	0.002	0.008	0.004
Configuration		VEJ3	VEJ3	VEJ3	VEJ3	VEJ3	VEJ3	VEJ3
		VEJ2	VEJ2	VEJ2	VEJ2	VEJ2	VEJ2	VEJ2
		VEJ1	VEJ1	VEJ1	VEJ1	VEJ1	VEJ1	VEJ1

Table B.8: Raw data of the system parameters for experimental points presented in Figure B.1. Units are shown in Table B.1.

ID name		1_3		1_4		1_5		1_11		1_12		1_13		1_18		1_19		1_20	
T_6	U_A	36.168	0.059	36.245	0.269	35.813	0.124	34.375	0.129	34.174	0.049	34.071	0.056	32.257	0.050	31.942	0.055	31.994	0.135
	U_B		0.555		0.556		0.553		0.545		0.544		0.543		0.533		0.531		0.531
T_{51}	U_A	12.093	0.055	11.903	0.030	11.920	0.036	12.092	0.061	11.864	0.056	11.948	0.024	12.128	0.040	11.880	0.036	11.966	0.117
	U_B		0.416		0.415		0.415		0.416		0.415		0.415		0.416		0.415		0.415
$T_{0,MT}$	U_A	-7.963	0.093	-8.085	0.113	-7.928	0.050	-8.010	0.066	-8.086	0.124	-7.884	0.038	-8.125	0.049	-7.935	0.026	-7.804	0.045
	U_B		0.300		0.300		0.301		0.300		0.300		0.301		0.299		0.301		0.301
P_{gc}	U_A	83.700	0.778	84.285	0.533	83.476	0.335	79.919	0.352	80.515	0.316	79.919	0.225	75.654	0.233	74.938	0.307	75.417	0.296
	U_B		0.290		0.292		0.289		0.277		0.279		0.277		0.262		0.260		0.261
P_{rec}	U_A	34.487	0.223	36.023	0.178	38.106	0.062	34.445	0.083	36.011	0.123	38.050	0.052	32.342	0.054	34.262	0.047	35.990	0.028
	U_B		0.119		0.125		0.132		0.119		0.125		0.132		0.112		0.119		0.125
$P_{0.MT}$	U_A	28.027	0.082	27.947	0.105	28.069	0.066	27.989	0.055	27.947	0.107	28.108	0.043	27.914	0.037	28.061	0.037	28.159	0.035
	U_B		0.097		0.097		0.097		0.097		0.097		0.097		0.097		0.097		0.098
P_{lift}	U_A	6.460	0.154	8.077	0.158	10.037	0.164	6.456	0.154	8.064	0.158	9.942	0.164	4.428	0.148	6.201	0.153	7.831	0.158
	U_B		0.154		0.158		0.164		0.154		0.158		0.164		0.148		0.153		0.158
$T_{ambient}$	U_A	20.631	0.677	20.631	0.677	20.631	0.677	19.870	0.111	19.870	0.111	19.870	0.111	19.940	0.092	19.940	0.092	19.926	0.151
	U_B		0.466		0.466		0.466		0.461		0.461		0.461		0.462		0.462		0.461
COP	U_A	2.170	0.022	2.313	0.043	2.459	0.021	2.446	0.017	2.571	0.024	2.662	0.020	2.530	0.017	2.772	0.020	2.911	0.032
	U_B		0.016		0.017		0.020		0.019		0.021		0.022		0.020		0.023		0.026
η_{ex}	U_A	0.105	0.001	0.113	0.001	0.119	0.002	0.113	0.000	0.120	0.001	0.122	0.001	0.117	0.000	0.131	0.000	0.135	0.001
	U_B		0.001		0.001		0.001		0.001		0.001		0.002		0.001		0.001		0.002
Q_{evap}	U_A	39.119	0.028	39.434	0.023	38.498	0.028	40.566	0.029	39.523	0.030	38.520	0.026	39.884	0.026	40.195	0.022	38.570	0.034
	U_B		0.184		0.185		0.181		0.190		0.185		0.181		0.187		0.188		0.181
$N_{el,CD1400H}$	U_A	6.041	0.057	7.710	0.074	9.733	0.095	6.451	0.060	7.884	0.052	9.850	0.079	4.835	0.050	6.565	0.044	7.895	0.052
	U_B		0.058		0.058		0.058		0.058		0.058		0.058		0.058		0.058		0.058
$N_{el,CD1000H}$	U_A	7.611	0.150	5.906	0.262	5.923	0.095	6.433	0.079	4.680	0.096	4.622	0.076	6.948	0.079	4.981	0.061	5.353	0.136
	U_B		0.058		0.058		0.058		0.058		0.058		0.058		0.058		0.058		0.058
$N_{el,CD380H}$	U_A	4.377	0.078	3.435	0.157	0.000	0.000	3.698	0.056	2.810	0.094	0.000	0.000	3.981	0.043	2.954	0.072	0.000	0.000
	U_B		0.058		0.058		0.058		0.058		0.058		0.058		0.058		0.058		0.058

Table B.9: Raw data of the system parameters for experimental points presented in Figure B.1. Units are shown in Table B.1.

ID name		1_26	U_A	U_B	1_27	U_A	U_B	1_28	U_A	U_B	1_34	U_A	U_B	1_35	U_A	U_B	1_36	U_A	U_B	1_51	U_A	U_B	1_52	U_A	U_B	1_53	U_A	U_B
T_6	$\frac{U_A}{U_B}$	29.801	0.061	0.518	30.203	0.062	0.521	30.015	0.079	0.520	28.186	0.252	0.509	28.283	0.064	0.510	27.715	0.155	0.506	34.439	0.069	0.119	35.989	0.153	0.554	35.996	0.063	0.554
T_{51}	$\frac{U_A}{U_B}$	11.889	0.054	0.415	11.907	0.083	0.415	11.874	0.085	0.415	11.933	0.113	0.415	12.161	0.057	0.417	11.853	0.080	0.415	15.092	0.071	0.434	14.804	0.039	0.432	15.273	0.054	0.435
$T_{0,MT}$	$\frac{U_A}{U_B}$	-7.927	0.022	0.301	-7.943	0.018	0.301	-8.008	0.079	0.300	-8.109	0.045	0.300	-7.958	0.100	0.300	-7.995	0.211	0.300	-7.964	0.042	0.300	-8.104	0.049	0.300	-7.729	0.051	0.302
P_{gc}	$\frac{U_A}{U_B}$	70.354	0.237	0.244	71.699	0.264	0.248	71.625	0.343	0.248	67.614	0.324	0.234	67.845	0.372	0.235	67.332	0.649	0.233	83.434	0.307	0.289	83.611	0.266	0.290	83.728	0.253	0.290
P_{rec}	$\frac{U_A}{U_B}$	32.160	0.068	0.111	34.264	0.058	0.119	35.820	0.073	0.124	31.990	0.115	0.111	34.213	0.067	0.119	35.863	0.143	0.124	34.439	0.069	0.119	36.201	0.061	0.125	38.133	0.052	0.132
$P_{0,MT}$	$\frac{U_A}{U_B}$	28.072	0.037	0.097	28.058	0.031	0.097	27.998	0.070	0.097	27.926	0.042	0.097	28.040	0.100	0.097	28.015	0.185	0.097	28.031	0.052	0.097	27.936	0.037	0.097	28.227	0.057	0.098
P_{lift}	$\frac{U_A}{U_B}$	4.088	0.148	0.148	6.206	0.153	0.153	7.823	0.157	0.157	4.064	0.147	0.147	6.173	0.153	0.153	7.847	0.158	0.158	6.409	0.154	0.154	8.266	0.158	0.158	9.906	0.164	0.164
$T_{ambient}$	$\frac{U_A}{U_B}$	19.926	0.151	0.461	19.998	0.050	0.462	19.998	0.050	0.462	20.181	0.004	0.463	20.181	0.004	0.463	20.181	0.004	0.463	20.429	0.011	0.464	20.181	0.004	0.463	20.181	0.004	0.463
COP	$\frac{U_A}{U_B}$	2.967	0.022	0.026	3.098	0.017	0.029	3.230	0.042	0.030	3.275	0.060	0.031	3.470	0.023	0.034	3.382	0.045	0.035	2.233	0.010	0.015	2.353	0.020	0.016	2.390	0.028	0.016
η_{ex}	$\frac{U_A}{U_B}$	0.140	0.000	0.001	0.145	0.001	0.002	0.153	0.003	0.003	0.158	0.001	0.002	0.166	0.001	0.003	0.159	0.004	0.004	0.088	0.000	0.001	0.093	0.000	0.001	0.094	0.001	0.001
Q_{evap}	$\frac{U_A}{U_B}$	39.465	0.028	0.185	38.792	0.031	0.182	39.581	0.026	0.185	40.104	0.033	0.187	40.727	0.049	0.190	36.894	0.028	0.174	44.827	0.030	0.208	45.153	0.032	0.209	47.345	0.033	0.218
$N_{el,CD1400H}$	$\frac{U_A}{U_B}$	4.713	0.056	0.058	6.605	0.038	0.058	8.177	0.054	0.058	4.945	0.055	0.058	7.026	0.055	0.058	7.863	0.104	0.058	7.380	0.056	0.058	9.338	0.095	0.058	11.976	0.181	0.058
$N_{el,CD1000H}$	$\frac{U_A}{U_B}$	5.469	0.056	0.058	5.919	0.054	0.058	4.079	0.150	0.058	4.617	0.183	0.058	4.710	0.052	0.058	0.000	0.000	0.058	8.080	0.051	0.058	6.248	0.101	0.058	4.879	0.097	0.058
$N_{el,CD380H}$	$\frac{U_A}{U_B}$	3.121	0.057	0.058	0.000	0.000	0.058	0.000	0.000	0.058	2.683	0.117	0.058	0.000	0.000	0.058	3.046	0.099	0.058	4.619	0.041	0.058	3.606	0.082	0.058	2.952	0.110	0.058

Table B.10: Raw data of the system parameters for experimental points presented in Figure B.1. Units are shown in Table B.1.

ID name		1_26	1_27	1_28	1_34	1_35	1_36	1_51	1_52	1_53
$\eta_{comp,CD1400H}$	value	0.743	0.758	0.734	0.747	0.743	0.729	0.766	0.743	0.682
	U_A	0.010	0.010	0.010	0.011	0.009	0.012	0.010	0.009	0.008
	U_B	0.016	0.016	0.016	0.017	0.016	0.016	0.015	0.014	0.013
$\eta_{comp,CD1000H}$	value	0.608	0.540	0.550	0.632	0.559	0.000	0.518	0.538	0.520
	U_A	0.008	0.008	0.008	0.010	0.008	0.000	0.007	0.008	0.007
	U_B	0.018	0.018	0.020	0.019	0.020	0.000	0.015	0.017	0.018
$\eta_{comp,CD380H}$	value	0.548	0.000	0.000	0.571	0.000	0.441	0.464	0.482	0.465
	U_A	0.007	0.000	0.000	0.009	0.000	0.006	0.007	0.007	0.006
	U_B	0.016	0.000	0.000	0.017	0.000	0.018	0.013	0.015	0.016
$\eta_{comp,overall}$	value	0.642	0.655	0.672	0.665	0.669	0.648	0.597	0.627	0.610
	U_A	0.005	0.006	0.007	0.006	0.006	0.007	0.005	0.005	0.005
	U_B	0.010	0.013	0.012	0.011	0.013	0.010	0.009	0.009	0.009
$\eta_{vol,CD1400H}$	value	0.870	0.879	0.865	0.879	0.878	0.873	0.855	0.844	0.806
	U_A	0.008	0.003	0.008	0.009	0.011	0.020	0.006	0.007	0.007
	U_B	0.023	0.023	0.022	0.023	0.023	0.023	0.022	0.021	0.020
$\eta_{vol,CD1000H}$	value	0.763	0.700	0.696	0.790	0.723	0.000	0.646	0.644	0.615
	U_A	0.005	0.003	0.019	0.022	0.005	0.000	0.003	0.007	0.006
	U_B	0.010	0.009	0.009	0.010	0.009	0.000	0.008	0.008	0.008
$\eta_{vol,CD380H}$	value	0.746	0.000	0.000	0.774	0.000	0.656	0.624	0.622	0.594
	U_A	0.005	0.000	0.000	0.021	0.000	0.013	0.003	0.007	0.006
	U_B	0.010	0.000	0.000	0.010	0.000	0.009	0.009	0.009	0.008
$\eta_{vol,overall}$	value	0.792	0.781	0.792	0.818	0.803	0.797	0.706	0.720	0.707
	U_A	0.004	0.002	0.009	0.010	0.006	0.013	0.002	0.004	0.004
	U_B	0.004	0.002	0.009	0.010	0.006	0.013	0.002	0.004	0.004
T_{53}	value	12.053	12.084	12.062	12.100	12.354	12.026	15.219	14.949	15.393
	U_A	0.054	0.080	0.087	0.109	0.061	0.081	0.070	0.041	0.059
	U_B	0.416	0.416	0.416	0.416	0.418	0.416	0.434	0.433	0.435
T_{54}	value	1.467	1.698	1.452	1.279	1.320	2.094	3.481	3.118	2.970
	U_A	0.047	0.115	0.043	0.068	0.070	0.115	0.070	0.035	0.048
	U_B	0.355	0.356	0.355	0.354	0.354	0.358	0.367	0.364	0.364
$m_{gl,evap}$	value	50.599	50.685	50.631	50.300	50.088	50.396	51.656	51.642	51.559
	U_A	0.018	0.018	0.016	0.020	0.031	0.016	0.016	0.019	0.018
	U_B	0.117	0.117	0.117	0.116	0.116	0.116	0.119	0.119	0.119
$m_{CO2,CD1400H}$	value	4.673	6.462	7.876	5.141	7.253	8.130	6.070	7.550	9.224
	U_A	0.021	0.016	0.059	0.029	0.069	0.157	0.028	0.048	0.077
	U_B	0.062	0.116	0.170	0.074	0.145	0.182	0.101	0.154	0.228
$m_{CO2,CD1000H}$	value	5.966	6.269	4.762	5.482	5.626	0.000	6.541	5.555	4.539
	U_A	0.045	0.031	0.112	0.150	0.042	0.000	0.032	0.063	0.038
	U_B	0.084	0.095	0.057	0.071	0.077	0.000	0.105	0.078	0.054
$m_{CO2,CD380H}$	value	3.120	0.000	0.000	2.873	0.000	3.288	3.377	2.867	2.341
	U_A	0.023	0.000	0.000	0.077	0.000	0.005	0.016	0.032	0.019
	U_B	0.045	0.000	0.000	0.038	0.000	0.020	0.055	0.040	0.028

Table B.11: Raw data of the system parameters for experimental points presented in Figure B.1. Units are shown in Table B.1.

ID name		1_59	1_60	1_61	1_66	1_67	1_68	1_69	1_74	1_75
T_6	value	34.011	33.777	33.938	31.984	31.866	31.976	31.795	29.835	30.132
	U_A	0.064	0.073	0.043	0.037	0.128	0.177	0.088	0.049	0.122
	U_B	0.543	0.541	0.542	0.531	0.530	0.531	0.530	0.519	0.520
T_{51}	value	15.084	15.030	15.063	14.819	15.290	15.237	15.004	14.786	15.109
	U_A	0.070	0.029	0.073	0.026	0.067	0.053	0.084	0.094	0.054
	U_B	0.433	0.433	0.433	0.432	0.435	0.434	0.433	0.432	0.434
$T_{0,MT}$	value	-7.901	-7.873	-7.898	-8.078	-7.868	-7.812	-7.854	-8.005	-7.981
	U_A	0.031	0.024	0.017	0.060	0.033	0.042	0.060	0.028	0.049
	U_B	0.301	0.301	0.301	0.300	0.301	0.301	0.301	0.300	0.300
P_{gc}	value	79.349	79.200	79.751	75.467	75.335	75.579	75.055	70.932	71.605
	U_A	0.243	0.214	0.258	0.213	0.292	0.386	0.290	0.238	0.432
	U_B	0.275	0.274	0.276	0.261	0.261	0.262	0.260	0.246	0.248
P_{rec}	value	34.093	36.061	38.031	32.287	34.142	36.174	37.487	32.030	33.962
	U_A	0.049	0.049	0.035	0.061	0.044	0.056	0.047	0.048	0.061
	U_B	0.118	0.125	0.132	0.112	0.118	0.125	0.130	0.111	0.118
$P_{0.MT}$	value	28.107	28.136	28.124	27.952	28.132	28.165	28.148	27.989	28.026
	U_A	0.044	0.024	0.029	0.048	0.031	0.021	0.028	0.036	0.064
	U_B	0.097	0.097	0.097	0.097	0.097	0.098	0.098	0.097	0.097
P_{lift}	value	5.986	7.925	9.907	4.334	6.010	8.009	9.339	4.041	5.936
	U_A	0.153	0.158	0.164	0.148	0.153	0.159	0.162	0.147	0.153
	U_B	0.153	0.158	0.164	0.148	0.153	0.159	0.162	0.147	0.153
$T_{ambient}$	value	20.429	20.429	20.429	21.623	21.623	21.623	20.429	21.623	21.623
	U_A	0.011	0.011	0.011	0.009	0.009	0.009	0.011	0.009	0.009
	U_B	0.464	0.464	0.464	0.471	0.471	0.471	0.464	0.471	0.471
COP	value	2.458	2.625	2.662	2.575	2.804	2.897	2.885	2.974	3.095
	U_A	0.017	0.021	0.040	0.012	0.022	0.032	0.025	0.018	0.028
	U_B	0.017	0.019	0.020	0.019	0.021	0.023	0.023	0.024	0.025
η_{ex}	value	0.098	0.105	0.104	0.116	0.124	0.128	0.114	0.136	0.139
	U_A	0.000	0.000	0.002	0.000	0.000	0.001	0.002	0.000	0.001
	U_B	0.001	0.001	0.002	0.001	0.001	0.002	0.002	0.001	0.002
Q_{evap}	value	45.481	45.675	44.523	45.400	47.089	46.356	44.432	45.506	46.450
	U_A	0.037	0.028	0.032	0.043	0.038	0.043	0.032	0.065	0.035
	U_B	0.211	0.211	0.207	0.210	0.217	0.214	0.206	0.210	0.214
$N_{el,CD1400H}$	value	7.332	9.366	11.582	6.055	7.901	9.917	11.460	5.862	7.797
	U_A	0.043	0.073	0.226	0.056	0.051	0.113	0.078	0.058	0.064
	U_B	0.058	0.058	0.058	0.058	0.058	0.058	0.058	0.058	0.058
$N_{el,CD1000H}$	value	7.109	5.069	5.140	7.369	5.629	6.084	3.938	5.997	4.532
	U_A	0.099	0.073	0.103	0.045	0.103	0.135	0.107	0.056	0.088
	U_B	0.058	0.058	0.058	0.058	0.058	0.058	0.058	0.058	0.058
$N_{el,CD380H}$	value	4.066	2.969	0.000	4.206	3.266	0.000	0.000	3.441	2.679
	U_A	0.064	0.092	0.000	0.031	0.068	0.000	0.000	0.042	0.084
	U_B	0.058	0.058	0.058	0.058	0.058	0.058	0.058	0.058	0.058

Table B.12: Raw data of the system parameters for experimental points presented in Figure B.1. Units are shown in Table B.1.

ID name		1_59	U_A	U_B	1_60	U_A	U_B	1_61	U_A	U_B	1_66	U_A	U_B	1_67	U_A	U_B	1_68	U_A	U_B	1_69	U_A	U_B	1_74	U_A	U_B	1_75	U_A	U_B
$\eta_{comp,CD1400H}$	U_A / U_B	0.761	0.009	0.015	0.731	0.009	0.015	0.676	0.008	0.013	0.757	0.009	0.016	0.747	0.009	0.015	0.705	0.008	0.014	0.661	0.008	0.014	0.754	0.009	0.016	0.740	0.009	0.016
$\eta_{comp,CD1000H}$	U_A / U_B	0.541	0.007	0.016	0.552	0.008	0.018	0.508	0.007	0.019	0.558	0.007	0.015	0.574	0.008	0.017	0.511	0.007	0.018	0.519	0.008	0.020	0.597	0.008	0.017	0.591	0.008	0.019
$\eta_{comp,CD380H}$	U_A / U_B	0.486	0.007	0.014	0.496	0.007	0.016	0.000	0.000	0.000	0.502	0.007	0.014	0.516	0.007	0.016	0.000	0.000	0.000	0.000	0.000	0.000	0.538	0.007	0.015	0.533	0.007	0.017
$\eta_{comp,overall}$	U_A / U_B	0.616	0.005	0.009	0.639	0.005	0.010	0.624	0.006	0.011	0.613	0.005	0.009	0.644	0.005	0.010	0.632	0.006	0.012	0.624	0.006	0.011	0.644	0.005	0.010	0.658	0.005	0.010
$\eta_{vol,CD1400H}$	U_A / U_B	0.861	0.004	0.022	0.845	0.006	0.022	0.810	0.004	0.021	0.865	0.008	0.022	0.862	0.004	0.022	0.837	0.007	0.021	0.810	0.005	0.021	0.874	0.008	0.023	0.867	0.006	0.022
$\eta_{vol,CD1000H}$	U_A / U_B	0.676	0.004	0.009	0.667	0.005	0.009	0.626	0.007	0.008	0.714	0.003	0.009	0.710	0.007	0.009	0.655	0.009	0.008	0.650	0.011	0.009	0.756	0.005	0.009	0.733	0.007	0.009
$\eta_{vol,CD380H}$	U_A / U_B	0.656	0.004	0.009	0.647	0.005	0.009	0.000	0.000	0.000	0.695	0.003	0.009	0.691	0.007	0.009	0.000	0.000	0.000	0.000	0.000	0.000	0.739	0.004	0.010	0.716	0.007	0.010
$\eta_{vol,overall}$	U_A / U_B	0.734	0.002	0.002	0.744	0.003	0.003	0.734	0.004	0.004	0.756	0.003	0.003	0.768	0.004	0.004	0.752	0.005	0.005	0.753	0.005	0.005	0.793	0.004	0.004	0.790	0.004	0.004
T_{53}	U_A / U_B	15.210	0.068	0.434	15.213	0.027	0.434	15.253	0.071	0.434	14.945	0.020	0.433	15.414	0.071	0.435	15.359	0.052	0.435	15.198	0.083	0.434	14.918	0.096	0.433	15.236	0.054	0.434
T_{54}	U_A / U_B	3.219	0.053	0.365	3.163	0.028	0.365	3.525	0.050	0.367	2.879	0.031	0.363	2.874	0.046	0.363	3.029	0.036	0.364	3.411	0.064	0.366	2.717	0.081	0.362	2.790	0.052	0.363
$m_{gl,evap}$	U_A / U_B	51.315	0.021	0.119	51.281	0.016	0.118	51.348	0.019	0.119	50.923	0.026	0.118	50.806	0.021	0.117	50.861	0.025	0.117	50.991	0.018	0.118	50.486	0.037	0.117	50.506	0.020	0.117
$m_{CO2,CD1400H}$	U_A / U_B	6.376	0.022	0.111	8.007	0.046	0.174	9.348	0.047	0.235	5.539	0.031	0.085	7.259	0.029	0.144	8.784	0.066	0.209	9.729	0.059	0.256	5.798	0.033	0.093	7.530	0.042	0.155
$m_{CO2,CD1000H}$	U_A / U_B	6.355	0.040	0.098	5.002	0.033	0.063	5.087	0.054	0.067	6.722	0.033	0.107	5.688	0.061	0.079	6.059	0.087	0.091	4.330	0.055	0.049	6.299	0.042	0.093	5.104	0.047	0.064
$m_{CO2,CD380H}$	U_A / U_B	3.294	0.021	0.051	2.592	0.017	0.033	0.000	0.000	0.000	3.498	0.017	0.056	2.959	0.030	0.041	0.000	0.000	0.000	0.000	0.000	0.000	3.291	0.022	0.049	2.663	0.024	0.034

Table B.13: Raw data of the system parameters for experimental points presented in Figure B.1. Units are shown in Table B.1.

ID name	U	1_76		1_81		1_82		1_83		1_84		1_90		1_91	
T_6	U_A	30.039	0.095	27.643	0.117	27.954	0.075	27.883	0.111	28.147	0.065	26.231	0.093	26.060	0.136
	U_B		0.520		0.506		0.508		0.507		0.509		0.498		0.497
T_{51}	U_A	15.035	0.127	15.353	0.032	14.860	0.038	14.977	0.137	14.920	0.021	14.969	0.047	15.056	0.061
	U_B		0.433		0.435		0.432		0.433		0.433		0.433		0.433
$T_{0,MT}$	U_A	-7.872	0.029	-7.702	0.051	-7.924	0.044	-8.104	0.046	-7.859	0.044	-7.954	0.029	-7.846	0.096
	U_B		0.301		0.302		0.301		0.300		0.301		0.300		0.301
P_{gc}	U_A	71.349	0.315	66.697	0.232	66.943	0.280	66.842	0.308	67.520	0.283	64.400	0.264	64.219	0.290
	U_B		0.247		0.231		0.232		0.232		0.234		0.223		0.222
P_{rec}	U_A	35.959	0.034	30.408	0.100	32.009	0.058	33.975	0.068	35.629	0.070	32.056	0.047	33.949	0.066
	U_B		0.125		0.105		0.111		0.118		0.123		0.111		0.118
$P_{0.MT}$	U_A	28.140	0.020	28.241	0.054	28.086	0.056	27.932	0.035	28.135	0.049	28.055	0.045	28.135	0.085
	U_B		0.097		0.098		0.097		0.097		0.097		0.097		0.097
P_{lift}	U_A	7.819	0.158	2.167	0.144	3.923	0.148	6.044	0.152	7.494	0.157	4.001	0.148	5.815	0.153
	U_B		0.158		0.144		0.148		0.152		0.157		0.148		0.153
$T_{ambient}$	U_A	20.969	0.014	20.156	0.008	20.969	0.014	20.969	0.014	20.506	0.038	20.969	0.014	20.969	0.014
	U_B		0.467		0.463		0.467		0.467		0.465		0.467		0.467
COP	U_A	3.184	0.034	3.096	0.016	3.356	0.032	3.527	0.033	3.510	0.027	3.672	0.029	3.924	0.057
	U_B		0.027		0.025		0.029		0.031		0.032		0.033		0.038
η_{ex}	U_A	0.135	0.002	0.122	0.000	0.147	0.001	0.154	0.002	0.145	0.002	0.162	0.001	0.170	0.003
	U_B		0.003		0.001		0.002		0.003		0.004		0.002		0.004
Q_{evap}	U_A	45.847	0.035	47.009	0.052	46.632	0.032	46.954	0.050	45.485	0.033	47.004	0.033	46.504	0.035
	U_B		0.212		0.216		0.215		0.216		0.210		0.216		0.214
$N_{el,CD1400H}$	U_A	9.953	0.074	4.883	0.056	6.120	0.052	8.233	0.092	9.536	0.068	6.186	0.050	7.726	0.111
	U_B		0.058		0.058		0.058		0.058		0.058		0.058		0.058
$N_{el,CD1000H}$	U_A	4.447	0.132	6.569	0.045	4.920	0.097	5.078	0.082	3.424	0.072	4.162	0.061	4.126	0.130
	U_B		0.058		0.058		0.058		0.058		0.058		0.058		0.058
$N_{el,CD380H}$	U_A	0.000	0.000	3.732	0.027	2.856	0.073	0.000	0.000	0.000	0.000	2.454	0.064	0.000	0.000
	U_B		0.058		0.058		0.058		0.058		0.058		0.058		0.058

Table B.14: Raw data of the system parameters for experimental points presented in Figure B.1. Units are shown in Table B.1.

ID name	U	1_76		1_81		1_82		1_83		1_84		1_90		1_91	
$\eta_{comp,CD1400H}$	U_A	0.691	0.008	0.744	0.009	0.749	0.010	0.719	0.009	0.685	0.008	0.745	0.009	0.719	0.011
	U_B		0.015		0.017		0.017		0.016		0.015		0.017		0.017
$\eta_{comp,CD1000H}$	U_A	0.541	0.007	0.598	0.008	0.622	0.008	0.559	0.008	0.544	0.008	0.631	0.008	0.571	0.008
	U_B		0.020		0.016		0.019		0.019		0.021		0.020		0.021
$\eta_{comp,CD380H}$	U_A	0.000	0.000	0.539	0.008	0.562	0.008	0.000	0.000	0.000	0.000	0.570	0.008	0.000	0.000
	U_B		0.000		0.015		0.017		0.000		0.000		0.018		0.000
$\eta_{comp,overall}$	U_A	0.644	0.006	0.630	0.005	0.665	0.005	0.658	0.006	0.647	0.006	0.674	0.005	0.668	0.007
	U_B		0.012		0.010		0.010		0.012		0.012		0.011		0.013
$\eta_{vol,CD1400H}$	U_A	0.838	0.004	0.877	0.011	0.881	0.009	0.866	0.008	0.842	0.006	0.886	0.006	0.873	0.009
	U_B		0.021		0.023		0.023		0.022		0.022		0.023		0.023
$\eta_{vol,CD1000H}$	U_A	0.691	0.014	0.781	0.004	0.786	0.010	0.733	0.009	0.705	0.005	0.798	0.005	0.749	0.018
	U_B		0.009		0.010		0.010		0.009		0.009		0.010		0.009
$\eta_{vol,CD380H}$	U_A	0.000	0.000	0.767	0.004	0.771	0.010	0.000	0.000	0.000	0.000	0.785	0.005	0.000	0.000
	U_B		0.000		0.010		0.010		0.000		0.000		0.010		0.000
$\eta_{vol,overall}$	U_A	0.779	0.006	0.807	0.004	0.820	0.006	0.805	0.006	0.793	0.004	0.833	0.003	0.819	0.009
	U_B		0.006		0.004		0.006		0.006		0.004		0.003		0.009
T_{53}	U_A	15.183	0.124	15.460	0.039	15.053	0.048	15.144	0.133	15.066	0.025	15.122	0.049	15.202	0.057
	U_B		0.434		0.436		0.433		0.434		0.433		0.434		0.434
T_{54}	U_A	2.880	0.058	2.654	0.043	2.349	0.031	2.338	0.073	2.721	0.038	2.131	0.034	2.347	0.068
	U_B		0.363		0.362		0.360		0.360		0.362		0.359		0.360
$m_{gl,evap}$	U_A	50.426	0.018	49.671	0.029	49.691	0.018	49.632	0.026	49.868	0.019	48.987	0.018	48.968	0.018
	U_B		0.116		0.115		0.115		0.115		0.115		0.113		0.113
$m_{CO2,CD1400H}$	U_A	9.208	0.047	5.190	0.037	6.480	0.045	8.373	0.071	9.361	0.063	6.853	0.031	8.371	0.075
	U_B		0.231		0.076		0.116		0.192		0.239		0.130		0.192
$m_{CO2,CD1000H}$	U_A	5.092	0.093	6.936	0.044	5.808	0.078	6.011	0.078	4.351	0.024	5.341	0.035	5.407	0.124
	U_B		0.065		0.110		0.079		0.086		0.048		0.068		0.070
$m_{CO2,CD380H}$	U_A	0.000	0.000	3.638	0.023	3.045	0.040	0.000	0.000	0.000	0.000	2.808	0.018	0.000	0.000
	U_B		0.000		0.059		0.042		0.000		0.000		0.036		0.000

Table B.15: Raw data of the system parameters for experimental points presented in Figure B.1. Units are shown in Table B.1.

ID name		2_1		2_2		2_3		2_4		2_5		2_9		2_10		2_11		2_12	
T_6	U_A	36.213	0.079	35.872	0.160	36.169	0.050	36.074	0.033	36.022	0.064	33.899	0.037	34.135	0.076	33.934	0.028	34.016	0.099
	U_B		0.555		0.554		0.555		0.555		0.554		0.542		0.543		0.542		0.543
T_{51}	U_A	12.206	0.025	12.035	0.104	12.044	0.027	12.069	0.014	12.006	0.028	12.152	0.033	11.982	0.047	11.780	0.016	12.080	0.051
	U_B		0.417		0.416		0.416		0.416		0.416		0.417		0.416		0.414		0.416
$T_{0,MT}$	U_A	0.045	0.301	0.036	0.301	0.038	0.301	0.018	0.301	0.038	0.300	0.042	0.301	0.038	0.301	0.036	0.300	0.047	0.300
	U_B		-2.493		-0.738		1.675		3.320		5.393		-2.576		-0.662		1.685		3.497
P_{gc}	U_A	83.525	0.200	83.363	0.220	83.619	0.237	83.749	0.291	83.515	0.238	79.007	0.207	79.660	0.402	79.264	0.182	79.475	0.314
	U_B		0.289		0.289		0.290		0.290		0.289		0.274		0.276		0.275		0.275
P_{rec}	U_A	30.263	0.066	31.952	0.104	34.229	0.067	35.957	0.106	38.057	0.082	30.231	0.090	31.895	0.134	34.205	0.083	35.992	0.069
	U_B		0.105		0.111		0.119		0.125		0.132		0.105		0.110		0.118		0.125
$P_{0.MT}$	U_A	28.137	0.045	28.047	0.037	28.133	0.039	28.069	0.020	28.017	0.047	28.086	0.038	28.050	0.038	28.019	0.040	28.021	0.046
	U_B		0.097		0.097		0.097		0.097		0.097		0.097		0.097		0.097		0.097
P_{lift}	U_A	2.127	0.080	3.905	0.110	6.097	0.078	7.887	0.108	10.040	0.094	2.145	0.098	3.845	0.139	6.186	0.092	7.972	0.083
	U_B		0.143		0.147		0.153		0.158		0.164		0.143		0.147		0.153		0.158
$T_{ambient}$	U_A	20.631	0.677	20.631	0.677	20.325	0.882	20.325	0.882	20.325	0.882	19.760	0.038	19.760	0.038	19.760	0.038	19.760	0.038
	U_B		0.466		0.466		0.464		0.464		0.464		0.460		0.460		0.460		0.460
COP	U_A	2.048	0.017	2.202	0.025	2.240	0.016	2.309	0.024	2.349	0.022	2.335	0.015	2.394	0.025	2.496	0.018	2.533	0.023
	U_B		0.018		0.021		0.022		0.023		0.024		0.022		0.023		0.025		0.025
η_{ex}	U_A	0.100	0.001	0.107	0.002	0.107	0.002	0.109	0.003	0.111	0.003	0.106	0.000	0.110	0.001	0.116	0.001	0.115	0.001
	U_B		0.001		0.001		0.001		0.002		0.002		0.001		0.001		0.002		0.002
Q_{evap}	U_A	41.151	0.024	39.556	0.030	39.677	0.023	39.284	0.022	38.969	0.023	39.827	0.025	39.787	0.030	39.563	0.031	39.535	0.040
	U_B		0.192		0.186		0.186		0.185		0.183		0.187		0.186		0.185		0.185
$N_{el,CD1400H}$	U_A	11.354	0.086	11.081	0.075	11.493	0.106	11.624	0.136	11.809	0.126	10.288	0.074	10.593	0.060	10.755	0.083	11.036	0.103
	U_B		0.131		0.128		0.133		0.134		0.136		0.119		0.122		0.124		0.127
$N_{el,CD1000H}$	U_A	5.516	0.097	6.885	0.188	6.223	0.067	5.386	0.109	4.778	0.094	6.770	0.083	6.024	0.164	5.097	0.079	4.574	0.096
	U_B		0.064		0.079		0.072		0.062		0.055		0.078		0.070		0.059		0.053
$N_{el,CD380H}$	U_A	3.222	0.102	0.000	0.000	0.000	0.000	0.000	0.000	0.000	0.000	0.000	0.000	0.000	0.000	0.000	0.000	0.000	0.000
	U_B		0.037		0.000		0.000		0.000		0.000		0.000		0.000		0.000		0.000

Table B.16: Raw data of the system parameters for experimental points presented in Figure B.1. Units are shown in Table B.1.

ID name		2_1			2_2			2_3			2_4			2_5			2_9			2_10			2_11			2_12		
		val	U_A	U_B	val	U_A	U_B	val	U_A	U_B	val	U_A	U_B	val	U_A	U_B	val	U_A	U_B	val	U_A	U_B	val	U_A	U_B	val	U_A	U_B
$\eta_{comp,CD1400H}$	U_A/U_B	0.695	0.008	0.013	0.700	0.008	0.014	0.696	0.008	0.013	0.690	0.008	0.013	0.683	0.008	0.013	0.709	0.008	0.014	0.702	0.008	0.014	0.697	0.008	0.014	0.690	0.008	0.014
$\eta_{comp,CD1000H}$	U_A/U_B	0.711	0.010	0.016	0.664	0.009	0.016	0.681	0.009	0.019	0.702	0.011	0.022	0.711	0.010	0.025	0.655	0.009	0.015	0.685	0.010	0.017	0.708	0.010	0.021	0.715	0.010	0.023
$\eta_{comp,CD380H}$	U_A/U_B	0.637	0.009	0.014	0.000	0.000	0.000	0.000	0.000	0.000	0.000	0.000	0.000	0.000	0.000	0.000	0.000	0.000	0.000	0.000	0.000	0.000	0.000	0.000	0.000	0.000	0.000	0.000
$\eta_{comp,overall}$	U_A/U_B	0.690	0.005	0.009	0.686	0.006	0.010	0.690	0.006	0.011	0.694	0.007	0.011	0.691	0.006	0.012	0.687	0.006	0.010	0.696	0.006	0.011	0.700	0.006	0.011	0.697	0.006	0.012
$\eta_{vol,CD1400H}$	U_A/U_B	0.814	0.005	0.021	0.817	0.004	0.021	0.816	0.005	0.021	0.811	0.004	0.020	0.807	0.004	0.020	0.834	0.005	0.021	0.827	0.004	0.021	0.825	0.004	0.021	0.820	0.005	0.021
$\eta_{vol,CD1000H}$	U_A/U_B	0.815	0.009	0.011	0.796	0.016	0.010	0.810	0.006	0.011	0.825	0.012	0.011	0.836	0.007	0.012	0.796	0.007	0.010	0.819	0.018	0.011	0.839	0.008	0.011	0.845	0.008	0.011
$\eta_{vol,CD380H}$	U_A/U_B	0.788	0.009	0.011	0.000	0.000	0.000	0.000	0.000	0.000	0.000	0.000	0.000	0.000	0.000	0.000	0.000	0.000	0.000	0.000	0.000	0.000	0.000	0.000	0.000	0.000	0.000	0.000
$\eta_{vol,overall}$	U_A/U_B	0.810	0.004	0.012	0.808	0.007	0.013	0.814	0.004	0.014	0.817	0.005	0.015	0.818	0.003	0.015	0.817	0.004	0.013	0.824	0.007	0.014	0.830	0.004	0.015	0.829	0.004	0.015
T_{53}	U_A/U_B	12.380	0.028	0.418	12.201	0.098	0.417	12.195	0.024	0.417	12.213	0.016	0.417	12.161	0.025	0.417	12.316	0.032	0.418	12.168	0.045	0.417	11.976	0.020	0.416	12.276	0.050	0.417
T_{54}	U_A/U_B	1.596	0.035	0.356	1.837	0.108	0.357	1.820	0.028	0.357	1.938	0.027	0.358	1.970	0.028	0.358	1.807	0.054	0.357	1.663	0.048	0.356	1.521	0.034	0.355	1.838	0.048	0.357
$m_{gl,evap}$	U_A/U_B	51.776	0.015	0.120	51.783	0.016	0.120	51.887	0.015	0.120	51.869	0.015	0.120	51.878	0.016	0.120	51.413	0.016	0.119	51.396	0.020	0.119	51.358	0.021	0.119	51.388	0.027	0.119
$m_{CO2,CD1400H}$	U_A/U_B	8.907	0.055	0.213	8.745	0.043	0.205	8.958	0.056	0.216	9.007	0.038	0.218	9.106	0.043	0.222	8.686	0.052	0.204	8.785	0.036	0.208	8.909	0.043	0.214	9.055	0.055	0.221
$m_{CO2,CD1000H}$	U_A/U_B	5.036	0.052	0.061	6.437	0.146	0.099	6.512	0.053	0.105	6.194	0.103	0.098	6.055	0.052	0.096	6.220	0.057	0.091	6.094	0.145	0.089	5.890	0.057	0.086	5.730	0.053	0.084
$m_{CO2,CD380H}$	U_A/U_B	2.600	0.025	0.032	0.000	0.000	0.000	0.000	0.000	0.000	0.000	0.000	0.000	0.000	0.000	0.000	0.000	0.000	0.000	0.000	0.000	0.000	0.000	0.000	0.000	0.000	0.000	0.000

Table B.17:   Raw data of the system parameters for experimental points presented in Figure B.1. Units are shown in Table B.1.

ID name		2_14	2_15	2_16	2_17	2_18	2_19	2_21	2_22	2_23
T_6	value	33.963	33.919	33.892	32.133	31.838	32.121	31.957	32.061	32.115
	U_A	0.060	0.039	0.053	0.079	0.060	0.093	0.085	0.131	0.080
	U_B	0.542	0.542	0.542	0.532	0.530	0.532	0.531	0.532	0.532
T_{51}	value	12.078	12.045	12.122	12.066	12.046	11.946	12.030	11.955	11.899
	U_A	0.034	0.013	0.038	0.038	0.015	0.065	0.037	0.095	0.047
	U_B	0.416	0.416	0.416	0.416	0.416	0.415	0.416	0.415	0.415
$T_{0,MT}$	value	0.012	0.021	0.086	0.052	0.033	0.021	0.029	0.054	0.047
	U_A	0.301	0.301	0.300	0.300	0.301	0.301	0.301	0.301	0.300
	U_B	7.316	9.234	10.724	-2.771	-0.755	1.579	5.364	7.198	9.026
P_{gc}	value	80.023	79.844	80.078	75.294	74.837	75.652	75.550	75.806	76.389
	U_A	0.216	0.191	0.254	0.236	0.191	0.269	0.309	0.369	0.270
	U_B	0.277	0.277	0.277	0.261	0.259	0.262	0.262	0.263	0.265
P_{rec}	value	40.006	42.112	44.054	30.120	31.922	34.174	38.044	40.035	42.124
	U_A	0.066	0.053	0.065	0.071	0.081	0.075	0.078	0.133	0.078
	U_B	0.139	0.146	0.153	0.104	0.111	0.118	0.132	0.139	0.146
$P_{0,MT}$	value	28.101	28.096	28.007	28.000	28.084	28.072	28.105	28.066	28.038
	U_A	0.010	0.024	0.105	0.053	0.031	0.022	0.029	0.060	0.054
	U_B	0.097	0.097	0.097	0.097	0.097	0.097	0.097	0.097	0.097
P_{lift}	value	11.906	14.015	16.047	2.120	3.838	6.102	9.939	11.969	14.086
	U_A	0.067	0.058	0.124	0.089	0.087	0.078	0.084	0.146	0.095
	U_B	0.169	0.175	0.181	0.142	0.147	0.153	0.164	0.169	0.175
$T_{ambient}$	value	19.760	19.760	19.870	20.740	20.740	20.740	20.740	19.940	19.940
	U_A	0.038	0.038	0.111	0.743	0.743	0.743	0.743	0.092	0.092
	U_B	0.460	0.460	0.461	0.466	0.466	0.466	0.466	0.462	0.462
COP	value	2.529	2.587	2.608	2.571	2.705	2.753	2.764	2.785	2.822
	U_A	0.017	0.018	0.030	0.018	0.020	0.023	0.032	0.024	0.027
	U_B	0.026	0.027	0.028	0.025	0.026	0.027	0.028	0.029	0.030
η_{ex}	value	0.111	0.114	0.115	0.128	0.135	0.137	0.133	0.126	0.128
	U_A	0.001	0.002	0.004	0.002	0.003	0.004	0.004	0.002	0.004
	U_B	0.002	0.003	0.004	0.002	0.002	0.003	0.003	0.003	0.005
Q_{evap}	value	36.708	36.327	36.257	40.926	40.511	39.904	37.317	36.887	36.126
	U_A	0.027	0.026	0.037	0.025	0.025	0.026	0.025	0.027	0.024
	U_B	0.174	0.172	0.172	0.191	0.189	0.187	0.176	0.174	0.171
$N_{el,CD1400H}$	value	10.629	10.738	11.053	9.934	9.917	10.160	9.772	10.020	10.124
	U_A	0.066	0.078	0.136	0.087	0.077	0.076	0.091	0.084	0.094
	U_B	0.123	0.124	0.128	0.115	0.115	0.117	0.113	0.116	0.117
$N_{el,CD1000H}$	value	0.000	0.000	0.000	5.988	5.061	4.336	0.000	0.000	0.000
	U_A	0.000	0.000	0.000	0.066	0.079	0.091	0.000	0.000	0.000
	U_B	0.000	0.000	0.000	0.069	0.058	0.050	0.000	0.000	0.000
$N_{el,CD380H}$	value	3.888	3.304	2.850	0.000	0.000	0.000	3.727	3.227	2.680
	U_A	0.068	0.061	0.080	0.000	0.000	0.000	0.126	0.076	0.076
	U_B	0.045	0.038	0.033	0.000	0.000	0.000	0.043	0.037	0.031

Table B.18: Raw data of the system parameters for experimental points presented in Figure B.1. Units are shown in Table B.1.

ID name		2_14			2_15			2_16			2_17			2_18			2_19			2_21			2_22			2_23		
		val	U_A	U_B	val	U_A	U_B	val	U_A	U_B	val	U_A	U_B	val	U_A	U_B	val	U_A	U_B	val	U_A	U_B	val	U_A	U_B	val	U_A	U_B
$\eta_{comp,CD1400H}$	$\frac{U_A}{U_B}$	0.702	0.008	0.014	0.699	0.008	0.014	0.691	0.008	0.014	0.702	0.009	0.014	0.702	0.008	0.014	0.698	0.008	0.014	0.707	0.009	0.015	0.703	0.008	0.014	0.702	0.008	0.014
$\eta_{comp,CD1000H}$	$\frac{U_A}{U_B}$	0.000	0.000	0.000	0.000	0.000	0.000	0.000	0.000	0.000	0.676	0.009	0.016	0.706	0.010	0.019	0.718	0.010	0.022	0.000	0.000	0.000	0.000	0.000	0.000	0.000	0.000	0.000
$\eta_{comp,CD380H}$	$\frac{U_A}{U_B}$	0.560	0.008	0.024	0.586	0.009	0.029	0.600	0.009	0.035	0.000	0.000	0.000	0.000	0.000	0.000	0.000	0.000	0.000	0.556	0.008	0.022	0.583	0.009	0.027	0.602	0.009	0.033
$\eta_{comp,overall}$	$\frac{U_A}{U_B}$	0.664	0.006	0.010	0.672	0.006	0.010	0.673	0.006	0.011	0.692	0.006	0.011	0.703	0.006	0.011	0.704	0.006	0.012	0.665	0.006	0.010	0.674	0.006	0.010	0.681	0.006	0.011
$\eta_{vol,CD1400H}$	$\frac{U_A}{U_B}$	0.827	0.003	0.021	0.826	0.004	0.021	0.820	0.009	0.021	0.835	0.004	0.021	0.837	0.003	0.021	0.832	0.004	0.021	0.839	0.004	0.021	0.837	0.006	0.021	0.835	0.006	0.021
$\eta_{vol,CD1000H}$	$\frac{U_A}{U_B}$	0.000	0.000	0.000	0.000	0.000	0.000	0.000	0.000	0.000	0.820	0.005	0.010	0.845	0.009	0.011	0.855	0.010	0.011	0.000	0.000	0.000	0.000	0.000	0.000	0.000	0.000	0.000
$\eta_{vol,CD380H}$	$\frac{U_A}{U_B}$	0.792	0.004	0.011	0.814	0.005	0.012	0.823	0.009	0.012	0.000	0.000	0.000	0.000	0.000	0.000	0.000	0.000	0.000	0.794	0.018	0.011	0.818	0.012	0.011	0.830	0.012	0.012
$\eta_{vol,overall}$	$\frac{U_A}{U_B}$	0.814	0.003	0.015	0.822	0.003	0.016	0.821	0.007	0.017	0.829	0.003	0.014	0.840	0.004	0.015	0.841	0.004	0.015	0.823	0.003	0.015	0.830	0.005	0.016	0.833	0.004	0.017
T_{53}	$\frac{U_A}{U_B}$	12.286	0.034	0.417	12.258	0.013	0.417	12.294	0.037	0.417	12.225	0.037	0.417	12.206	0.011	0.417	12.114	0.062	0.416	12.206	0.034	0.417	12.126	0.091	0.416	12.074	0.045	0.416
T_{54}	$\frac{U_A}{U_B}$	2.608	0.032	0.361	2.679	0.034	0.362	2.748	0.062	0.362	1.355	0.041	0.354	1.431	0.026	0.355	1.507	0.045	0.355	2.311	0.036	0.360	2.345	0.080	0.360	2.496	0.054	0.361
$m_{gl,evap}$	$\frac{U_A}{U_B}$	51.429	0.020	0.119	51.420	0.019	0.119	51.494	0.027	0.119	51.100	0.016	0.118	51.026	0.016	0.118	51.051	0.016	0.118	51.150	0.017	0.118	51.148	0.017	0.118	51.154	0.017	0.118
$m_{CO2,CD1400H}$	$\frac{U_A}{U_B}$	8.808	0.034	0.209	8.897	0.044	0.214	9.022	0.096	0.219	8.793	0.043	0.209	8.853	0.035	0.212	8.923	0.040	0.215	8.731	0.036	0.206	8.844	0.063	0.212	8.841	0.056	0.212
$m_{CO2,CD1000H}$	$\frac{U_A}{U_B}$	0.000	0.000	0.000	0.000	0.000	0.000	0.000	0.000	0.000	5.946	0.041	0.082	5.695	0.060	0.078	5.442	0.062	0.074	0.000	0.000	0.000	0.000	0.000	0.000	0.000	0.000	0.000
$m_{CO2,CD380H}$	$\frac{U_A}{U_B}$	4.698	0.008	0.042	4.528	0.007	0.043	4.267	0.006	0.042	0.000	0.000	0.000	0.000	0.000	0.000	0.000	0.000	0.000	4.522	0.017	0.036	4.396	0.013	0.037	4.041	0.009	0.035

Table B.19: Raw data of the system parameters for experimental points presented in Figure B.1. Units are shown in Table B.1.

ID name		2_24		2_25		2_26		2_28		2_29		2_30		2_33		2_35		2_36	
T_6	U_A	32.121	0.085	29.804	0.101	29.927	0.136	29.902	0.043	30.078	0.085	30.113	0.109	27.854	0.079	28.056	0.056	28.076	0.155
	U_B		0.532		0.518		0.519		0.519		0.520		0.520		0.507		0.508		0.509
T_{51}	U_A	11.976	0.043	12.182	0.041	12.079	0.058	11.868	0.014	11.824	0.058	11.995	0.069	11.895	0.103	11.865	0.057	12.083	0.079
	U_B		0.416		0.417		0.416		0.415		0.415		0.416		0.415		0.415		0.416
$T_{0,MT}$	U_A	0.028	0.301	0.046	0.301	0.025	0.301	0.029	0.301	0.051	0.300	0.067	0.301	0.059	0.301	0.032	0.300	0.034	0.301
	U_B		10.769		-2.675		-0.655		3.281		5.261		7.193		-2.707		1.552		3.396
P_{gc}	U_A	76.205	0.288	70.401	0.302	70.596	0.355	71.001	0.189	71.674	0.313	71.692	0.392	66.770	0.219	67.232	0.196	67.248	0.337
	U_B		0.264		0.244		0.245		0.246		0.248		0.248		0.231		0.233		0.233
P_{rec}	U_A	44.055	0.061	30.162	0.081	31.965	0.083	35.888	0.071	37.976	0.087	39.969	0.070	30.112	0.086	34.123	0.083	35.929	0.056
	U_B		0.153		0.104		0.111		0.124		0.132		0.138		0.104		0.118		0.124
$P_{0.MT}$	U_A	28.124	0.031	28.133	0.047	28.051	0.030	28.082	0.026	28.039	0.055	28.076	0.061	28.102	0.044	28.029	0.033	28.076	0.033
	U_B		0.097		0.097		0.097		0.097		0.097		0.097		0.097		0.097		0.097
P_{lift}	U_A	15.931	0.068	2.028	0.093	3.914	0.088	7.806	0.076	9.937	0.104	11.894	0.093	2.011	0.097	6.094	0.089	7.853	0.065
	U_B		0.181		0.143		0.147		0.158		0.164		0.169		0.143		0.153		0.158
$T_{ambient}$	U_A	19.940	0.092	19.998	0.050	20.702	0.015	20.702	0.015	20.702	0.015	20.702	0.015	20.345	0.013	20.345	0.013	20.345	0.013
	U_B		0.462		0.462		0.466		0.466		0.466		0.466		0.464		0.464		0.464
COP	U_A	2.843	0.028	2.944	0.027	2.991	0.026	3.019	0.015	3.057	0.027	3.100	0.032	3.231	0.024	3.263	0.031	3.345	0.028
	U_B		0.030		0.029		0.030		0.030		0.032		0.033		0.032		0.033		0.034
η_{ex}	U_A	0.127	0.004	0.138	0.001	0.149	0.002	0.149	0.001	0.151	0.003	0.150	0.005	0.159	0.002	0.158	0.003	0.159	0.003
	U_B		0.005		0.002		0.003		0.004		0.005		0.006		0.003		0.004		0.005
Q_{evap}	U_A	35.761	0.024	40.750	0.026	40.766	0.029	38.241	0.024	37.928	0.026	37.647	0.027	40.368	0.033	38.709	0.025	38.828	0.029
	U_B		0.170		0.190		0.190		0.180		0.178		0.177		0.188		0.181		0.182
$N_{el,CD1400H}$	U_A	10.181	0.091	9.077	0.069	9.353	0.090	9.133	0.045	9.396	0.081	9.547	0.104	8.447	0.060	8.513	0.064	8.687	0.082
	U_B		0.118		0.105		0.108		0.105		0.108		0.110		0.098		0.098		0.100
$N_{el,CD1000H}$	U_A	0.000	0.000	4.764	0.104	4.276	0.073	0.000	0.000	0.000	0.000	0.000	0.000	4.048	0.068	0.000	0.000	0.000	0.000
	U_B		0.000		0.055		0.049		0.000		0.000		0.000		0.047		0.000		0.000
$N_{el,CD380H}$	U_A	2.400	0.085	0.000	0.000	0.000	0.000	3.535	0.043	3.013	0.072	2.596	0.069	0.000	0.000	3.350	0.090	2.922	0.051
	U_B		0.028		0.000		0.000		0.041		0.035		0.030		0.000		0.039		0.034

Table B.20: Raw data of the system parameters for experimental points presented in Figure B.1. Units are shown in Table B.1.

ID name		2_24	U_A/U_B	2_25	U_A/U_B	2_26	U_A/U_B	2_28	U_A/U_B	2_29	U_A/U_B	2_30	U_A/U_B	2_33	U_A/U_B	2_35	U_A/U_B	2_36	U_A/U_B
$\eta_{comp,CD1400H}$	U_A/U_B	0.700	0.008 / 0.014	0.706	0.008 / 0.015	0.700	0.008 / 0.015	0.707	0.008 / 0.015	0.703	0.008 / 0.015	0.700	0.008 / 0.015	0.711	0.009 / 0.016	0.710	0.008 / 0.016	0.705	0.008 / 0.016
$\eta_{comp,CD1000H}$	U_A/U_B	0.000	0.000 / 0.000	0.701	0.009 / 0.018	0.708	0.009 / 0.020	0.000	0.000 / 0.000	0.000	0.000 / 0.000	0.000	0.000 / 0.000	0.706	0.010 / 0.019	0.000	0.000 / 0.000	0.000	0.000 / 0.000
$\eta_{comp,CD380H}$	U_A/U_B	0.599	0.010 / 0.039	0.000	0.000 / 0.000	0.000	0.000 / 0.000	0.557	0.007 / 0.021	0.587	0.008 / 0.026	0.598	0.008 / 0.031	0.000	0.000 / 0.000	0.560	0.007 / 0.020	0.580	0.008 / 0.024
$\eta_{comp,overall}$	U_A/U_B	0.681	0.006 / 0.011	0.704	0.006 / 0.012	0.703	0.006 / 0.012	0.665	0.006 / 0.010	0.675	0.006 / 0.011	0.678	0.006 / 0.011	0.709	0.007 / 0.012	0.667	0.006 / 0.011	0.674	0.006 / 0.011
$\eta_{vol,CD1400H}$	U_A/U_B	0.835	0.005 / 0.021	0.849	0.006 / 0.022	0.845	0.005 / 0.022	0.849	0.004 / 0.022	0.845	0.005 / 0.022	0.844	0.006 / 0.022	0.861	0.007 / 0.022	0.859	0.005 / 0.022	0.857	0.006 / 0.022
$\eta_{vol,CD1000H}$	U_A/U_B	0.000	0.000 / 0.000	0.846	0.012 / 0.011	0.853	0.008 / 0.011	0.000	0.000 / 0.000	0.000	0.000 / 0.000	0.000	0.000 / 0.000	0.856	0.008 / 0.011	0.000	0.000 / 0.000	0.000	0.000 / 0.000
$\eta_{vol,CD380H}$	U_A/U_B	0.831	0.009 / 0.012	0.000	0.000 / 0.000	0.000	0.000 / 0.000	0.799	0.004 / 0.011	0.823	0.015 / 0.011	0.834	0.007 / 0.012	0.000	0.000 / 0.000	0.805	0.014 / 0.011	0.824	0.008 / 0.011
$\eta_{vol,overall}$	U_A/U_B	0.834	0.004 / 0.017	0.848	0.006 / 0.015	0.848	0.005 / 0.015	0.832	0.003 / 0.015	0.838	0.004 / 0.016	0.841	0.004 / 0.017	0.860	0.005 / 0.015	0.841	0.004 / 0.016	0.846	0.004 / 0.016
T_{53}	U_A/U_B	12.151	0.042 / 0.417	12.363	0.048 / 0.418	12.237	0.056 / 0.417	12.045	0.014 / 0.416	11.997	0.058 / 0.416	12.168	0.066 / 0.417	12.055	0.099 / 0.416	12.062	0.054 / 0.416	12.273	0.082 / 0.417
T_{54}	U_A/U_B	2.669	0.021 / 0.362	1.438	0.047 / 0.355	1.298	0.044 / 0.354	1.812	0.029 / 0.357	1.855	0.038 / 0.357	2.109	0.059 / 0.359	1.137	0.094 / 0.353	1.606	0.034 / 0.356	1.770	0.056 / 0.357
$m_{gl,evap}$	U_A/U_B	51.147	0.018 / 0.118	50.614	0.016 / 0.117	50.578	0.018 / 0.117	50.707	0.016 / 0.117	50.747	0.018 / 0.117	50.768	0.018 / 0.117	50.191	0.019 / 0.116	50.239	0.016 / 0.116	50.155	0.018 / 0.116
$m_{CO2,CD1400H}$	U_A/U_B	8.928	0.053 / 0.216	8.735	0.059 / 0.207	8.910	0.054 / 0.216	8.732	0.040 / 0.207	8.837	0.047 / 0.212	8.942	0.056 / 0.217	8.686	0.063 / 0.206	8.663	0.047 / 0.205	8.823	0.055 / 0.213
$m_{CO2,CD1000H}$	U_A/U_B	0.000	0.000 / 0.000	5.351	0.071 / 0.067	5.294	0.048 / 0.068	0.000	0.000 / 0.000	0.000	0.000 / 0.000	0.000	0.000 / 0.000	4.975	0.040 / 0.058	0.000	0.000 / 0.000	0.000	0.000 / 0.000
$m_{CO2,CD380H}$	U_A/U_B	3.917	0.007 / 0.037	0.000	0.000 / 0.000	0.000	0.000 / 0.000	4.284	0.003 / 0.030	4.125	0.009 / 0.030	3.972	0.003 / 0.031	0.000	0.000 / 0.000	4.077	0.006 / 0.025	3.997	0.004 / 0.026

Table B.21: Raw data of the system parameters for experimental points presented in Figure B.1. Units are shown in Table B.1.

ID name		2_37	2_49	2_50	2_51	2_57	2_58	2_59	2_65	2_66
T_6	value	28.214	35.762	36.032	35.978	34.294	34.086	33.978	32.190	32.129
	U_A	0.060	0.050	0.200	0.137	0.040	0.160	0.067	0.095	0.053
	U_B	0.509	0.553	0.554	0.554	0.544	0.543	0.543	0.532	0.532
T_{51}	value	11.891	14.860	14.682	14.679	15.120	14.836	14.761	15.196	15.164
	U_A	0.100	0.086	0.034	0.092	0.050	0.123	0.109	0.042	0.082
	U_B	0.415	0.432	0.431	0.431	0.434	0.432	0.432	0.434	0.434
$T_{0,MT}$	value	0.058	0.032	0.046	0.057	0.031	0.050	0.070	0.018	0.041
	U_A	0.301	0.302	0.302	0.301	0.303	0.301	0.302	0.301	0.301
	U_B	5.246	-2.653	-0.558	1.532	-2.571	-0.608	1.474	-2.523	-0.610
P_{gc}	value	67.650	82.853	83.670	83.649	79.823	79.697	79.496	75.581	75.604
	U_A	0.301	0.198	0.454	0.406	0.188	0.291	0.198	0.260	0.292
	U_B	0.234	0.287	0.290	0.290	0.277	0.276	0.275	0.262	0.262
P_{rec}	value	37.897	30.115	32.066	34.090	30.110	31.958	33.975	30.181	32.070
	U_A	0.099	0.065	0.091	0.115	0.055	0.093	0.066	0.062	0.070
	U_B	0.131	0.104	0.111	0.118	0.104	0.111	0.118	0.105	0.111
$P_{0.MT}$	value	28.082	28.303	28.297	28.122	28.335	28.125	28.284	28.099	28.143
	U_A	0.054	0.028	0.039	0.045	0.021	0.047	0.059	0.015	0.043
	U_B	0.097	0.098	0.098	0.097	0.098	0.097	0.098	0.097	0.097
P_{lift}	value	9.816	1.811	3.770	5.968	1.775	3.833	5.691	2.082	3.927
	U_A	0.113	0.071	0.099	0.123	0.059	0.105	0.089	0.064	0.082
	U_B	0.163	0.143	0.148	0.153	0.143	0.147	0.153	0.143	0.148
$T_{ambient}$	value	20.345	21.000	21.000	21.000	21.000	21.000	21.000	21.000	20.870
	U_A	0.013	0.095	0.095	0.095	0.095	0.095	0.095	0.095	0.012
	U_B	0.464	0.468	0.468	0.468	0.468	0.468	0.468	0.468	0.467
COP	value	3.395	2.081	2.124	2.237	2.244	2.380	2.484	2.482	2.631
	U_A	0.035	0.016	0.019	0.020	0.014	0.028	0.017	0.023	0.019
	U_B	0.036	0.018	0.019	0.022	0.020	0.023	0.024	0.023	0.026
η_{ex}	value	0.163	0.089	0.091	0.094	0.095	0.101	0.106	0.105	0.110
	U_A	0.006	0.000	0.000	0.001	0.000	0.001	0.001	0.001	0.001
	U_B	0.007	0.001	0.001	0.001	0.001	0.001	0.002	0.001	0.002
Q_{evap}	value	38.253	45.865	44.941	43.474	46.840	45.103	44.840	47.170	46.382
	U_A	0.032	0.036	0.030	0.047	0.029	0.046	0.055	0.037	0.052
	U_B	0.180	0.212	0.208	0.202	0.216	0.209	0.208	0.217	0.214
$N_{el,CD1400H}$	value	8.784	12.737	12.833	12.720	12.388	12.164	12.274	11.769	11.781
	U_A	0.076	0.084	0.092	0.123	0.070	0.109	0.091	0.121	0.105
	U_B	0.101	0.147	0.148	0.147	0.143	0.140	0.142	0.136	0.136
$N_{el,CD1000H}$	value	0.000	5.886	5.234	6.718	5.373	6.787	5.777	4.536	5.851
	U_A	0.000	0.116	0.113	0.120	0.069	0.198	0.075	0.081	0.073
	U_B	0.000	0.068	0.060	0.078	0.062	0.078	0.067	0.052	0.068
$N_{el,CD380H}$	value	2.483	3.413	3.088	0.000	3.110	0.000	0.000	2.702	0.000
	U_A	0.087	0.094	0.113	0.000	0.089	0.000	0.000	0.099	0.000
	U_B	0.029	0.039	0.036	0.000	0.036	0.000	0.000	0.031	0.000

Table B.22: Raw data of the system parameters for experimental points presented in Figure B.1. Units are shown in Table B.1.

ID name	2_37	U_A	U_B	2_49	U_A	U_B	2_50	U_A	U_B	2_51	U_A	U_B	2_57	U_A	U_B	2_58	U_A	U_B	2_59	U_A	U_B	2_65	U_A	U_B	2_66	U_A	U_B
$\eta_{comp,CD1400H}$	0.705	0.009	0.016	0.656	0.008	0.013	0.657	0.008	0.013	0.662	0.008	0.013	0.653	0.008	0.013	0.658	0.008	0.013	0.655	0.008	0.013	0.652	0.008	0.013	0.652	0.008	0.013
$\eta_{comp,CD1000H}$	0.000	0.000	0.000	0.703	0.009	0.015	0.719	0.010	0.018	0.672	0.009	0.018	0.709	0.010	0.016	0.658	0.009	0.016	0.693	0.009	0.020	0.718	0.010	0.017	0.682	0.009	0.018
$\eta_{comp,CD380H}$	0.595	0.008	0.029	0.630	0.009	0.014	0.645	0.010	0.016	0.000	0.000	0.000	0.637	0.009	0.015	0.000	0.000	0.000	0.000	0.000	0.000	0.646	0.009	0.016	0.000	0.000	0.000
$\eta_{comp,overall}$	0.680	0.007	0.012	0.665	0.006	0.009	0.670	0.006	0.009	0.665	0.006	0.010	0.665	0.005	0.009	0.658	0.006	0.010	0.667	0.006	0.011	0.667	0.005	0.009	0.662	0.006	0.011
$\eta_{vol,CD1400H}$	0.856	0.007	0.022	0.790	0.003	0.020	0.789	0.004	0.020	0.794	0.006	0.020	0.793	0.002	0.020	0.797	0.007	0.020	0.796	0.006	0.020	0.800	0.006	0.020	0.801	0.006	0.020
$\eta_{vol,CD1000H}$	0.000	0.000	0.000	0.813	0.004	0.010	0.826	0.008	0.011	0.808	0.011	0.011	0.825	0.003	0.011	0.803	0.016	0.010	0.831	0.006	0.011	0.840	0.009	0.011	0.830	0.008	0.011
$\eta_{vol,CD380H}$	0.836	0.024	0.011	0.786	0.004	0.011	0.801	0.008	0.011	0.000	0.000	0.000	0.799	0.003	0.011	0.000	0.000	0.000	0.000	0.000	0.000	0.817	0.008	0.011	0.000	0.000	0.000
$\eta_{vol,overall}$	0.850	0.005	0.017	0.796	0.002	0.012	0.801	0.003	0.013	0.800	0.006	0.014	0.803	0.002	0.012	0.799	0.007	0.013	0.810	0.005	0.014	0.813	0.004	0.013	0.812	0.005	0.014
T_{53}	12.122	0.103	0.416	14.994	0.088	0.433	14.823	0.034	0.432	14.815	0.087	0.432	15.263	0.050	0.435	15.013	0.127	0.433	14.916	0.115	0.433	15.343	0.043	0.435	15.293	0.077	0.435
T_{54}	1.788	0.072	0.357	2.981	0.085	0.364	3.044	0.031	0.364	3.430	0.096	0.366	2.912	0.032	0.363	3.130	0.047	0.364	3.103	0.133	0.364	2.816	0.040	0.363	2.956	0.057	0.363
$m_{gl,evap}$	50.226	0.019	0.116	51.666	0.020	0.119	51.637	0.018	0.119	51.665	0.028	0.119	51.315	0.016	0.119	51.355	0.026	0.119	51.366	0.031	0.119	50.950	0.021	0.118	50.869	0.029	0.117
$m_{CO2,CD1400H}$	8.862	0.064	0.215	9.671	0.035	0.250	9.645	0.044	0.249	9.556	0.077	0.246	9.777	0.030	0.256	9.624	0.084	0.249	9.764	0.078	0.256	9.773	0.075	0.257	9.815	0.072	0.260
$m_{CO2,CD1000H}$	0.000	0.000	0.000	5.295	0.024	0.067	5.156	0.047	0.065	6.823	0.118	0.114	5.107	0.018	0.062	6.610	0.156	0.104	6.410	0.051	0.101	4.715	0.041	0.053	6.271	0.069	0.094
$m_{CO2,CD380H}$	3.783	0.009	0.026	2.732	0.013	0.035	2.671	0.024	0.034	0.000	0.000	0.000	2.645	0.008	0.032	0.000	0.000	0.000	0.000	0.000	0.000	2.451	0.021	0.028	0.000	0.000	0.000

Table B.23:   Raw data of the system parameters for experimental points presented in Figure B.1. Units are shown in Table B.1.

ID name		2_67		2_73		2_74		2_75		2_76		2_81		2_82	
T_6	U_A	32.188	0.143	30.182	0.072	30.204	0.035	29.953	0.061	29.904	0.158	28.037	0.093	28.190	0.135
	U_B		0.532		0.521		0.521		0.519		0.519		0.508		0.509
T_{51}	U_A	14.969	0.080	14.966	0.036	15.004	0.065	15.058	0.237	14.896	0.048	14.951	0.113	14.909	0.104
	U_B		0.433		0.433		0.433		0.433		0.432		0.433		0.432
$T_{0,MT}$	U_A	0.029	0.302	0.046	0.300	0.033	0.301	0.095	0.300	0.036	0.301	0.068	0.300	0.062	0.301
	U_B		1.697		-2.658		-0.666		1.456		3.550		-2.824		-0.737
P_{gc}	U_A	75.793	0.311	71.540	0.288	71.378	0.256	70.867	0.244	71.240	0.322	66.940	0.248	67.453	0.308
	U_B		0.263		0.248		0.247		0.245		0.247		0.232		0.234
P_{rec}	U_A	34.280	0.125	30.046	0.048	31.945	0.069	34.024	0.071	36.352	0.143	29.998	0.078	31.981	0.075
	U_B		0.119		0.104		0.111		0.118		0.126		0.104		0.111
$P_{0.MT}$	U_A	28.302	0.023	28.009	0.047	28.056	0.035	28.007	0.083	28.147	0.036	27.986	0.061	28.126	0.052
	U_B		0.098		0.097		0.097		0.097		0.098		0.097		0.097
P_{lift}	U_A	5.978	0.127	2.037	0.067	3.889	0.077	6.017	0.109	8.205	0.147	2.012	0.099	3.855	0.092
	U_B		0.154		0.142		0.147		0.153		0.159		0.142		0.148
$T_{ambient}$	U_A	20.870	0.012	20.870	0.012	20.870	0.012	20.870	0.012	20.506	0.038	20.870	0.012	21.195	0.012
	U_B		0.467		0.467		0.467		0.467		0.465		0.467		0.469
COP	U_A	2.708	0.033	2.844	0.030	2.935	0.020	3.040	0.029	3.010	0.035	3.219	0.056	3.317	0.053
	U_B		0.027		0.028		0.029		0.031		0.030		0.032		0.033
η_{ex}	U_A	0.114	0.002	0.120	0.001	0.124	0.001	0.128	0.002	0.119	0.002	0.140	0.003	0.146	0.004
	U_B		0.002		0.002		0.002		0.003		0.003		0.003		0.004
Q_{evap}	U_A	45.409	0.032	46.413	0.036	46.185	0.030	46.091	0.050	42.547	0.033	47.275	0.045	46.020	0.040
	U_B		0.210		0.214		0.213		0.213		0.198		0.217		0.212
$N_{el,CD1400H}$	U_A	11.754	0.147	10.786	0.159	10.864	0.084	11.069	0.124	10.284	0.155	10.111	0.239	9.996	0.203
	U_B		0.136		0.125		0.125		0.128		0.119		0.117		0.115
$N_{el,CD1000H}$	U_A	5.014	0.140	5.533	0.069	4.874	0.063	4.092	0.072	0.000	0.000	4.573	0.085	3.877	0.086
	U_B		0.058		0.064		0.056		0.047		0.000		0.053		0.045
$N_{el,CD380H}$	U_A	0.000	0.000	0.000	0.000	0.000	0.000	0.000	0.000	3.850	0.049	0.000	0.000	0.000	0.000
	U_B		0.000		0.000		0.000		0.000		0.044		0.000		0.000

Table B.24: Raw data of the system parameters for experimental points presented in Figure B.1. Units are shown in Table B.1.

ID name		2_67		2_73		2_74		2_75		2_76		2_81		2_82	
$\eta_{comp,CD1400H}$	U_A	0.656	0.008	0.662	0.008	0.662	0.008	0.652	0.007	0.680	0.008	0.663	0.010	0.667	0.008
	U_B		0.013		0.014		0.014		0.014		0.014		0.015		0.015
$\eta_{comp,CD1000H}$	U_A	0.707	0.011	0.683	0.009	0.703	0.010	0.713	0.010	0.000	0.000	0.702	0.009	0.717	0.010
	U_B		0.021		0.017		0.019		0.023		0.000		0.018		0.021
$\eta_{comp,CD380H}$	U_A	0.000	0.000	0.000	0.000	0.000	0.000	0.000	0.000	0.538	0.009	0.000	0.000	0.000	0.000
	U_B		0.000		0.000		0.000		0.000		0.020		0.000		0.000
$\eta_{comp,overall}$	U_A	0.671	0.006	0.669	0.006	0.675	0.006	0.669	0.006	0.642	0.005	0.675	0.007	0.681	0.007
	U_B		0.011		0.011		0.011		0.012		0.010		0.012		0.012
$\eta_{vol,CD1400H}$	U_A	0.805	0.008	0.815	0.005	0.818	0.004	0.811	0.010	0.833	0.005	0.827	0.006	0.831	0.005
	U_B		0.020		0.021		0.021		0.021		0.021		0.021		0.021
$\eta_{vol,CD1000H}$	U_A	0.851	0.019	0.834	0.006	0.853	0.007	0.864	0.011	0.000	0.000	0.858	0.009	0.871	0.009
	U_B		0.011		0.010		0.011		0.011		0.000		0.011		0.011
$\eta_{vol,CD380H}$	U_A	0.000	0.000	0.000	0.000	0.000	0.000	0.000	0.000	0.789	0.006	0.000	0.000	0.000	0.000
	U_B		0.000		0.000		0.000		0.000		0.011		0.000		0.000
$\eta_{vol,overall}$	U_A	0.822	0.008	0.822	0.004	0.831	0.003	0.829	0.008	0.819	0.004	0.838	0.005	0.844	0.005
	U_B		0.015		0.014		0.015		0.016		0.015		0.015		0.016
T_{53}	U_A	15.098	0.076	15.183	0.033	15.147	0.066	15.194	0.240	15.021	0.050	15.123	0.115	15.036	0.103
	U_B		0.434		0.434		0.434		0.434		0.433		0.434		0.433
T_{54}	U_A	3.022	0.032	2.751	0.038	2.765	0.048	2.830	0.124	3.644	0.043	2.280	0.065	2.552	0.108
	U_B		0.364		0.362		0.362		0.363		0.367		0.360		0.361
$m_{gl,evap}$	U_A	50.881	0.018	50.525	0.020	50.478	0.016	50.444	0.022	50.588	0.020	49.832	0.023	49.897	0.020
	U_B		0.118		0.117		0.117		0.116		0.117		0.115		0.115
$m_{CO2,CD1400H}$	U_A	9.857	0.099	9.639	0.058	9.729	0.043	9.871	0.127	9.496	0.058	9.737	0.080	9.723	0.064
	U_B		0.262		0.251		0.257		0.264		0.246		0.258		0.257
$m_{CO2,CD1000H}$	U_A	6.111	0.146	5.831	0.045	5.785	0.051	5.517	0.071	0.000	0.000	5.399	0.052	5.115	0.047
	U_B		0.092		0.079		0.080		0.075		0.000		0.068		0.063
$m_{CO2,CD380H}$	U_A	0.000	0.000	0.000	0.000	0.000	0.000	0.000	0.000	4.530	0.012	0.000	0.000	0.000	0.000
	U_B		0.000		0.000		0.000		0.000		0.033		0.000		0.000

Table B.25: Raw data of the system parameters for experimental points presented in Figure B.1. Units are shown in Table B.1.

ID name		2_84		2_85		2_89		2_91		2_92	
T_6	U_A	28.074	0.075	27.850	0.064	26.052	0.087	25.750	0.075	26.020	0.092
	U_B		0.508		0.507		0.497		0.495		0.497
T_{51}	U_A	15.108	0.054	15.036	0.047	15.181	0.080	14.885	0.066	14.876	0.040
	U_B		0.434		0.433		0.434		0.432		0.432
$T_{0,MT}$	U_A	0.059	0.301	0.061	0.301	0.045	0.301	0.030	0.300	0.037	0.301
	U_B		3.415		5.299		-2.873		1.361		3.284
P_{gc}	U_A	67.090	0.193	66.880	0.221	63.996	0.223	63.730	0.200	63.992	0.218
	U_B		0.232		0.232		0.222		0.221		0.222
P_{rec}	U_A	35.955	0.078	37.996	0.076	30.100	0.059	34.029	0.056	35.969	0.032
	U_B		0.125		0.132		0.104		0.118		0.125
$P_{0.MT}$	U_A	28.111	0.046	28.073	0.065	28.069	0.044	28.000	0.036	28.047	0.046
	U_B		0.097		0.097		0.097		0.097		0.097
P_{lift}	U_A	7.844	0.091	9.923	0.100	2.031	0.073	6.029	0.067	7.922	0.056
	U_B		0.158		0.164		0.143		0.153		0.158
$T_{ambient}$	U_A	20.870	0.012	20.506	0.038	21.195	0.012	21.195	0.012	21.195	0.012
	U_B		0.467		0.465		0.469		0.469		0.469
COP	U_A	3.347	0.037	3.431	0.060	3.575	0.047	3.684	0.031	3.704	0.064
	U_B		0.034		0.036		0.036		0.038		0.039
η_{ex}	U_A	0.137	0.003	0.138	0.008	0.159	0.004	0.161	0.004	0.163	0.010
	U_B		0.004		0.006		0.004		0.006		0.007
Q_{evap}	U_A	43.809	0.040	43.771	0.036	47.593	0.040	44.233	0.036	44.885	0.036
	U_B		0.203		0.203		0.218		0.204		0.207
$N_{el,CD1400H}$	U_A	9.827	0.130	10.095	0.208	9.566	0.161	9.160	0.092	9.532	0.199
	U_B		0.113		0.117		0.110		0.106		0.110
$N_{el,CD1000H}$	U_A	0.000	0.000	0.000	0.000	3.746	0.067	0.000	0.000	0.000	0.000
	U_B		0.000		0.000		0.043		0.000		0.000
$N_{el,CD380H}$	U_A	3.260	0.063	2.662	0.075	0.000	0.000	2.848	0.037	2.585	0.061
	U_B		0.038		0.031		0.000		0.033		0.030

Table B.26: Raw data of the system parameters for experimental points presented in Figure B.1. Units are shown in Table B.1.

ID name		2_84		2_85		2_89		2_91		2_92	
$\eta_{comp,CD1400H}$	U_A	0.672	0.008	0.665	0.008	0.663	0.008	0.675	0.008	0.664	0.008
	U_B		0.015		0.015		0.015		0.016		0.015
$\eta_{comp,CD1000H}$	U_A	0.000	0.000	0.000	0.000	0.716	0.009	0.000	0.000	0.000	0.000
	U_B		0.000		0.000		0.020		0.000		0.000
$\eta_{comp,CD380H}$	U_A	0.563	0.008	0.593	0.008	0.000	0.000	0.589	0.008	0.595	0.008
	U_B		0.023		0.028		0.000		0.022		0.026
$\eta_{comp,overall}$	U_A	0.645	0.006	0.650	0.006	0.678	0.006	0.655	0.006	0.650	0.006
	U_B		0.011		0.011		0.012		0.012		0.012
$\eta_{vol,CD1400H}$	U_A	0.836	0.005	0.831	0.006	0.834	0.005	0.844	0.003	0.837	0.004
	U_B		0.021		0.021		0.021		0.022		0.021
$\eta_{vol,CD1000H}$	U_A	0.000	0.000	0.000	0.000	0.874	0.007	0.000	0.000	0.000	0.000
	U_B		0.000		0.000		0.011		0.000		0.000
$\eta_{vol,CD380H}$	U_A	0.819	0.008	0.847	0.011	0.000	0.000	0.841	0.004	0.850	0.006
	U_B		0.011		0.011		0.000		0.011		0.011
$\eta_{vol,overall}$	U_A	0.831	0.004	0.835	0.005	0.847	0.004	0.843	0.002	0.840	0.003
	U_B		0.016		0.017		0.016		0.017		0.017
T_{53}	U_A	15.264	0.054	15.175	0.048	15.298	0.083	15.015	0.071	14.997	0.046
	U_B		0.435		0.434		0.435		0.433		0.433
T_{54}	U_A	3.365	0.048	3.292	0.043	2.169	0.078	2.834	0.077	2.619	0.041
	U_B		0.366		0.365		0.359		0.363		0.362
$m_{gl,evap}$	U_A	49.804	0.023	49.830	0.021	49.074	0.021	49.145	0.020	49.086	0.020
	U_B		0.115		0.115		0.113		0.113		0.113
$m_{CO2,CD1400H}$	U_A	9.660	0.060	9.789	0.070	9.785	0.061	9.564	0.036	9.804	0.051
	U_B		0.255		0.261		0.261		0.250		0.262
$m_{CO2,CD1000H}$	U_A	0.000	0.000	0.000	0.000	4.856	0.033	0.000	0.000	0.000	0.000
	U_B		0.000		0.000		0.055		0.000		0.000
$m_{CO2,CD380H}$	U_A	4.303	0.008	4.059	0.005	0.000	0.000	3.854	0.003	3.851	0.003
	U_B		0.030		0.029		0.000		0.022		0.024